Biofunctionalization strategies for continuous monitoring biosensors

BIOFUNCTIONALIZATION STRATEGIES FOR CONTINUOUS MONITORING BIOSENSORS

PROEFSCHRIFT

ter verkrijging van de graad van doctor aan de Technische Universiteit Eindhoven, op gezag van de rector magnificus prof.dr.ir. F.P.T. Baaijens, voor een commissie aangewezen door het College voor Promoties, in het openbaar te verdedigen op dinsdag 22 februari 2022 om 16:00 uur

door

YU-TING LIN

geboren te Kaohsiung, Taiwan

Dit proefschrift is goedgekeurd door de promotoren en de samenstelling van de promotiecommissie is als volgt:

voorzitter:	prof.dr.ir. G.M.W. Kroesen
1e promotor:	prof.dr.ir. M.W.J. Prins
copromotor:	dr.ir. A.M. de Jong
leden:	prof.dr.ir. I.K. Voets
	dr. dipl.-ing. A. Sobota
	prof.dr.ir. J. Huskens (Universiteit Twente)
	dr. R.J. de Vries (Wageningen University & Research)

Het onderzoek of ontwerp dat in dit proefschrift wordt beschreven is uitgevoerd in overeenstemming met de TU/e Gedragscode Wetenschapsbeoefening.

Dedicated to my family, Li-Chun Chen, Wen-Hao Lin,
and Tsung-You Lin for their unwavering support.

The work described in this thesis was performed in the Faculty of Applied Physics of Eindhoven University of Technology and was financially supported by Applied Engineering Science (project number 15481), which is part of the Netherlands Organization for Scientific Research (NWO).

COLOPHON

Cover design by Y. Lin and Ehsanfaridi. Printed by ADC Dereumaux, 's-Hertogenbosch, the Netherlands.

This document was typeset using the typographical look-and-feel `classicthesis` developed by André Miede and Ivo Pletikosić.

A catalogue record is available from the Eindhoven University of Technology Library.
ISBN: 978-90-386-5453-9

SUMMARY

Sensing technologies for the continuous monitoring of biomolecules will allow studies of dynamic changes in biological systems and control based on measured responses. Biosensing by particle mobility (BPM) is a novel sensing technology for continuous biomarker monitoring, based on measuring the motion of particles near a surface and resolving their interactions with single-molecule resolution. A critical aspect that determines the functionality, stability, and generalizability of the sensor is the biofunctionalization of the surface. This thesis investigates click-based coupling to an anti-fouling polymer as a strategy for realizing assays with oligonucleotides and antibodies as binder molecules, for achieving stable and generalizable continuous monitoring biosensors.

In chapter one, an introduction is given into the field of continuous monitoring biosensors for applications in healthcare. Strategies for biofunctionalization of biosensor surfaces are compared, with special attention to recent developments in fast and oriented immobilization methods.

In chapter two, we describe a molecular architecture consisting of anti-fouling bottlebrush polymers (PLL-g-PEG) and covalently coupled affinity binders. The aim is to make biosensors with stable responses over long durations. With the molecular architecture, reversible responses were observed over long durations with BPM biosensors having a dsDNA tether between particle and surface, for a sandwich oligonucleotide assay, a competitive oligonucleotide assay and a competitive small molecule immunoassay, in buffer and in filtered blood plasma, with picomolar, nanomolar, and micromolar analyte concentrations, and with continuous sensor operation over 10 hours.

In chapter three we present a BPM sensing principle with free diffusional motion of particles, called f-BPM, that does not include a dsDNA tether between particle and surface. Here, target-induced reversible bonds are detected by changes of the

diffusion coefficient between unbound states (free Brownian motion) and bound states (confined motion). The sensing principle is demonstrated with a DNA competition assay in buffer and in undiluted filtered blood plasma. An operational lifetime of 6 days is achieved, demonstrating the high stability of the biofunctionalized surface.

In chapter four, we investigate how to preserve and store both the biofunctionalized surfaces and the sensor device, aiming to fabricate ready-to-use sensor cartridges. We studied different sugar compositions and demonstrate that a coating of sucrose and trehalose preserves the functionality of the particles and sensor surface in a dry state. We report a protocol that allows for at least three weeks of dry storage of the f-BPM biosensors.

In chapter five, we study site-specific antibody modification based on glycan remodeling to covalently couple oligonucleotides onto the fragment crystallizable region of the antibodies. The aim is to immobilize antibodies on PLL-g-PEG surfaces with a defined orientation. Since the coupling anchor is specific, the antibody activity is expected to be maximally retained. We quantified the coupling efficiency with quadrupole time-of-flight (QTOF) mass spectrometry and SDS-PAGE. The functionality of oriented anti-PCT antibodies on both particles and PLL-g-PEG surfaces is demonstrated in f-BPM experiments. Finally, chapter six summarizes the findings of the thesis, discusses the impact for applications, and describes directions for further research.

CONTENTS

LIST OF ABBREVIATIONS

AntiDIG	Anti-digoxigenin antibodies
Asn	Asparagine
BCN	Bicyclononyne
BPM	Biosensing by particle mobility
bp	Base pair
BSA	Bovine serum albumin
COC	Cyclic olefin copolymer
CRP	C-reactive protein
CV	Coefficient of variation
DBCO	Dibenzocyclooctyne
DIG	Digoxigenin
DNA	Deoxyribonucleic acid
DNA-PAINT	DNA points accumulation in nanoscale topography
dsDNA	Double-stranded deoxyribonucleic acid
DTT	Dithiothreitol
ELISA	Enzyme-linked immunosorbent assay
Fab	Antigen-binding fragment
f-BPM	Free-diffusion-based biosensing by particle mobility
Fc	Crystallizable fragment
IL-6/IL-8	Interleukin-6/Interleukin-8

LC-MS	Liquid chromatography-mass spectrometry
LOD	Limit of detection
MSD	Mean squared displacement
nt	Nucleotide
PBS	Phosphate buffered saline
PC	Polycarbonate
PCT	Procalcitonin
PEG	Poly(ethylene glycol)
PLL	Poly(l-lysine)
PLL-g-PEG	Poly(l-lysine)-grafted-poly(ethylene glycol)
PLL-g-PEG-N_3	Poly-l-lysine-graft poly(ethylene glycol)-azide
POCT	Point-of-care testing
QCM	Quartz crystal microbalance
RNA	Ribonucleic acid
SDS-PAGE	Sodium dodecyl sulphate-polyacrylamide gel electrophoresis
SPR	Surface plasmon resonance
ssDNA	Single-stranded deoxyribonucleic acid
t-BPM	Biosensing by mobility of tethered particles
TNF-α	Tumor necrosis factor-alpha
QTOF	Quadrupole time-of-flight
UDP	Uridine diphosphate
UV	Ultraviolet

1

INTRODUCTION

Applications in the fields of fundamental biological research, health care, bioprocessing industry, and environmental surveillance call for continuous monitoring techniques which allow rapid and sensitive measurement of molecular substances as a function of time. Developments in biofunctionalization strategies play a large role in the analytical performance of continuous monitoring devices. There are unmet needs for robust molecular architectures and coupling processes to immobilize biomolecules on anti-fouling surfaces with good stability. This chapter introduces the topic of the thesis, explains the roles of biofunctionalizations in sensing devices, and specifies the central questions that will be studied.

1.1 CONTINUOUS MONITORING BIOSENSORS

A biosensor can be defined as a "compact analytical device or unit incorporating a biological or biologically derived sensitive recognition element integrated or associated with a physico-chemical transducer that transforms a measurand into an output signal".[1] There are three main components of a biosensor: (i) the biological recognition elements that differentiate the target molecules in the presence of non-relevant biomolecules or chemicals, (ii) a transducer that converts the biorecognition event into a measurable signal, and (iii) a signal processing system that converts the signal into a readable form. The general diagram of a biosensor is demonstrated in Figure 1.1.[1] The molecular recognition elements include antibodies, aptamers, enzymes, and nucleic acids for example.

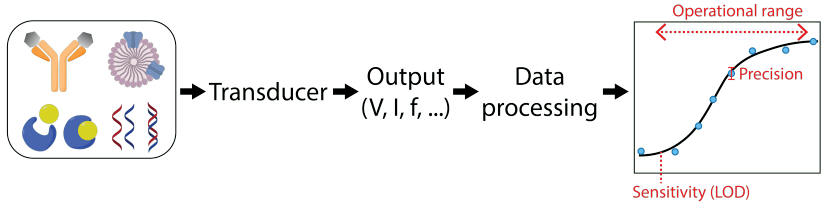

Figure 1.1: General diagram of a sensor system. The biological recognition elements include antibodies, aptamers, enzymes, and nucleic acids for example. Biorecognition events are converted into measurable signals by a transducer. The signals are processed and finally converted into a concentration. The sensing performance of biosensors can be evaluated and compared in terms of e.g. sensitivity, precision, and operational range.

A biosensor should be able to measure the relevant concentration range of the target of interest with good analytical performances.[2] The analytical performance of biosensors is often characterized by sensitivity, precision, and operational range, as shown in Figure 1.1. The sensitivity (limit of detection) is defined as the lowest quantity of a target that can be distinguished by the biosensor from the absence of the target. Precision demonstrates the ability of providing alike concentration outputs for duplicate measurements, while accuracy indicates how close the mean value of the concentration value distribution is to the true value. The range of concentrations over which the biosensor functions is the operational range. In general, biosensors are needed with a

high sensitivity, broad operational range and high precision. To meet the requirements, the ratio between the detected output signal and the analyte concentration should be large, resulting in a steep slope in the dose-response curve. Furthermore, parameters such as reproducibility and stability are important for biosensor development.

One of the well-known categories of biosensors is point-of-care testing (POCT), defined as "biochemical testing at or near the site of patient care whenever the medical care is needed". For example, control of blood glucose levels by POCT is widely applied. A new trend in biosensors is towards continuous monitoring of biomarkers. The concentration of interest, the desired frequency of sampling, and the turnaround time are important factors for the development of continuous monitoring biosensors.[3]

Various continuous monitoring devices have been developed for detecting subcutaneous glucose. Enzymatic electrochemical biosensors offer the required analytical performance and ease of use.[4] Also for other targets, wearable and noninvasive electrochemical biosensors are being investigated e.g. for monitoring electrolytes and metabolites in sweat, tears, or saliva.

Enzymatic electrochemical biosensors are based on enzymatic catalytic reactions that cause changes in electrical properties. Improvements of the enzyme stability have been important research topics to ensure the operation over longer periods. Enzymatic electrochemical biosensors have been demonstrated for precise detection of millimolar concentrations during several weeks.[5–8]

A continuous monitoring sensing principle that achieves higher sensitivities is electrochemical aptamer-based sensing, based on analyte-induced conformational changes of surface-coupled aptamers.[9] The specificity is achieved by the binding properties of an electrode-bound RNA or DNA aptamer. Research groups have demonstrated the monitoring of micromolar and nanomolar analyte concentrations.[10–12] Electrochemical aptamer-based biosensors have been demonstrated for the detection of targets in whole blood with micromolar precision over many hours.[13]

1.2 FROM ENSEMBLE TO SINGLE-MOLECULE DETECTION

Biosensing techniques such as surface plasmon resonance (SPR), enzyme-linked immunosorbent assay (ELISA) and quartz crystal microbalance (QCM) typically measure large numbers of molecules in an ensemble manner, i.e. averages over a large number of molecules, without resolving individual molecules. Single-molecule biosensors aim at detecting individual biomolecules with high specificity and accuracy. Single-molecule detection of biomolecular interactions can reveal kinetic parameters, including lifetimes, rates, binding events, and distributions of these parameters. Since high numbers of biorecognition events are collected, non-specific interactions or outliers can be distinguished and filtered out, which leads to a higher specificity, precision and accuracy.[14]

An example of biosensor development towards single-molecule measurements is the category of digital assays. ELISA has been used for decades for detecting and quantifying e.g. antibodies, antigens, proteins, peptides and food allergens. To improve the sensitivity and specificity, an enzyme-linked digital immunoassay platform with a single-molecule array technology was introduced in 2010, called digital ELISA.[15] The digital assay employs femtoliter-sized reaction chambers for single-molecule entrapments. Each chamber is loaded with one magnetic bead ,with capture and labelled detection antibodies. At low protein concentrations, only a small fraction of beads demonstrate catalytic enzyme activity, which is the typical signature due to beads carrying either a single immunocomplex or none.[16] Femtomolar sensitivity and single molecule resolution have been achieved in digital ELISA assays. However, multiple reagent and washing steps are required, which limits developments towards continuous monitoring devices.

A sensing technology that combines single-molecule resolution with continuous monitoring is Biosensing by Particle Mobility (BPM), which is based on particles that are tethered to a substrate via flexible double-stranded DNA (dsDNA). The particles and substrate are coated with binder molecules such as proteins, oligonucleotides or antibodies, as shown in the left panel of Figure 1.2. In a sandwich assay format, target molecules can

simultaneously bind to a binder molecule on the particle and another binder molecule on the substrate. The formation of a target-induced sandwich bond between the particle and substrate causes the particle motion to become more restricted, which can optically be detected. By recording binding and unbinding events, DNA and protein biomarkers can be monitored with picomolar to nanomolar sensitivity. The sensing principle is reversible and does not consume or produce any reagents, making it suited for continuous monitoring with single-molecule resolution over long durations.

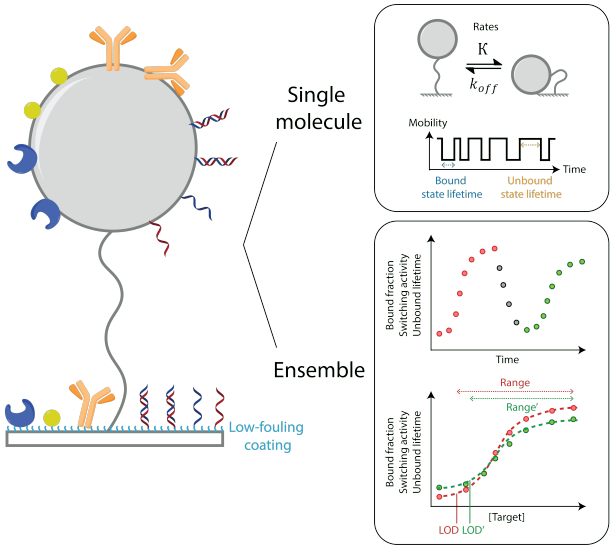

Figure 1.2: Schematic overview of the basic sensing principle and the output parameters of BPM biosensors. Particles are tethered to a substrate via flexible double-stranded DNA. The particles and substrate are coated with binder molecules such as proteins, antibodies, and oligonucleotides. Once the targets bind to the binders, the motion patterns of the particles are changed, which can be optically detected. Single-molecule events and ensemble signals are recorded for the understanding of molecular kinetics and the detection of target concentrations. Analytical performance can be evaluated in terms of sensitivity (LOD), precision and operational range, which are influenced by the stability and reproducibility of the system.

The BPM biosensors are capable of extracting both single-molecule kinetics of targets and reporting ensemble output signals based on large statistics, as shown in the right panel of Figure 1.2. Firstly, since the target binding causes the particle to intermittently switch between unbound states and bound states,

the effective association rate and dissociation rate of the particle can be obtained. Secondly, the unbound states and bound states are distinguished based on the changes in mobilities or motion patterns of particles. Therefore, the corresponding unbound state and bound state lifetimes can be extracted, reflecting the binding affinities, on-rate and off-rate kinetics of target molecules. In addition, ensemble signals such as average switching activity, bound fraction and characteristic lifetimes can also be extracted, due to the large number of particles (500-1000) tracked at the same time. The strength of single-molecule based measurement is its capability of recording both single-molecule events and multiple output parameters.

To enable applications of the BPM biosensor, investigations of the stability and reproducibility of analytical performance over long durations are of importance. Table 1.1 describes mechanisms in the molecular systems of BPM biosensors and their potential consequences in terms of analytical parameters. In principle, the loss of responsive beads, biomolecules, or anti-fouling properties might lead to loss of sensitivity of BPM biosensors. As shown in the bottom right panel of Figure 1.2, a signal decay and a higher background both cause a shift in the measured does-response curve, resulting in a higher detection limit and a smaller dynamic range. Therefore, we aim at developing robust coupling strategies and anti-fouling coating materials, and quantifying changes in sensing performance.

Table 1.1: Potential degradation mechanisms in the molecular systems of BPM biosensors and their possible consequences in terms of analytical parameters.

Potential degradation mechanisms in BPM biosensors	**Potential consequences for analytical performances**
Lose responsive beads	Lower statistics and larger error bars: limited operational lifetime
Lose responsive biomolecules	EC_{50} shifts to higher concentrations: LOD goes up. The contrast becomes smaller: smaller dynamic range
Loss of anti-fouling properties	Higher background and smaller contrast: Lose sensitivity, dynamic range, and LOD

1.3 MOLECULAR ASSEMBLY STRATEGIES

1.3.1 *Anti-fouling polyelectrolytes*

Since the surface of a biosensor comes into contact with complex biological mixtures, efforts have been dedicated over the years to engineer anti-fouling coatings for modifications of sensor surfaces.[17,18] Anti-fouling coatings are designed to be biologically "inert"; i.e., the anti-fouling materials should not directly influence the bio-recognition process or the chemical reactions involved in a biosensor.[19] Bottle-brush (comb-like) polymers, peptides, non-amphoteric hydrophilic materials, zwitterionic compounds, PEG-based materials, and polysaccharides-based materials are the main categories of anti-fouling coatings that have been developed for the field of biosensing.[20,21]

PLL-g-PEG is a commonly used bottle-brush polymer for preventing the non-specific binding of proteins or particles. The adsorption mechanism of PLL-g-PEG on the substrate involves multivalent electrostatic interactions between the positively charged PLL backbones and the negatively charged oxide surface, which can be either glass or plastic substrates. As a result, the polymer backbone lies parallel to the substrate and the PEG side-chains stretch perpendicularly into the bulk environment, resulting in a brush-like structure. In literature, it was shown that protein resistance is maintained when the PLL-g-PEG coating is exposed to multiple serum injections over several hours or stored dry for several months.[18] Due to the good anti-fouling properties and the simple, fast and robust physisorption process, PLL-g-PEG is highly suitable for incorporation in a multi-step molecular architecture designed for a biosensor. The goal is to achieve simple application of the anti-fouling intermediate layer, which enables further coupling of biomolecules such as oligonucleotides and antibodies.

1.3.2 *Coupling strategies*

Physisorption

Physisorption is the interfacial adsorption of biomolecules through Van der Waals, hydrophobic, polar, or electrostatic interac-

tions.[22] It is a simple coupling method but the orientation of immobilized biomolecules can vary. In imunoassays, structural changes and inadequate orientation of binding paratopes upon physisorption can negatively influence the functionality of antibodies.

Covalent coupling

Biomolecules can be coupled to surfaces by chemical reactions between an activated solid substrate and the complementary functional groups on the biomolecule itself. The most common covalent coupling strategies include the use of amine groups, carboxy groups, or thiol groups in lysine or cysteine residues. These covalent strategies give strong coupling but can lead to undesirable orientation or multipoint attachment of biomolecules due to a relatively high abundance of both amine and carboxy groups on the surfaces of proteins, resulting in an increase in the heterogeneity and the loss of bioactivity.[22]

Affinity-based attachment

Affinity-based immobilization techniques include DNA-directed immobilizations, recombinant proteins with engineered histidine-tag, protein A or protein G-mediated immobilization for specific interactions with Fc fragments of antibodies, and immobilization of glycoproteins through their carbohydrate moiety.[22] Another popular bioaffinity immobilization method is based on the specific binding of biotin to avidin and streptavidin, since the biotin-avidin interaction is the strongest noncovalent bond found in nature.

Antibody orientation

The orientation of immobilized bioreceptors, such as antibodies affects the sensitivity of the biosensor in detecting the analyte. The sensitivity is dependent on presentation of functional antibodies, requiring the antigen binding sites be directed toward the solution phase, as shown in the end-on orientation in Figure 1.3.[23]

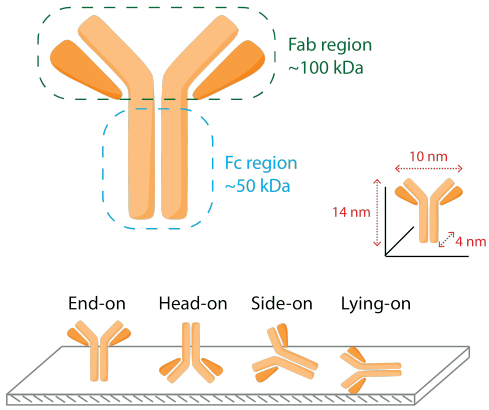

Figure 1.3: The structure, orientations, and dimensions of an antibody. The molecular mass of an antibody is approximately 150 kDa and the dimension is $14 \times 10 \times 4$ nM. An antibody is comprised of two fragment antigen binding (Fab) regions and a fragment crystallizable region (Fc). The ideal orientation of immobilized antibodies is referred to as "end-on". With end-on orientation, the two Fab regions are accessible, allowing the maximum binding capacity of antigens. Other possible orientations include "head-on," "side-on," and "lying-on".[23]

Antibody immobilization via physisorption often results in a low proportion of antibodies with accessible and functional binding sites. Covalent attachment of antibodies to chemically activated substrates via functional groups has resulted in improvements in antibody density and stability, though these covalent methods are generally not site-directed. An example of splitting the Fab fragments from the antibodies and covalently immobilizing the Fab fragments on substrates has been demonstrated. The Fab fragments were oriented via their functional groups and coupled on an activated thiol surface.[24] Other approaches study how antibodies can be immobilized in their native form in a homogeneous arrangement such that their antigen binding sites are free from steric hindrance and are oriented so as to maximize the binding capacity of targets.[23]

DNA is a highly stable molecule which better tolerates covalent immobilization onto reactive surfaces without losing its binding capacity. Also, oligonucleotides bearing chemical modifications for the direct attachment to surfaces are readily available via click chemistry. Hence the DNA-directed immobilization method has been used to generate biofunctionalized surfaces for antibody-

based immunoassays. The binding of DNA strands to antibodies can be conducted in homogeneous solution with higher efficiency compared to heterogeneous reactions on a surface. Thereafter, the DNA-antibody conjugates can be captured subsequently by robust DNA hybridization onto the surface.[8]

1.3.3 *Molecular assembly strategies*

To develop a robust biofunctionalization strategy for biosensors, strong and stable coupling methods can be combined with anti-fouling coatings. For example, a biotin-poly(L-lysine)-g-poly(ethylene glycol) (biotin-PLL-g-PEG) and protein A-based technique was developed to immobilize antibody on the surface of microchannels.[25] The surface was first activated with functional carboxyl group for subsequent binding of biotin-PLL-g-PEG molecules through the electrostatic interactions. Biotinylated protein A was immobilized on the surface through a linking molecule, neutravidin.[25] In this case, the PLL-g-PEG polymers reduce the non-specific interactions, while the biotin-neutravidin bond offers a robust and stable coupling strategy for immobilizing antibodies onto the polymer surface.

Another example is based on the combination of anti-fouling polymer coatings and a DNA-directed coupling method. Complexes of streptavidin and biotinylated ssDNA were arrayed onto a PLL-g-PEG/ PEGbiotin coated microarray chip.[26] A mixture of liposomes covalently tagged with different complementary DNA sequences was sorted via the specific binding of DNA strands. Single liposome arrays may increase the throughput due to the increased spot density, and may enlarge the understanding of biorecognition events on the single-molecule level.[26] In conclusion, anti-fouling polymers and covalent coupling strategies offer advantages such as minimized non-specific interactions and stronger anchoring bonds which can be combined into a promising strategy for developing a biofunctionalization strategy, while the use of DNA-directed immobilization prevents the loss of antibody bioactivity upon attachment to the biofunctionalized surface.

1.3.4 *Preservation strategies to achieve ready-to-use biosensors*

A challenge in the development of protein-based biosensors like immuno-sensors is maintaining the functional activity and the three-dimensional structure of proteins during processing and storage. A common method of stabilizing proteins for long-term storage and later use is lyophilization (freeze drying). However, freeze-dried reagents are not easily integrated into a biosensor cartridge.[27]

Anhydrous, or dry state, preservation such as sugar-based drying is commonly used in biosensor devices, e.g. in immunoassay lateral flow tests. For example, anhydrous preservation in a trehalose matrix is suitable for the preservation of biological samples.[28] Trehalose is a disaccharide found at high concentrations in many organisms that naturally survive dehydration.[28] The preservation principle is based on restricting molecular motion to a small volume over a finite time period, which can prevent the degradation of proteins.[27]

An example of a successfully demonstrated ready-to-use biosensor is the Magnotech system, which is an immunoassay technology based on magnetically controlled movement of particles detected optically.[29,30] The biosensor with dry-reagents was demonstrated with blood plasma and whole saliva. In this thesis, we will study the functionality of a biofunctionalized surface with anhydrous preservation strategies for a ready-to-use biosensor with long-term operational lifetime.

1.4 OUTLINE OF THE THESIS

Sensing technologies for the continuous monitoring of biomolecules will allow studies of dynamic changes in biological systems and control based on measured responses. Biosensing by particle mobility (BPM) is a novel sensing technology for continuous biomarker monitoring, based on measuring the motion of particles near a surface and resolving their interactions with single-molecule resolution. A critical aspect that determines the functionality, stability, and generalizability of the sensor is the biofunctionalization of the surface. This thesis investigates click-based coupling to an anti-fouling polymer as a strategy for realizing assays with oligonucleotides and antibodies as binder molecules, for achieving stable and generalizable continuous monitoring biosensors.

In chapter two, we describe a molecular architecture consisting of anti-fouling bottlebrush polymers (PLL-g-PEG) and covalently coupled affinity binders. The aim is to make biosensors with stable responses over long durations. With the molecular architecture, reversible responses were observed over long durations with BPM biosensors having a dsDNA tether between particle and surface, for a sandwich oligonucleotide assay, a competitive oligonucleotide assay and a competitive small molecule immunoassay, in buffer and in filtered blood plasma, with picomolar, nanomolar, and micromolar analyte concentrations, and with continuous sensor operation over 10 hours.

In chapter three we present a BPM sensing principle with free diffusional motion of particles, called f-BPM, that does not include a dsDNA tether between particle and surface. Here, target-induced reversible bonds are detected by changes of the diffusion coefficient between unbound states (free Brownian motion) and bound states (confined motion). The sensing principle is demonstrated with a DNA competition assay in buffer and in undiluted filtered blood plasma. An operational lifetime of 6 days was achieved, demonstrating the high stability of the biofunctionalized surface.

In chapter four, we investigate how to preserve and store both the biofunctionalized surfaces and the sensing particles, aiming to fabricate ready-to-use sensor cartridges. We studied different

sugar compositions and demonstrate that a coating of sucrose and trehalose preserves the functionality of the particles and sensor surface in a dry state. We report a protocol that allows for at least three weeks of dry storage of the f-BPM biosensors.

In chapter five, we study site-specific antibody modification based on glycan remodeling to covalently couple oligonucleotides onto the Fc fragment region of the antibodies. The aim was to immobilize antibodies on PLL-g-PEG surfaces with a defined orientation. Since the coupling anchor is specific, the antibody activity is expected to be maximally retained. We quantified the coupling efficiency with quadrupole time-of-flight (QTOF) mass spectrometry and SDS-PAGE. The functionality of oriented anti-PCT antibodies on both particles and PLL-g-PEG surfaces was demonstrated in f-BPM experiments.

Finally, chapter six summarizes the findings of the thesis, discusses the impact for applications, and describes directions for further research.

2

CLICK-COUPLING TO ANTI-FOULING POLYMERS FOR CONTINUOUS MONITORING WITH SINGLE-MOLECULE RESOLUTION

Sensing technologies for the real-time monitoring of biomolecules will allow studies of dynamic changes in biological systems and control based on measured responses. Here we describe a molecular architecture and coupling process that allows continuous measurements of low-concentration biomolecules over long durations in a sensing technology with single-molecule resolution. The sensor is based on measuring temporal changes of the motion of particles upon binding and unbinding of analyte molecules. The biofunctionalization involves covalent coupling by click chemistry to PLL-g-PEG bottlebrush polymers. The polymer is coupled to a surface by multivalent electrostatic interactions, while the grafted poly(ethylene glycol) suppresses non-specific binding of biomolecules. With this biofunctionalization strategy, we demonstrate the continuous monitoring of single-stranded DNA and a medically relevant small-molecule analyte (creatinine), in sandwich and competitive assays, in buffer and in filtered blood plasma, with picomolar, nanomolar as well as micromolar analyte concentrations, with continuous sensor operation over 10 hours.

Parts of this Chapter have been published as:

Lin, Y., Vermaas, R., Yan, J., de Jong, A. M., & Prins, M. W. J. "Click-Coupling to Electrostatically Grafted Polymers Greatly Improves the Stability of a Continuous Monitoring Sensor with Single-Molecule Resolution." *ACS Sensors* (2021).

Alvisi, N., Gutiérrez-Mejía, F. A., Lokker, M., Lin, Y. T., de Jong, A. M., van Delft, F., & de Vries, R. "Self-Assembly of Elastin-like Polypeptide Brushes on Silica Surfaces and Nanoparticles." *Biomacromolecules* (2021).

2.1 INTRODUCTION

Biological systems exhibit dynamics that are at the most basic level driven by time-dependent changes of molecules such as metabolites, hormones, proteins, and nucleic acids. For healthcare and engineering purposes, it would be highly valuable to be able to continuously monitor specific molecules that critically reflect the biological dynamics, so that timely actions can be taken and changes can be managed. A good example are sensors for continuous glucose monitoring which are used for patient self-monitoring[31] as well as for controlling industrial fermentations and bioreactors.[32]

Glucose is a metabolite that is present at millimolar concentrations. Biomarkers at lower concentrations can be measured with well-established detection techniques such as surface plasmon resonance (SPR), quartz crystal microbalance (QCM), and enzyme-linked immunosorbent assays (ELISA). However, these methods involve fluid handling steps (e.g. washing steps) which complicate the design of a monitoring system. A sensing principle that does not require wash steps is electrochemical aptamer-based sensing, based on analyte-induced conformational changes of surface-coupled aptamers.[9] Research groups have demonstrated the monitoring of micromolar and nanomolar analyte concentrations.[10–12] However, the continuous monitoring of biomarkers in the picomolar concentration range has not come within reach.

We have recently demonstrated a sensing technology for continuous biomarker monitoring at micromolar, nanomolar and picomolar concentrations, called Biosensing by Particle Mobility (BPM).[33–35] The BPM sensing method has single-molecule resolution and gives digital signals, which enables measurements at low concentrations.[36] BPM is based on particles tethered to a substrate, where the particles and the substrate are functionalized with specific binder molecules. Temporal changes are detected in the mobility of the particles caused by the reversible binding and unbinding of analyte molecules, generating digital on-off switching related to single-molecule events. The BPM sensing principle has been demonstrated with oligonucleotides and proteins as binder molecules, for sensing DNA, protein, as well as

small-molecule biomarkers. However, the reported data show a decay of sensor signals, limiting the duration of the experiments as well as the duration of sensor operation in prospective applications. Potential causes of the signal decay are imperfect anti-fouling strategies and a loss of binder molecules over time due to non-covalent coupling methods.

In this paper, we describe a molecular architecture with anti-fouling bottlebrush polymers (PLL-g-PEG)[37] and covalent click coupling[38,39] for achieving real-time continuous monitoring of analytes at low concentrations with stable response over long durations. The bottlebrush polymer serves four purposes: (i) it is strongly attached to the substrate by multivalent electrostatic interactions for high sensor stability, (ii) polyethylene glycol groups give anti-fouling properties[18,40] in order to reduce non-specific binding of biomolecules, (iii) the polymer serves as a spacer between binder molecules and the solid substrate for minimizing loss of biomolecular activity over time, and (iv) integrated click-functional groups allow facile covalent coupling of binder molecules. We show that the molecular architecture with click-coupling to anti-fouling polymers greatly improves the stability of the BPM continuous monitoring sensor with single-molecule resolution. We describe the molecular architecture, compare it to previous coupling methods, and demonstrate the continuous monitoring of single-stranded DNA (ssDNA) and a small-molecule analyte (creatinine), in sandwich and competitive assay formats, in buffer and in filtered blood plasma. Picomolar, nanomolar as well as micromolar analyte concentrations are measured with continuous sensor operation over long durations.

2.1.1 *Sensing approach*

Biosensing by Particle Mobility (BPM) is based on particles that are tethered to a substrate via double-stranded DNA (dsDNA), with the particles and substrate coated with binder molecules such as oligonucleotides or antibodies.[33,35] The particles show Brownian motion and explore a region related to the length of the dsDNA tether. In a sandwich assay format (see Figure 2.1), target molecules can simultaneously bind to a binder molecule

on the particle (particle-side binder, also referred to as 'particle binder') and a binder molecule on the substrate (substrate-side binder, also referred to as 'substrate binder'). The formation of a target-induced sandwich bond between the particle and substrate causes the particle motion to become more restricted (bound state), which can optically be detected. Upon dissociation of the target molecule, the larger motion amplitude of the particle is restored (unbound state). The increase and decrease of particle motion, as a result of binding and unbinding of target molecules, is detected over time.[33] The output of the BPM biosensor is the particle switching activity, defined as the average frequency of binding and unbinding events per particle, which can be quantitatively related to the target concentration. The sensing principle is reversible and does not consume or produce any reagents, making it highly suited for continuous monitoring over long durations. However, operation over long durations requires a high stability of the biofunctionalizations in the system, which is the topic of this study.

2.2 RESULTS AND DISCUSSION

2.2.1 *Develop a stable particle-based biosensor by covalent coupling to anti-fouling polyelectrolytes*

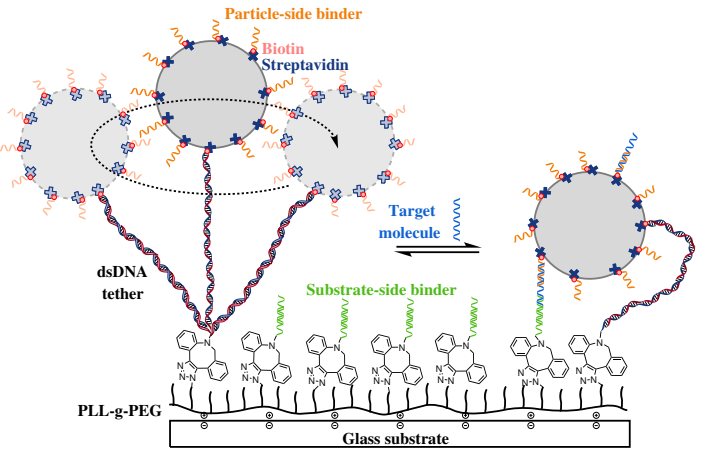

Figure 2.1: Schematic overview of Biosensing by Particle Mobility (BPM) using click-coupling to anti-fouling bottlebrush polymer, exemplified by a sandwich assay for detecting ssDNA target molecules (not to scale). The substrate is coated with PLL-g-PEG-N_3 molecules, for anti-fouling properties and for click-coupling of DBCO-tagged double-stranded DNA tether molecules (red-blue). The particle and the substrate are provided with binders that have a specific affinity to the target molecule. Target molecules (blue) hybridize with the complementary particle and substrate binders, forming a sandwich arrangement (right). The formed sandwich bond leads to a restriction of the motion of the particle. Due to the reversible affinity interactions, the particle switches between the unbound state (left) and the bound state (right). The switching frequency depends on the target concentration: the frequency is low for low target concentration, and the frequency is high for high target concentration.

The design of the molecular architecture and the particle-based biosensor are shown in Figure 2.1. A mixture of cationic PLL-g-PEG and PLL-g-PEG-N_3 polymers are adsorbed onto the negatively charged glass substrate. The grafted polyethylene glycol (PEG) groups are strongly hydrophilic and provide biofouling resistant properties, used here to reduce non-specific interactions between particles, substrate and matrix components. The dsDNA tether as well as the substrate-side binder molecules are coupled to the PLL-g-PEG layer via the integrated azide groups, using second generation click chemistry that is copper-free, catalyst-free,

specific and biocompatible.[41–44] The surface density of clickable azide groups was controlled by mixing PLL-g-PEG and PLL-g-PEG-N_3 polymers at a 10:1 ratio. This provides a sufficient number of azide groups on the surface while still enabling a low degree of non-specific binding. The single-tethering of particles was created by coupling DBCO-dsDNA-biotin tethers to the azide groups and thereafter exposing the surface to particles functionalized with streptavidin moieties.

The stability of the tethered particles was characterized by measuring the number of tethered particles over time. Figure 2.2 shows the percentage of particles that remain tethered to the surface over a 24 h monitoring period. In the reference experiment the dsDNA tethers were provided with digoxigenin tags and coupled to the substrate using anti-digoxigenin antibodies (see our earlier work[33]). The observed time profiles of the two coupling methods are fitted with single-exponential decay curves. The curves show that the click-based coupling is much more stable than the antibody-antigen based coupling: the rate of particle loss is about 50 times slower for the click-based coupling.

For the click-based coupling, the loss of particles over a period of 24 h is about 20%. Possible origins of the observed loss are the detachment of the PLL-g-PEG layer from the glass substrate, the breaking of the DBCO-azide bond, or the dissociation of the biotin-streptavidin bond on the particle. The dissociation rate of biotin-streptavidin is about $(5.5 \pm 2.2) \times 10^{-6} s^{-1}$,[45] which is very close to the rate observed in Figure 2.2. The DBCO-azide conjugate, formed through click chemistry, has been proven to be stable under a pulling force of 150 pN for more than 24 h.[42,46] The strength of the PLL-g-PEG coupling to the glass substrate is dependent on the surface charge density of the substrate; studies have shown that PLL-g-PEG modified surfaces stay passivated over days.[47–50] Therefore, the loss rate of particles in the PLL-g-PEG experiment in Figure 2.2 is most likely caused by the dissociation of biotin-streptavidin bonds between the biotinylated dsDNA tether and the streptavidin-functionalized particle.

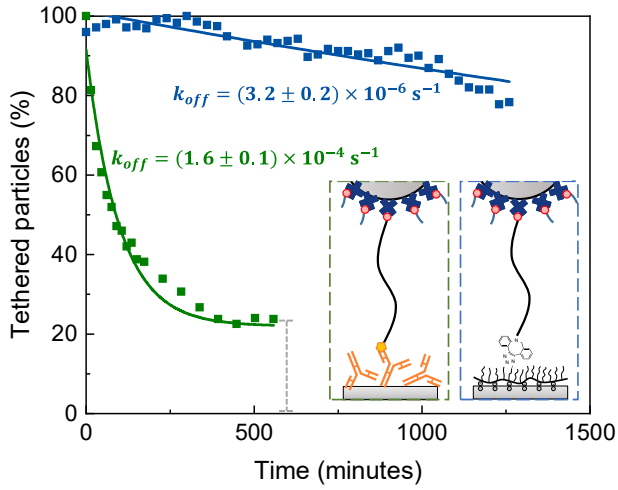

Figure 2.2: Number of tethered particles measured over time, for two methods of coupling the dsDNA tether to the substrate: DIG-AntiDIG coupling (green) and click chemistry (blue). The fluid cell was turned over so that dissociated particles sediment and move away from the glass substrate. The curves were normalised at t=0 and have been fitted with an exponential decay function: $f(t) = (1-a) + a \times exp(-t \cdot k_{off})$, with $f(t)$ the fraction of particles bound to the substrate as a function of time, k_{off} the dissociation rate constant of single-tethered particles, a the initial fraction of single-tethered particles, and $(1-a)$ the initial fraction of particles that are strongly bound, i.e. double-tethered or non-specifically bound. The fitted k_{off} values are indicated at the curves. The initial number of particles in the experiments was around 500. Negative control experiments are discussed in Appendix 2.5.1.

2.2.2 *DNA sandwich assay performed in buffer and in filtered blood plasma*

The reversibility of the BPM sensor with click-based coupling is studied in Figure 2.3, for a DNA sandwich assay as sketched in Figure 2.1. The particle and substrate are provided with ssDNA molecules having 10-bp and 9-bp complementarity to the ssDNA target respectively, resulting in a bound state lifetime in the order of seconds. Figure 2.3a shows the applied concentration profile (top panel) and the measured switching activity (bottom panel). The switching activity is the frequency of binding and unbinding events observed per particle, averaged over the number of tethered particles in the microscopic field of view and over a

measurement duration of 5 minutes. Typically, a few hundred particles are simultaneously imaged and tracked. The averaging makes the switching activity a normalized parameter that is independent of the number of observed particles. The total number of particles is important for achieving good event statistics and small error bars in the measured switching activity parameter. Measurements with less particles give lower numbers of switching events, and therefore larger measurement uncertainties due to lower event statistics. We typically have 500 to 1000 particles in one field of view. To achieve a CV of 5%, at least 400 events need to be collected per measurement point.[35]

The switching activity signal in Figure 2.3a dynamically responds to both increasing and decreasing target concentrations. The activity increases for increasing target concentration, as is expected for a sandwich assay. When the target concentration is decreased to zero in a single step, the activity drops with a finite response time. The three measured step responses are fitted with exponential decay curves, see the grey lines, showing that the dynamic response can be described with a single time constant τ_{off} of 26.5±2.0 min. The fitted τ_{off} values of the three subsequent step responses are equal within their uncertainty intervals, demonstrating that the time constant is independent of analyte concentration. This implies that the binding between particle and substrate is monovalent and that the relaxation time reflects the single-molecule dissociation constant of the weakest link, i.e. the binding between target molecule and substrate binder. Furthermore, the data prove that the sensor system is reversible and stable over a time period of several hours.

Figure 2.3b shows the data points measured in panel a, but now plotted as a dose-response graph, i.e. the measured signal as a function of the applied target concentration. The correspondence between the data points in the two panels is highlighted by their colors. Figure 2.3b shows that the data measured with the click-coupling is consistent over the different time periods. The data is fitted with a Hill equation $A([T]) = A_{bg} + A_a \times \frac{[T]}{EC50+[T]}$, with A the switching activity, A_{bg} the background activity, A_a the activity amplitude, $[T]$ the target concentration, and $EC50$ the target concentration at which the response reaches 50% of the activity amplitude. The data show that the sensor response is consistent

over a period of 10 hours, using the molecular architecture with click-based coupling on anti-fouling polymer. Other than PBS buffer, the capability of performing DNA sandwich assay in high ionic strength buffers has been tested (see Appendix 2.5.9). The interactions between PLL-g-PEG and DNA have been further investigated by varying salt concentration.

The PEG side chains of the PLL-g-PEG polymer are expected to function as an anti-fouling layer that resists protein adsorption. Figure 2.3c and Figure 2.3d show the response of the BPM sensor in filtered undiluted blood plasma. The data in plasma and in buffer show good correspondence, both in time response and in dose-response curve, proving that ssDNA target in the picomolar concentration range can be dynamically monitored in very different solutions over long durations. The anti-fouling properties of the PLL-g-PEG polymer are also apparent in other parameters: (i) the percentage of non-specifically bound particles is less than 10% (see Appendix 2.5.1), (ii) the room-temperature shelf-life of the PLL-g-PEG surface functionalized with oligonucleotides and dsDNA tethers is at least three months (see Appendix 2.5.2), and (iii) analyte measurements in 10% unfiltered blood plasma can be done over a period of 9 hours (see Appendix 2.5.3).

The stability of the click-based BPM sensor is improved relative to that of the antibody-anchoring BPM sensor (Appendix 2.5.4). Under similar conditions, the click-based sensor responds quantitatively to the target in filtered undiluted blood plasma with a signal decay rate of $(8.3 \pm 1.1) \times 10^{-6} s^{-1}$ (on average less than 10% signal loss was observed over five hours), while the antibody-anchored sensor exhibits a higher loss of signal (approximately 50% signal loss was observed over five hours) with a decay rate of $(4.5 \pm 0.3) \times 10^{-5} s^{-1}$.

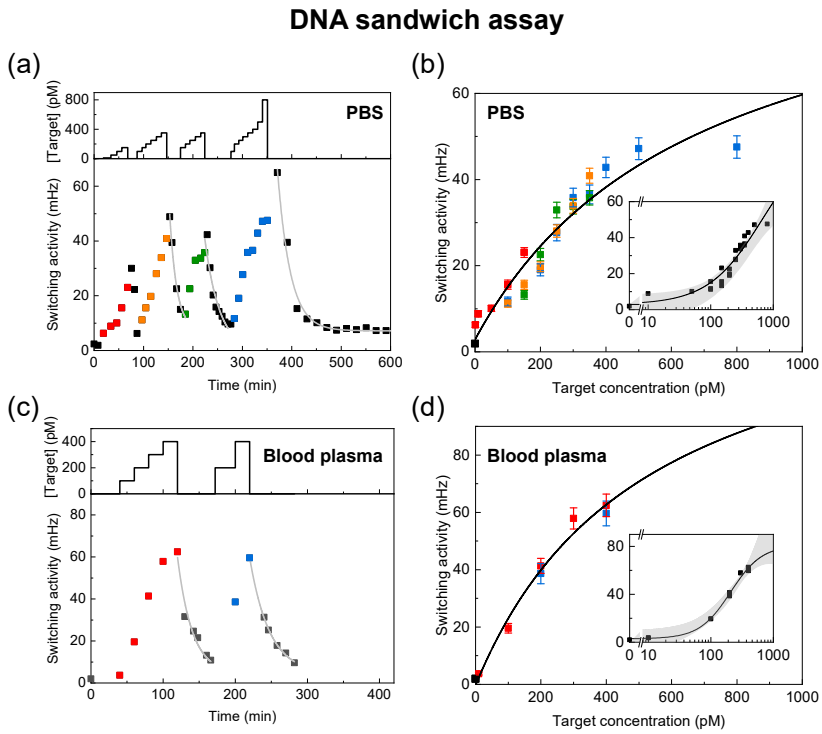

Figure 2.3: Dynamic response to target concentration of a BPM sensor with click-coupling to PLL-g-PEG polymer, for a DNA sandwich assay in buffer and in filtered undiluted blood plasma. The substrate is functionalized with ssDNA oligonucleotide binders having 9-bp complementarity to the ssDNA target. Particles are provided with ssDNA oligonucleotide binders having 10-bp complementarity. (a) The switching activity measured over time for ssDNA target in PBS. The top panel shows the concentration-time profile applied to the flow cell. The target concentration was gradually increased in small steps and thereafter returned to zero in a single step; four such profiles were consecutively applied. The bottom panel shows the switching activity of the BPM sensor. The switching activity, defined as the average frequency of binding and unbinding events per particle, shows a positive and reversible response to target concentration. The signal response after application of zero concentration was fitted with a single-exponential decay function (indicated as light grey lines), revealing a time constant of = 26.5±2.0 min. (b) The data of panel a plotted in a dose-response graph, i.e. the measured signal as a function of target concentration. The colors of the data points refer to the consecutive concentration-time profiles in panel a. The inset shows the data with a logarithmic concentration scale. The data points collapse onto a single curve, demonstrating the consistent response and reversibility of the sensor. The data were fitted with a Hill equation $A([T]) = A_{bg} + A_a \times \frac{[T]}{EC50+[T]}$ (black line), revealing $EC50$ = 680 ± 268 pM. The measurement errors are the standard errors given by the standard deviation of switching activity divided by the square root of the number of particles.[51] The standard errors show the accuracy of the mean and are strongly dependent on sample size. The grey shade indicates the 95% confidence range of the fit. (c) The switching activity measured for ssDNA target in 50 kDa spin-filtered bovine blood plasma. The single-exponential decay fits (light grey lines) reveal a time constant of τ_{off} = 27.0±2.0 min. The protein composition of the filtered blood plasma was determined with SDS-PAGE, see Appendix 2.5.5. (d) The data of panel c plotted in a dose-response graph. The data points collapse onto a single curve with $EC50$ = 524 ± 257 pM

2.2.3 *Continuous small molecule monitoring via competition assays*

Sandwich assays are suitable for measuring analytes that have two binding sites, since the analyte needs to simultaneously bind to both the particle binder and the substrate binder. For monitoring small molecules with only one binding site, it is necessary to employ a competition assay. Figure 2.4 shows the sensor design and the sensor response for two competition assays, namely for monitoring ssDNA and creatinine.[35] Creatinine is a byproduct of muscle metabolism and an important biomarker for monitoring kidney function.[52] In the competition assays, either the particles or the substrate are provided with molecular binders that compete with the analyte for transient binding of the particles.

In the ssDNA competition assay, the PLL-g-PEG surface is covalently functionalized with partially double stranded substrate binders that function as the analogues (green) with a 9-nt single stranded binding region pointing outward. Particles are provided with initial biotinylated oligos (grey) having 20-nt complementarity to particle binders (orange). The reversible 9 bp hybridization between substrate binders (ssDNA analogues) and particle binders results in transient switching of particle mobility. In the presence of the 11-nt analyte (blue), the binding region on particle binders is blocked, causing a decrease of switching events. In the creatinine assay, the PLL-g-PEG surface is covalently functionalized with substrate binders (grey) having 20-nt complementarity to ssDNA-creatinine conjugates that function in the assay as the analogues (green). Particles are functionalized with anti-creatinine antibodies (orange) by biotin-streptavidin coupling. In the absence of creatinine analyte, the reversible binding of creatinine antibodies to analogues results in switching of particles. When creatinine analyte is present in solution, then the binding sites on the anti-creatinine antibodies are blocked by analyte and the switching events of the particles are reduced. For a detailed explanation of the competition assays, see Appendix 2.5.6 and Appendix 2.5.7.

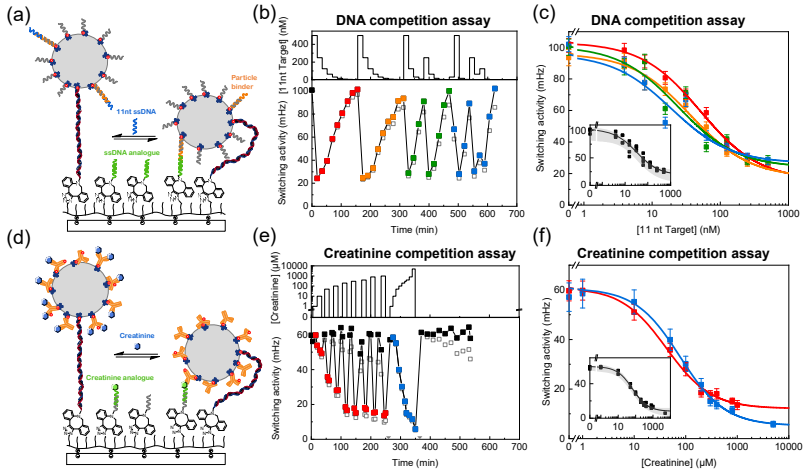

Figure 2.4: BPM competition assays on anti-fouling PLL-g-PEG polymer, for measuring ssDNA (a, b, c) and creatinine (d, e, f) in PBS. (a) Schematic drawing of ssDNA competition assay (molecules are not to scale). (b) The switching activity measured over time for ssDNA target. The top panel shows the concentration-time profiles and the bottom panel the measured switching activity. The switching activity shows an inverted response (high analyte concentration gives low switching activity), as expected for a competition assay. The open squares show the uncorrected data and the solid squares show the signal corrected for loss; the correction method is described in Appendix 2.5.6. Red and orange data points represent equal decreasing concentration series; green and blue data points represent sequences of alternating concentration values. Lines are guides to the eye. (c) Dose-response graph containing all data points of panel b. The data were fitted with a Hill equation (colored lines). The fitted $EC50$ values are 51±6 nM (red), 37±8 nM (orange), 24±17 nM (green), and 19±13 nM (blue). Small variations in flow conditions within experiments and incomplete exchange of fluid cause small differences in the measured $EC50$ values. The inset shows the Hill equation fit through all data points simultaneously, with an $EC50$ of 35±9 nM. The measurement errors are the standard errors of the mean, given by the standard deviation of switching activity divided by the square root of the number of particles.[51] Lines are guides to the eye. (d) Schematic drawing of creatinine competition assay (molecules are not to scale). (e) Competitive BPM assay with creatinine-analogue on the substrate and anti-creatinine antibody on the particle. The colored squares show the signal corrected for signal loss. The open squares represent the uncorrected data. Two grey triangles on the x-axis mark the time points when a chemical reactivation processes was applied. The correction method and the reactivation process are described in Appendix 2.5.7. Lines are guides to the eye. (f) Dose-response graph containing all data points of panel e. Dose-response curves for the two time periods (red, blue) were separately fitted with a Hill equation. The fitted $EC50$ values are 42±6 μM (red) and 78±9 μM (blue). The inset shows the Hill equation fit through all data points simultaneously, with an $EC50$ of 66±8 μM.

The data in Figure 2.4 show reversible sensor responses over long durations for the two very different molecular systems,

namely the competitive oligonucleotide assay (panels a-c) and the competitive small molecule immuno-assay (panels d-f). The time-dependent data in Figure 2.4b and Figure 2.4e show that the signal dynamically responds to repeated increases as well as decreases of analyte concentration, applied over a time period of many hours. Compared to the sandwich assays, three interesting differences are seen. First, the competition assays give a sensor with inverted response: an increase of analyte concentration causes a decrease of switching activity, because the analyte molecules compete with the analogues. Second, the responses in the competition assays are much faster than the responses in the sandwich assays. The faster response is caused by the law of mass action, as the analyte concentrations are higher in the competition assays compared to the sandwich assays. Third, the competition assays are prepared with a reduced density of binders on the particle side or on the substrate side. A low density is essential in order to achieve reversible monovalent bonds and avoid irreversible multivalent bonds between particle and substrate. The density of binders is approximately three orders of magnitude lower in the competition assays compared to the sandwich assay. The open squares in Figure 2.4b show the raw data of the DNA competition assay. The observed signal decrease follows a straight line with a loss rate of $6 \times 10^{-6} s^{-1}$ (see Appendix 2.5.6). This rate is equal to the dissociation rate constant of the biotin-streptavidin bonds that are involved in the coupling of the particle-side binders (see Figure 2.4a). A similar time-dependent dissociation of particle-side binders should have occurred in the sandwich assay experiment of Figure 2.3, but in that data the dissociation is not visible due to the small loss of signal compared to the error bars. The predictable nature of the signal loss allows the application of a mathematical correction method. The solid data points in Figure 2.4b represent the measured signal after correction for the loss (see Appendix 2.5.6). The resulting dose-response curves are shown in Figure 2.4c.

In the creatinine assay, a signal loss rate is observed of $2 \times 10^{-5} s^{-1}$ (see Appendix 2.5.7). Since proteins are generally less stable than oligonucleotides, the higher loss rate is potentially caused by a gradual loss of activity of the antibodies. Again, the observed rate of signal loss allows the application of a mathemat-

ical correction. The solid data points in Figure 2.4e represent the measured signal after correction for the loss (see Appendix 2.5.7). Alternatively, the original signal can be recovered by supplementing fresh analogues into the flow cell (see experimental results in Appendix 2.5.7). In summary, Figure 2.4 shows consistent time-dependent responses and dose-response curves, for two very different competition assays (ssDNA oligonucleotide assay, and small-molecule immunoassay), over a wide concentration range (nM to mM), over monitoring periods of many hours.

2.3 CONCLUSION

We have described a biofunctionalization strategy based on click-coupling to an anti-fouling polymer for improving the control and durability of real-time continuous biosensing with single-molecule resolution. The bottlebrush polymer (PLL-g-PEG) is strongly attached to the substrate by multivalent electrostatic interactions and serves as a spacer between immobilized molecules and the solid substrate. Reversible and consistent responses were observed over long durations in different molecular systems, namely a sandwich oligonucleotide assay, a competitive oligonucleotide assay and a competitive small molecule immunoassay, showing the general applicability of the approach. Picomolar, nanomolar as well as micromolar analyte concentrations were measured with continuous sensor operation over many hours. The presented molecular architecture is suited for a variety of substrates (see Appendix 2.5.8) and for further industrialization with inexpensive fabrication cost. We tested that the shelf life of the modified surface in wet state is several months (Appendix 2.5.2). We expect that the sensor with novel biofunctionalization strategy will enable real-time monitoring for a wide range of applications that can benefit from series of biochemical data and dynamic process control, including biological research as well as medical, pharmaceutical and industrial applications.

2.4 MATERIALS AND METHODS

2.4.1 *DNA and chemicals*

The ssDNA oligonucleotides (standard desalting and HPLC purification for chemically modified DNA) used in the study were purchased from IDT (Integrated DNA Technologies). Chemicals used in this protocol were purchased from Sigma, except if stated otherwise.

2.4.2 *PLL-g-PEG functionalization and tether anchoring*

Poly(l-lysine)-grafted poly(ethylene glycol) was purchased from SuSoS (Switzerland) with a grafting ratio of 3.5. The molecular weight of the PLL backbone and PEG side chains are 20 kDa and 2 kDa respectively. Azide functionalized PLL-g-PEG (Nanosoft Biotechnology LLC, USA) is composed of a 15 kDa PLL backbone and 2 kDa PEG chain with a grafting ratio of 3.5.

Glass slides (25 x 75 mm, #5, Menzel-Gläser) were pre-cleaned by 30 minutes of sonication in isopropanol (VWR, absolute) and 10 minutes of sonication in MilliQ. After the substrate was dried with a nitrogen stream, 1 minute of oxygen plasma was applied to the slides to plasma-oxidize the surface. PLL(20)-g[3.5]-PEG(2) and PLL(15)-g[3.5]-PEG(2)-N_3 were pre-mixed in MilliQ with the ratio of 9:1 by weight at a final concentration of 0.45 mg/mL and 0.05 mg/mL respectively. Custom-made fluid cell stickers (Grace Biolabs) with an approximate volume of 20 μL were then attached to the substrate and the PLL-g-PEG/PLL-g-PEG-N_3 polymer mixture was immediately injected to the flow chamber and incubated for two hours. After the polymer self-assembled onto the negatively charged substrate, the unbound or loosely bound polymers were removed by withdrawing the solution out of the chamber. Then, a double-stranded DNA tether (dsDNA) modified at one end with DBCO and the other end with biotin was injected and coupled to the azide group on PLL-g-PEG at a final concentration of 0.5 nM in 500 mM NaCl in PBS (130 mM NaCl, 7 mM Na_2HPO_4, 3 mM NaH_2PO_4 at pH 7.4).[53] The dsDNA tether was incubated for approximately 15 hours at room temperature.

2.4.3 *Surface functionalization and dose-response experiments for ssDNA sandwich assay in PBS and filtered blood plasma*

The substrate-side binder is a partially double stranded DNA consisting of two complementary oligos, namely a 31nt oligo (3 ′ C ATT ATT ACA AGC TAA GCT CTT GCA CTG ACG 5 ′) and a DBCO functionalized oligo (5 ′ CGA TTC GAG AAC GTG ACT GCT TTT T 3 ′ DBCO). The 100 μM 31nt oligo was pre-hybridized with 100 μM DBCO functionalized oligo at a volume ratio of four to one, making the DBCO functionalized oligo the limiting reagent. After the glass substrate was modified with PLL-g-PEG and dsDNA tether, the partially double stranded DNA was diluted to 1 μM with 500 mM NaCl in PBS (130 mM NaCl, 7 mM Na_2HPO_4, 3 mM NaH_2PO_4 at pH 7.4) and injected into the flow cell, followed by 48 hours of incubation at room temperature. The coupling of the substrate-side binder to the PLL-g-PEG saturated most of the binding sites, preventing the exposure of azide groups, which reduces non-specific interactions. These modified substrates can be stored at room temperature in a humid chamber for months.

One microliter of streptavidin-coated magnetic particles (10 mg/mL, Dynabeads MyOne Streptavidin C1, 65001, Thermo Scientific) was incubated with 4 μL of 11nt biotinylated ssDNA (5 ′ TCACGGTACGA 3 ′ Biotin) at a final concentration of 2 μM in PBS buffer for 70 min on a rotating fin (VWR, The Netherlands). The particle mixture was washed with 0.05 vol.-% Tween-20 (Sigma-Aldrich) in PBS and reconstituted in 500 μL of 500 mM NaCl in PBS. Right before injecting particles into flow cells, the particle solution was sonicated with 10 pulses at 70% with 0.5 duty cycle (Hielscher, Ultrasound Technology). Particle solution was injected into the flow chamber with a flow rate of 40 μL/min and a volume of 400 μL in total. After the flowing procedure was completed, the reaction was continued for another 5 minutes, allowing capture of the particles by the biotin groups on dsDNA tethers. Then the flow cell was turned over to allow the unbound particles to sediment away from the functionalized surface. 200 μL of 100 μM mPEG-biotin (PG1-BN-1k Nanocs) in high salt buffer (500 mM NaCl in PBS) was added to the flow cell to avoid the formation of multiple-tethered particles. The high salt buffer

in the flow cell was replaced by PBS before adding the ssDNA analytes. For each target concentration, 200 μL of the ssDNA target (5 ′ TCG TAC CGT GTG TAA TAA TGC G 3 ′) in PBS was injected into the chamber with a flow rate of 40 μL per minute, after which the particle motion was recorded for 5 min in the absence of flow. For the DNA sandwich assay in filtered blood plasma, bovine plasma (P4639-10ML, Sigma Aldrich) was reconstituted in MilliQ and then filtered with 50-kDa molecular weight cut-off centrifugal filter (UFC905008, Millipore). The ssDNA target (5 ′ TCG TAC CGT GTG TAA TAA TGC G 3 ′) in plasma filtrate was injected into the flow cell with a flow rate of 40 μL per minute and a total volume of 200 μL.

2.4.4 *Surface functionalization and dose-response experiments for the ssDNA competition assay*

The surface was first functionalized with PLL-g-PEG/PLL-g-PEG-N_3, dsDNA tether and substrate-side binder (which in this case also functions as ssDNA analogue) via the same procedure as described in the ssDNA sandwich assay. The particles were coated with 20 nt biotinylated ssDNA (Biotin 3 ′ CAT CTG TAG GTT GGA CTG AT 5 ′) at a concentration of 2 μM in high salt buffer (500 mM NaCl in PBS). After the standard wash and sonication of the particles, the particles were added to the flow cell and captured by the biotin groups on dsDNA tethers. 200 μL of 100 μM mPEG-biotin (PG1-BN-1k, Nanocs) in high salt buffer (500 mM NaCl in PBS) was added to the flow cell to avoid the formation of multiple-tethered particles. The high salt buffer in the flow cell was replaced by PBS before adding the particle-side binder (5 ′ GTA GAC ATC CAA CCT GAC TA C GTG A GT AAT AAT G CG 3 ′). The particle-side binder has 20 bp complementarity to the 20 nt ssDNA on the particle and 9 bp complementarity to the substrate-side binder on the surface. When the switching activity of the BPM sensor reached the baseline signal, the unbound particle-side binder was removed and 300 μL of 11nt ssDNA (5′ TCA TTA TTA CGA AAA 3′) analyte in PBS was injected into the flow cell with a flow rate of 30 μL per minute via a fully automated flow and sampling

system (see below), after which the particle motion was recorded for 5 min in the absence of flow.

2.4.5 *Surface functionalization and dose-response experiments for the creatinine competition assay*

The DBCO modified ssDNA (5 ′ GTC TGT AGA CAG TTT CAT CGG TGA C 3 ′ -PEG4-DBCO) was prepared by labeling amine-modified oligo (5 ′ GTC TGT AGA CAG TTT CAT CGG TGA C -3 ′ amine) with Dibenzocyclooctyne-PEG4-N-hydroxysuccinimidyl ester (Sigma-Aldrich). The DBCO-PEG4-NHS Ester was dissolved in DMSO at a final concentration of 10 mM. Then, amine-modified oligo at a final concentration of 100 μM was added to the DBCO-PEG4-NHS Ester solution and incubated at room temperature for 2 hours. The oligonucleotides were purified via ethanol precipitation and stored in PBS. The glass substrate was first functionalized with PLL-g-PEG/PLL-g-PEG-N_3 and dsDNA tether via the same procedure as described in section 2.4.3. 1 μM of DBCO modified ssDNA was provided to the surface and incubated for 48 hours. These modified substrates can be stored at room temperature in a humid chamber for months.

Two microliters of streptavidin-coated magnetic particles (10 mg/mL, Dynabeads MyOne Streptavidin C1, 65001, Thermo Scientific) was incubated with 2 μL of biotinylated antibody against creatinine at a concentration of 400 nM in PBS buffer for 40 min on a rotating fin (VWR, The Netherlands). The biotinylation of the creatinine antibody was described in a previous paper.[35] An additional blocking process was done by incubating the particle solution with 5 μL of 2 μM PolyT (5 ′ Biotin - TTT TTT TTT TTT TTT T 3 ′) for 40 min on a rotating fin. The creatinine-antibody coated particles were tethered to the substrate and 200 μL of 100 μM mPEG-biotin (PG1-BN-1k, Nanocs) in high salt buffer (500 mM NaCl in PBS) was added to the flow cell to avoid the formation of multiple-tethered particles. The preparation of creatinine-DNA conjugates (5 ′ GTC ACC GAT GAA ACT GTC TAC AGA C-3 ′ creatinine) was discussed in the previous publication.[35] The high salt buffer in the flow cell was replaced by PBS before adding the creatinine-DNA conjugates (also referred to as creatinine analogues). When the switching activity of the

BPM sensor reached the baseline signal, the unbound creatinine analogues were removed and 200 μL of creatinine analyte in PBS was injected into the chamber with a flow rate of 40 μL per minute, after which the particle motion was recorded for 5 min in the absence of flow.

2.4.6 *Automated flow and sampling system*

The flow cell was connected to a 10 mL syringe (Norm Jet) at one side and to a microfluidic distribution valve device (MUX distributor, Elveflow) at the other side with flexible tubing (Freudenberg Medical). A control program written with Matlab provides a simple user interface to control the syringe pump (Standard Infuse/Withdraw 11 Elite, Harvard Apparatus), valve device, camera and particle localization software. The system allows sample taking from reservoirs with specific analyte concentrations, with control of flow rate, sample volume, and timing of the measurement. Once the valve tubing was primed with a specific analyte solution, 300 μL of sample was injected with a flow rate of 30 μL per minute, after which the particle motion was recorded for 5 min in the absence of flow.

2.4.7 *Particle tracking and event analysis*

The 5 min particle motion measurements in the absence of flow, were recorded on a Nikon Ti-E inverted microscope (Dark field microscopy, Nikon Instruments Europe BV, The Netherlands) and a Leica DMI5000M microscope (Dark field microscopy, Leica Microsystems GmbH, Germany). The position of the particles was recorded in a field of view of 883×552 μm^2 on Leica microscope or 405×405 μm^2 on Nikon microscope for 5 minutes at a frame rate of 30 Hz with an integration time of 5 ms. By applying a Gaussian fitting over the intensity of pixels around the particle, the center of every particle could be determined over each time frame. We also used another particle tracking method, based on a phasor based localization.[54] The tracking of particles is independent of microscope models and analysis algorithms. The details of the particle tracking and event detection were described in a previous publication.[33]

2.5 APPENDIX

2.5.1 *Negative control experiments for the click-based coupling approach*

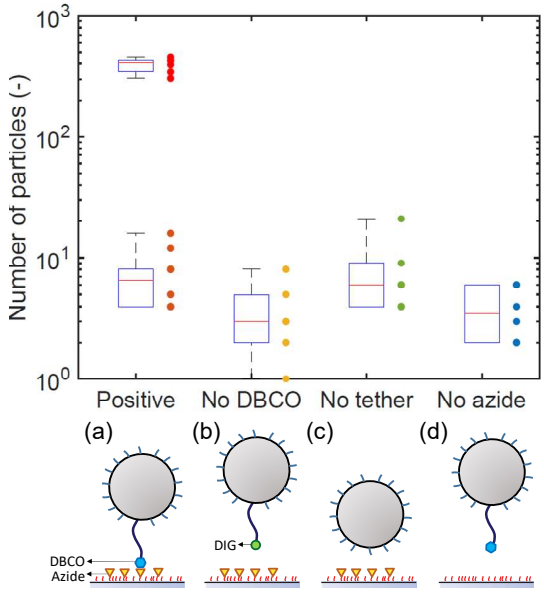

Figure 2.5: The negative control experiments showing the number of properly tethered particles anchored to the surface based on click coupling and the physisorption of PLL-g-PEG polymer. The circles represent the number of particles observed in four or five different field of views. (a) Positive control experiments, showing a high number of properly tethered particles (bright red circles) and a low number of non-specifically bound particles (dark red circles). The percentage of non-specifically bound particles is less than 10%; (b) Negative control experiment, where the DBCO group on the dsDNA tether was replaced by a non-relevant functional group, Digoxigenin (DIG); (c) Negative control experiment, with absence of dsDNA tether; (d) Negative control experiment, with absence of azide groups. A low number of bound particles were observed in experiments b, c, and d, in the absence of DBCO, tether, or azide.

The described click-based BPM sensor has PLL-g-PEG with azide groups on the surface and dsDNA tethers with a DBCO group, which connect the particles to the PLL-g-PEG coated surface. If the DBCO group on the dsDNA tether is replaced by a non-relevant functional group, such as a Digoxigenin, the chemistry should not work. Moreover, by removing the dsDNA anchor or the azide groups on the polymer, the system should show a rela-

tively low number of non-specific binding. To demonstrate the specificity of the click-based coupling approach, negative control experiments were performed with the absence of either the DBCO group, dsDNA tether, or azide group. After standard cleaning steps, the substrates were treated with 1 minute of oxygen plasma and a pure PLL-g-PEG or PLL-g-PEG/PLL-g-PEG-N_3 mixture was applied to the surface, followed by 2 hours of incubation. The substrates then were either provided with DBCO modified tether, Digoxigenin modified tether, or without tether. In both the positive control and negative control experiments, particles were partially blocked by mPEG-biotin (PG1-BN-1k, Nanocs) and washed with standard procedure described in Appendix 2.4.2 before injecting to the modified substrate. After 10 minutes of incubation, all samples were turned over and unbound particles gradually sedimented to the bottom of the chamber. The focal plane was fixed at the top of the chamber and the motion patterns of particles tethered to the upper surface were recorded. Particles are designated as singly tethered, based on the shape, radius, and symmetry of their motion patterns. Based on the contour length of the 221 base pairs dsDNA tether used in our system, properly tethered particles show a circular motion pattern with a radius of 150 nm. In contrast, the non-specifically bound particles show a much more confined motion.[33] The number of properly tethered particles (bright red) and non-specifically bound particles (dark red, yellow, green and blue) are shown in Figure 2.5. Colored circles represent independent measurements from different field of views. The percentage of non-specifically bound particles was less than 10%. Further tests for characterizing the anti-fouling properties of polymer coated surfaces are demonstrated in Appendix 2.5.10.

2.5.2 *Shelf-life of the biofunctionalized surface*

The stability of biomolecules and the coupling approaches influence the shelf-life of a biosensor, which is an important feature for further development of sensors. Thus, we tested the shelf-life of the PLL-g-PEG surface functionalized with substrate binders and dsDNA tether. After the glass substrate was modified with PLL(20)-g[3.5]-PEG(2) and PLL(15)-g[3.5]-PEG(2)-N_3 mixture, ds-

DNA tether solution and substrate binder solution were added to the sensor chamber sequentially. Then the sensor was sealed and stored in a humid chamber at room temperature for approximately three months (82 days). Particles were freshly prepared and the covalent-based BPM biosensor was produced with the experimental procedures described in Section 2.4.3. The time dependent measurements and the dose response curve were recorded as shown in Figure 2.6. The good performance of the sensor demonstrates the high stability of the covalent bonds and the components such as PLL-g-PEG, dsDNA and ssDNA.

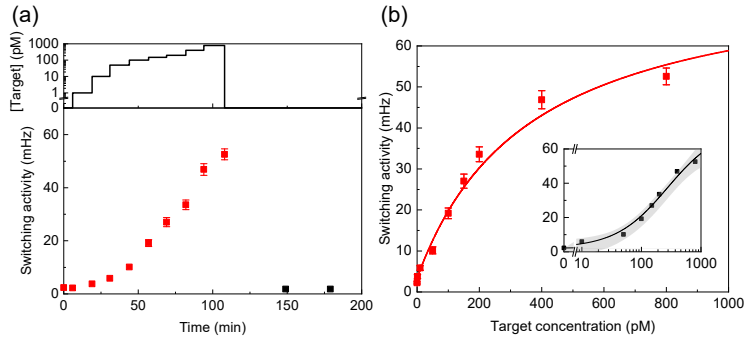

Figure 2.6: The ssDNA sandwich assay measured with the sample that was stored for 82 days. (a) The switching activity of the BPM sensor as a function of time recorded under a step-wise increased concentration of ssDNA analyte (red solid squares) followed by a complete removal of analyte (black solid squares). The concentration profile is shown in the top panel. (b) The dose response curve plotted with linear scales. The curve was fitted with a Hill equation, revealing $EC50 = 362 \pm 121$ pM. The inset shows the data with a logarithmic concentration scale. The measurement errors are calculated by the standard deviation of switching activity divided by the square root of the sample size.

2.5.3 *DNA competition assay in 10% blood plasma over 9 hours*

The sensing principle for a competition assay is the competition for binding between analogues and analytes. The particle binder (5 ′ GTA GAC ATC CAA CCT GAC TAC GTG AGT AAT AAT GCG 3 ′) for the ssDNA competition assay has 20 bp complementarity to the initial biotinylated oligo (Biotin 3 ′ CAT CTG TAG GTT GGA CTG AT 5 ′) coupled on particles, and 9 bp complementarity to the ssDNA analogue on the substrate (substrate binder). The particle binder hybridizes and de-hybridizes to the substrate binder on a relatively fast time scale of around

20 seconds and causes the particle to switch between bound state and unbound state. When the 11 nt ssDNA analyte is added, it competes with the substrate binder (ssDNA analogue) by partly hybridizing to the particle binder. The hybridization of 11 nt ssDNA analyte to the 9 bp binding region on particle binders hinders the particle to switch from unbound state to bound state. The particle binder cannot bind to the substrate binder (ssDNA analogue) again, until the analyte molecule dissociates. Therefore, the BPM biosensor shows high switching activity at low analyte concentration and shows low switching activity at high analyte concentration.

To investigate the capabilities for measuring ssDNA analytes in complex matrices over long durations, we performed the DNA competition assay in 10% bovine blood plasma over many hours. Without filtration, the resuspended lyophilized blood plasma contained aggregated materials that perturb the optical tracking and the motion of the particles. Filtration of the plasma resulted in reproducible biosensing data. Bovine blood plasma (P4639-10ML, Sigma Aldrich) reconstituted in MilliQ was first diluted to 10% and then filtered through a 0.22 μm filter. The protein composition of the diluted bovine blood plasma (1% and 2.5%) was determined with SDS-PAGE, see Appendix 2.5.5. In Figure 2.7, the switching activity rises (green square) after adding 250 pM of particle binder (5 ′ GTA GAC ATC CAA CCT GAC TAC GTG AGT AAT AAT GCG 3 ′). When enough switching events were observed, the particle binders in bulk solution were removed and the measurement chamber was washed with 10% bovine blood plasma. The 10% bovine blood plasma was then spiked with the 11nt ssDNA (5 ′ TCA TTA TTA CGA AAA 3 ′) analyte at the concentration indicated in the top panel of Figure 2.7. The switching activity shown in the bottom panel of Figure 2.7 inversely responds to different concentrations of the 11nt ssDNA analyte, demonstrating the reversibility of the DNA competitive assay over 9 hours in the complex matrix. Compared to assays in pure buffer, the 10% bovine blood plasma solution gave more non-specifically bound particles over time. The inactive and non-specifically bound particles were excluded via data processing. The signal at zero analyte concentration, measured right after the supply of analyte with higher concentrations (500 nM and 1 μM),

was generally much lower than the initial baseline signal. This reduction of switching activity is attributed to remaining analyte in the system because of incomplete fluid exchange. To calculate the signal decay rate, measurements at zero analyte concentration were analyzed (excluding measurements after high analyte concentration); the corresponding data points are indicated as red squares. A fit with single-exponential decay gives a decay rate of $(5.3 \pm 2.0) \times 10^{-6} s^{-1}$.

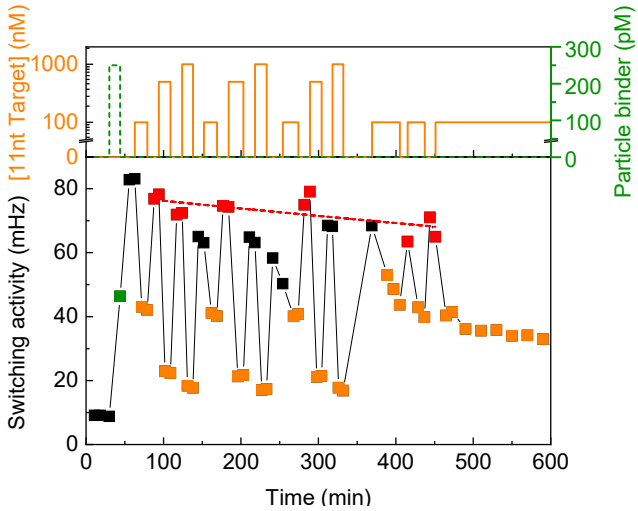

Figure 2.7: DNA competition assay performed in 10% bovine blood plasma over 9 hours. The top panel shows the concentration profile of the particle binder (green) and the 11nt ssDNA analyte (orange). The bottom panel shows the switching activity measured for ssDNA target in 10% bovine blood plasma. The switching activity rises with the addition of particle binder (green square) and responds inversely to different concentrations of the 11nt ssDNA analyte. The signals measured in the presence of analyte are represented by orange squares. The signal at zero concentration measured right after 100 nM analyte concentration, is indicated by red squares; the fitted curve gives a decay rate of $(5.3 \pm 2.0) \times 10^{-6} s^{-1}$.

2.5.4 *Signal decay rate of the click-based and antibody anchoring-based BPM sensor*

The stability of the BPM sensor was characterized by measuring the number of tethered particles over time (see Figure 2.2) and the signal decay rate. The time dependent measurements in undiluted bovine blood plasma filtered with 50 kDa molecular weight cut-off membranes, were recorded with the antibody-anchored

sensor and the click-based sensor, as shown in Figure 2.8. Under similar conditions, the antibody anchoring-based sensor exhibits a signal decay rate of $(4.5 \pm 0.3) \times 10^{-5} s^{-1}$ and the click-based sensor shows a decay rate of $(8.3 \pm 1.1) \times 10^{-6} s^{-1}$. Figure 2.8 indicates that less than 10% signal loss was observed in the click-based sensor over five hours, while the antibody anchoring-based sensor exhibits approximately 50% signal loss. Potential causes of the larger signal loss observed in the antibody anchoring-based sensor are larger non-specific interactions of particles and a loss of substrate-side binders over time due to non-covalent coupling methods.

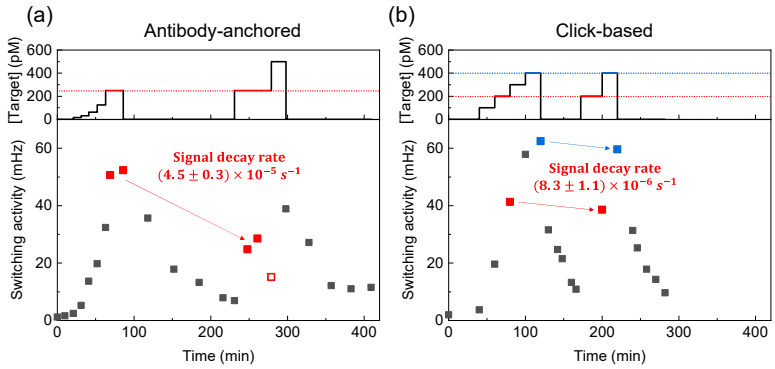

Figure 2.8: DNA sandwich assay measured with antibody-anchored BPM sensor in 50 kDa spin-filtered undiluted bovine blood plasma (see Figure 4c in our earlier work[33]). The top panel shows the concentration-time profile applied to the flow cell. The bottom panel shows the corresponding switching activity of the BPM sensor, defined as the average frequency of binding and unbinding events per particle. The signal measured at the same concentration but at different time points are highlighted in red (250 pM). The data point with open square is considered to be an outlier, as it deviates from measurements before and after. The signal decay rate of the antibody-anchored BPM sensor is $(4.5 \pm 0.3) \times 10^{-5} s^{-1}$. (b) The DNA sandwich assay measured with the click-based BPM sensor under similar conditions in 50 kDa spin-filtered undiluted bovine blood plasma. The top panel and the bottom panel show the concentration profile and the signal response respectively. The signal measured with the same concentration but at different time points are highlighted with red (200 pM) and blue (400 pM). The click-based BPM sensor exhibits less than 10% signal loss over five hours with a signal decay rate of $(8.3 \pm 1.1) \times 10^{-6} s^{-1}$.

2.5.5 *SDS-PAGE characterization of filtered blood plasma and diluted blood plasma*

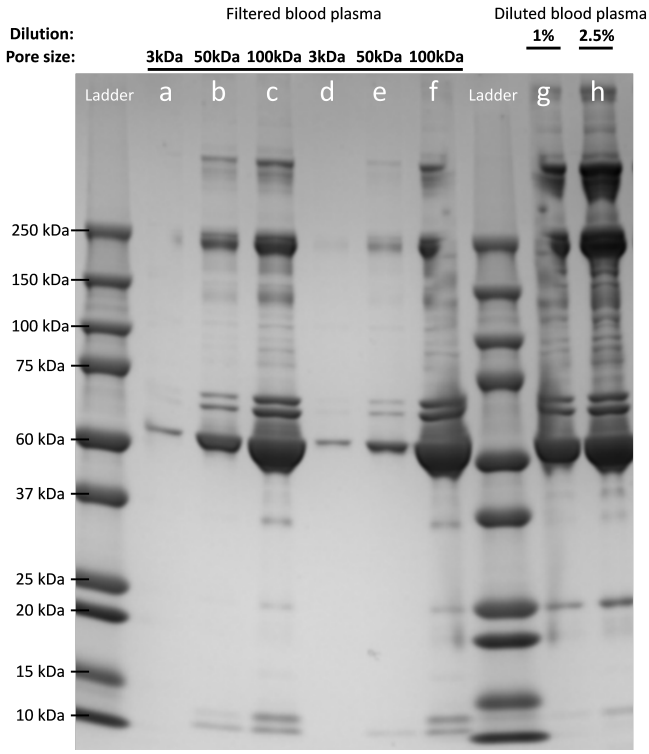

Figure 2.9: (lane a-f) The undiluted bovine blood plasma filtered with 3 kDa, 50 kDa, or 100 kDa molecular weight cut-off membranes. Lane a-c and lane d-f originate from two different batches of bovine blood plasma. (lane g, h) The bovine blood plasma was first diluted to 1% and 2.5%, then filtered through a 0.22 μm filter.

The protein composition of undiluted bovine blood plasma spin-filtered with different membrane pore sizes, and of diluted bovine blood plasma, was determined with SDS-PAGE, see Figure 2.9. The gel was stained with Coomassie blue for 10 min after electrophoresis was performed for 2 hours with 120 V at room temperature. The 50 kDa filtered undiluted blood plasma was used as complex medium in Figure 2.3c and Figure 2.3d, while 10% diluted blood plasma was used in Figure 2.7.

The clear band detected in all sample lanes at around 67 kDa is assigned to bovine serum albumin. In lanes b and e (50 kDa

filtered) we observe two bands at around 10 kDa, three major bands at 60-70 kDa and another clear band at 250 kDa. Bands in the range 50-250 kDa and above, indicate that possibily large stretched proteins passed through the membrane or that smaller proteins aggregated after the filtration.

The protein concentration in 1% blood plasma is too high for SDS-PAGE experiments, thus we measured 1% and 2.5% plasma. As expected, the diluted plasma (lanes g-h) contains larger proteins compared to the spin-filtered blood plasma (lanes a-f).

2.5.6 *Correction of signal decay for ssDNA competition assay*

The molecular design and sensing principle of the DNA competition assay are described in Appendix 2.5.3. To summarize, the sensing principle for a competition assay is the competition for binding between analogues and analytes. When the 11 nt ssDNA analyte is added, it competes with the substrate binder (ssDNA analogue) by partly hybridizing to the particle binder and therefore hinders the particle to switch from unbound state to bound state. In a competition assay, the BPM biosensor shows high switching activity at low analyte concentration and shows low switching activity at high analyte concentration.

The first and second dose-response curves in Figure 2.13 were measured with equal decreasing concentration series, while the third and forth curves were measured with randomly alternating concentration series. The alternating concentration variations result in stronger dispersion and flow effects. Hence, the effective concentrations are between the consecutive feed concentrations, resulting in a signal response that is effectively more averaged.

alternating concentration variations result in stronger dispersion and flow effects, resulting in concentrations that are between the consecutive feed concentrations. This leads to a signal response that is effectively more averaged.

We observed a decay of baseline signal (red open squares) during a period of 10 hours. The red open squares can be fitted with a decay rate k of $(6.3 \pm 1.8) \times 10^{-6} s^{-1}$. This can be used to correct the measured signals (light-grey open squares). The corrected switching activity signal $A_{corrected}$ is shown as solid squares in

Figure 2.13, calculated by implementing a correction factor e^{kt} as given in the following equation: $A_{corrected}(t) = A(t) \times (e^{kt})$

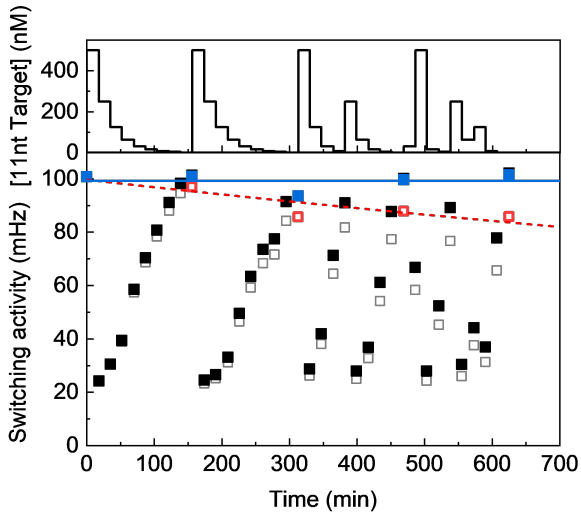

Figure 2.10: The signal loss correction for the ssDNA competition assay. The corrected (solid squares) and non-corrected (open squares) switching activity of the BPM biosensor as a function of time, for monitoring different concentrations of 11nt ssDNA analyte. The signal measured over time at zero analyte concentration (red open square) was fitted with an exponential function, showing a decay rate of $(6.3 \pm 1.8) \times 10^{-6} s^{-1}$. Due to the predictable and steady loss rate, the signal loss correction can be applied to all data points, giving a flat baseline (blue solid squares).

2.5.7 *Correction of signal decay for creatinine competition assay*

The sensing principle for the creatinine competition assay is shown in Figure 2.4d. The analogue, in this case an ssDNA-creatinine conjugate, induces switching of particles while the analyte competes with the analogue and therefore reduces the switching frequency. The concentration profile of the creatinine analogues is shown with green dashed lines in the top panel of Figure 2.11. The switching activity rises (green open squares) with the gradual increase of analogue concentration. When enough switching events were observed, the analogues in bulk solution were removed and the measurement chamber was washed with PBS buffer. Free analogues bound to the antibodies on particles dissociate during the washing steps due to the weak affinity, while the analogues bound to the surface by the 20 base

pair hybridization remain after each activation process (green open squares).

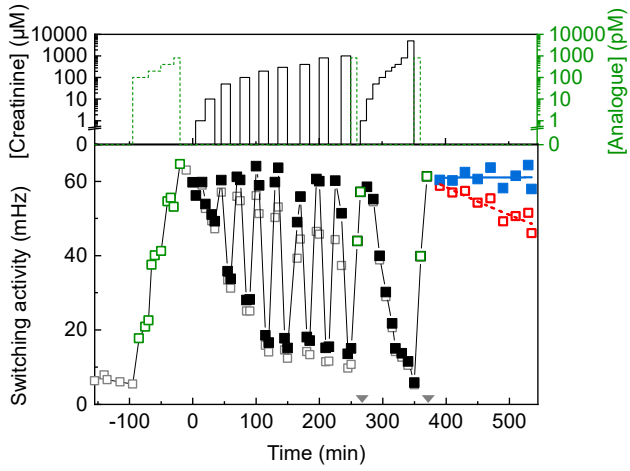

Figure 2.11: Top panel: The concentration-time profile of creatinine analogues (green) and creatinine (black). Bottom panel: Measured switching activity as a function of time. Grey open squares: non-corrected data. Green open squares: non-corrected data in the presence of creatinine analogue, indicating the activation processes. Black solid squares: corrected signals based on a decay rate of $(2.2 \pm 0.5) \times 10^{-5} s^{-1}$. Red open squares: non-corrected signals measured at zero creatinine concentration, giving an estimated decay rate of $(2.2 \pm 0.5) \times 10^{-5} s^{-1}$. Blue solid squares: corrected signals measured at zero creatinine concentration, using a decay rate of $(2.2 \pm 0.5) \times 10^{-5} s^{-1}$.

It is expected that the analogues on the surface should not dissociate over time, causing the system to show a stable baseline activity at zero analyte concentration. However, variations in flow conditions within experiments and incomplete exchange of fluid can lead to residual amounts of analytes in the chamber, causing an underestimated baseline signal, as shown in the first section (up to 250 min). Moreover, the analogues can still slowly detach from the surface due to dissociation of 20 base pair ds-DNA and the total number of active antibodies on particles can also decrease because of the dissociation of biotin-streptavidin complexes or a gradual loss of activity of the antibodies, resulting in a signal decay (red open squares) as shown in Figure 2.11. The decay rate of the baseline signal, $(2.2 \pm 0.5) \times 10^{-5} s^{-1}$, was calculated by fitting the recorded signal at zero creatinine

concentration (red open squares) with a single-exponential decay curve. Due to the predictable and steady loss rate, the signal loss correction described in Appendix 2.5.6 can be applied to all data points, giving a flat baseline (blue solid squares). The corrected (solid squares) and non-corrected (open squares) switching activity of the BPM biosensor are shown in the bottom panel of Figure 2.4 as a function of time.

Reactivation (grey triangles) was performed by providing the system with the same concentration of creatinine analogues as in the first activation process. The switching activity goes back to the baseline level, compensating for the loss of active antibodies or binders with the addition of creatinine analogues.

2.5.8 *Biofunctionalization of plastic substrates*

A balance between production cost and biosensor performance is of major importance for industrial applications. The proposed biofunctionalization approach can be easily adapted to different substrates such as plastic slides, as long as the substrate can be modified to carry a net negative surface charge. Plastic slides (e.g., polycarbonate, cyclic olefin copolymer) are all optically transparent and potentially suitable for particle-based biosensing. In addition, one of the advantages of using plastic materials is that the flexibility allowed by the plastic molding process meets the requirement for industrial applications. We successfully functionalized polycarbonate (PC) slides with PLL-g-PEG polymer and subsequently attached oligonucleotides on the surface. The molecular design and sensing principle of the DNA sandwich assay are described in Section 2.2.2.

The results showed that particles can be properly tethered onto PLL-g-PEG-N_3 functionalized plastic slides. Figure 2.12a indicates that the activity signal responds to both increase and decrease of target concentrations. As shown in Figure 2.12b, the data of the first dose-response curve measured with the PC slide was fitted with a Hill equation $A([T]) = A_{bg} + A_a \times \frac{[T]}{EC50+[T]}$ (red line), revealing $EC50$ = 590 $\pm$ 164 pM. Since the plateau value of the second dose-response curve was not measured, a plateau of approximately 85 mHz was set manually and the estimated $EC50$ is 1728 $\pm$ 490 pM. Moreover, the time dependent data

in Figure 2.12a shows that the relaxation process after the first dose-response is slower than the second one. The possible cause is due to incomplete exchange of fluids, since the last applied concentration in the first dose-response curve is relatively high compared to the second curve.

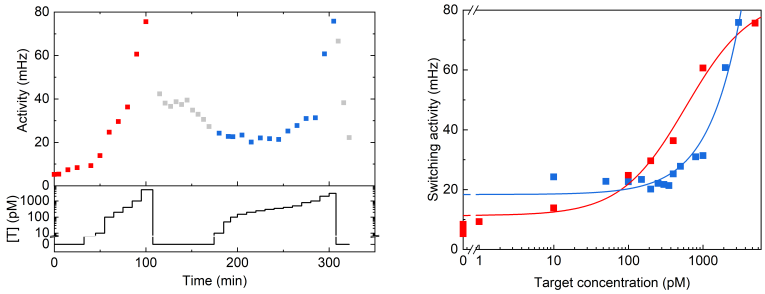

(a) (b)

Figure 2.12: (a) DNA sandwich assay performed on the PC slide. The switching activity of the BPM sensor as a function of time recorded under two series of stepwise increased concentration of ssDNA analyte (red and blue solid squares). In between the two concentration series, a complete removal of analyte (grey solid squares) was applied. The top panel shows the measured switching activity, while the bottom panel shows the concentration-time profile. (b) Dose-response graph containing all data points of panel a. The data were fitted with the Hill equation. The fitted EC50 values are 590 ± 164 pM (red) and 1728 ± 490 pM (blue).

Compared to the DNA sandwich assay performed on glass slides, as shown in Section 2.2.2, two major differences are observed for the DNA sandwich assay performed with PC slides. Firstly, the EC50 values extracted from the two dose-response curves in Figure 2.12b are less consistent. Secondly, the sensor is sensitive in the range of 10-5000 pM, while the activity signal is generally saturated at 500 pM for the system using glass slides. The hypothesis is that the coupling conditions are different for plastic materials like PC and therefore lead to a different density of immobilized molecules on the surface. Further investigations on tuning the binder densities and surface modification conditions are needed to optimize the sensitivity, operational range and stability.

2.5.9 *DNA sandwich assay performed in high salt buffer*

Schlapak et al. proved that an increased salt concentration within the PEG layer would lead to a screening of positive charges in the PLL layer. In the absence of salt, stronger electrostatic interactions between DNAs and PLL-g-PEG polymer layers were observed. These attractive interactions between the negatively charged DNA tethers and positively charged PLL backbone are non-specific. In the presence of salt, the interactions can be shielded by the addition of salt. That is, weak interactions at high ionic strengths and strong interactions at low ionic strengths.[53] To avoid the non-specific interactions, 500mM of NaCl was used for tethering particles and attaching DNA molecules onto the surface.

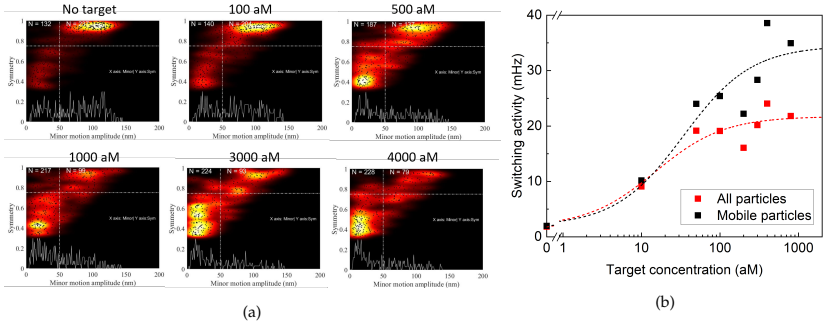

Figure 2.13: Dynamic response of the DNA sandwich assay performed in high salt buffer. (a) Motion distribution plot of 1 μm particles tethered with dsDNA. Each black dot corresponds to the symmetry and minor motion amplitude of a single particle motion pattern. The color-map indicates the local density of the black dots. The dashed line corresponds to the thresholds for identifying particles with or without switching behaviors. Particles that have a symmetry larger than 0.75 and a minor motion amplitude higher than 50 nm are single-tethered particles at their unbound states. After applying 4 fM of target, the particle population shifts to the bound state region, indicating more binding events occurring. (b) The corresponding switching activity measured at different target concentrations. The black data points represent the average switching activity of the particles that have a symmetry larger than 0.75 and a minor motion amplitude higher than 50 nm. The red data points represent the average switching activity of all the particles.

The interactions between PLL-g-PEG and DNA have been investigated by varying salt concentration. Under high salt condition, a shift of the dose-response curve to lower concentrations is observed. But when the target solution is mixed with high concentration of mismatch ssDNA, the dose-response curve shifts back

to the original level. The hypothesis is that the structure of the PEG side chains changes while the ionic strength becomes larger. It is hypothesized that the negatively charged DNA accumulates in the PLL-g-PEG layer. The resulting high local concentration of target thus enhances the sensitivity of the BPM system and shifts the limit of detection to the femtomolar range. However, further investigations on the reversibility and the relaxation of the system is needed to achieve continuous monitoring of targets.

2.5.10 *Characterization of bottle-brush polyelectrolytes via particle mobility analysis, zeta potential and supernatant assay*

The anti-fouling properties of bottlebrush polymers or polypeptide brushes (see Appendix 2.5.11) play an important role in biosensing systems and immunoassays, since the hydrophilic character and high grafting density of the side chains of the bottlebrush polymer can significantly reduce the background signal by avoiding non-specific binding of proteins to the surface. Since the fabrication strategies and the composition of polymer solution lead to different structures and molecular ordering of the polymer adlayer, which significantly influence the performance of the anti-fouling surfaces, the characterization of the particles and surfaces is essential.

In Appendix 2.5.1, we tested the anti-fouling properties of the PLL-g-PEG polymer by evaluating the the percentage of non-specifically bound particles after the tethering process, which is less than 10%. Another simpler way to study the anti-fouling properties of the surface is to estimate the fraction of nonspecifically bound particles before the tethering process, that is based on freely-moving particles. We apply video microscopy to study particle-surface interactions with mean squared displacement analysis to extract the diffusion coefficient of freely moving particles. Furthermore, the excursion of immobilized particles provides information about the interactions between particles and surfaces with different coatings. In order to optimize parameters of the coating procedure and lower the non-specific interactions, we estimated the degree of polymer coverage on particles by calculating the fraction of stuck particles. Zeta potential measurements were used to measure the effective total surface charge

of particles, which is related to the amount of electrostatically adsorbed polymers.

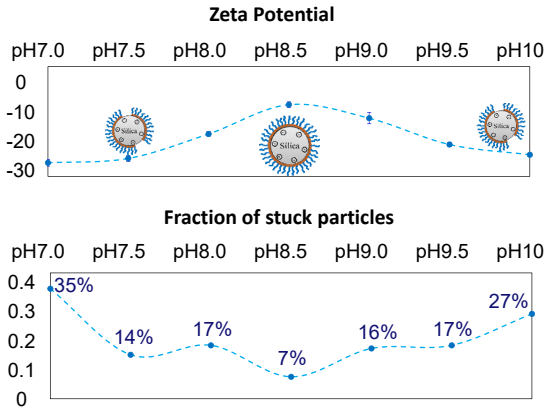

Figure 2.14: The top panel shows the measured zeta potential of the PLL-g-PEG coated silica particles prepared at different pH. The magnitude of the zeta potential serves as an indirect measure of the grafting density and is measured for different pH values. The bottom panel shows the corresponding fraction of stuck particles. The PLL-g-PEG coated silica particles prepared at different pH were added onto PLL-g-PEG coated glass substrates respectively and the mobility of particles were measured after 30 minutes of incubation. The degree of polymer coverage reached a maximum value at pH 8.5.

Based on the zeta potential measurements and particle mobility analysis shown in Figure 2.14, we conclude that pH 8.5 is the appropriate conditions for achieving the highest loading of PLL-g-PEG polymers on particles, resulting in the lowest degree of non-specific binding. We also study the influence of pH values on the particle size and the zeta potential for both bare carboxyl functionalized silica particles and PLL-g-PEG coated silica particles. By lowering the pH, carboxylate moieties at the particle surface gradually become more protonated, thus becoming neutralized. As for the PLL-g-PEG coated particles, the absolute value of zeta potential also decreases. The DLS measurements indicate a higher degree of cluster formation in buffers with lower pH values.[55] Furthermore, as shown in Table 2.1, the anti-fouling behaviour and the stability of PLL-g-PEG layer was compared with that of traditionally used blocking agents such as bovine serum albumin (BSA). The result shows that PLL-g-PEG is a relatively stable coating material and its anti-fouling property can be maintained over one day.

Table 2.1: Particles and surfaces blocked with PLL-g-PEG and BSA were tested separately considering the degree of non-specific interactions. The stability of the two aforementioned blocking materials were characterized by measuring the fraction of stuck particles after two hours and one day of incubation. The fraction of stuck particles for the PLL-g-PEG blocked system are approximately 17% (2 hours) and 13% (1 day). The fraction of stuck particles for the BSA blocked system are approximately 37% (2 hours) and 86% (1 day).

Surface blocking	**Particle coating**	**Incubation time**	**Stuck particles**
PLL-g-PEG	PLL-g-PEG	2 hours	17 %
PLL-g-PEG	PLL-g-PEG	1 day	13 %
BSA	BSA	2 hours	37 %
BSA	BSA	1 day	86 %

2.5.11 *Characterization of the anti-fouling properties of the brush-forming polypeptides*

Direct covalent immobilization or physissorption of antibodies on surfaces may lead to significant loss of antibody activity. To avoid misorientation or denaturation, one of the solutions is to indirectly attach biomolecules to the surface via anti-fouling polymer brushes. Besides the commercially available PLL-g-PEG polymers, recombinant or synthetic polypeptides are another options. Polypeptides offer the advantage of precise control of polymer chemistry including the conjugation of biomolecules such as antibodies, and the possibility to directly include other functional peptide or protein blocks in the design. The polypeptide shown in Figure 2.15 was made by Alvisi et al. and was designed for immobilizing biomolecules on the substrate-side in the BPM system introduced in Section 2.1.1.

In a particle-based biosensor system, it is essential to avoid the non-specific interactions between the particles and the surface. As a first demonstration of the functionality of the self-assembled brushes in a biosensing application, we demonstrate the effectiveness of the BRT-ES40 diblocks in blocking non-specific particle-surface interactions in Figure 2.16.

Blocking of non-specific interactions by polypeptide brushes formed by BRT-ES40 diblocks on silica nanoparticles and glass slides was tested using a particle mobility assay, illustrated in

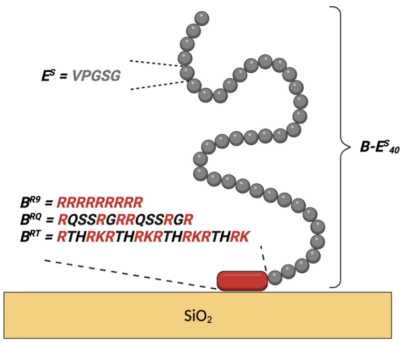

Figure 2.15: Schematic structure of BRT-ES40 diblocks for forming hydrophilic polypeptide brushes on silica surfaces.

Figure 2.16. The interactions between particles and surface are directly reflected by the mobility. To record the mobility of micron-sized particles over time, we used dark field microscopy. The position of every particle at each frame is localized with an accuracy of about 20 nm and then reconstructed into a trajectory over time. Silica particles and polystyrene particles with specific modifications are sedimented onto the surface of coated glass slides and their trajectories are reconstructed. For each particle, the diffusion coefficient D is determined from the mean squared displacement.

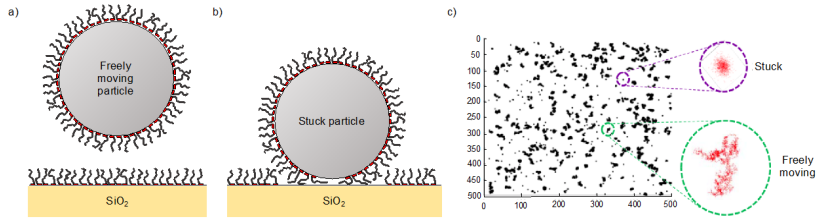

Figure 2.16: Schematic representation of the particle mobility assay. Particles coated with biomolecules such as ssDNA, streptavidin, and BRT-ES40 sediment to the surface of the substrate and show Brownian motion. The mobility and fraction of stuck particles is influenced by the interactions between particles and surfaces. (a,b) Schematic of a particle not interacting with the surface and a particle strongly interacting. (c) Example of particle position trajectories recorded over time for multiple particles. The insets show typical observed trajectories for a stuck and freely moving particle.

By analyzing the particle trajectories and setting a threshold for the diffusion coefficient, freely moving particles and stuck particles are distinguished and percentages are obtained for particles that ultimately become stuck. Results are given in Table 2.2, for various types of particles, and for particle and surface

coatings with BRT-ES40 diblock polypeptides and PLL-g-PEG copolymers, the current standard for self-assembled anti-fouling brushes. While both BRT-ES40 and PLL-g-PEG coatings are effective in preventing non-specific interactions if both the particle and the surface are non-functionalized, various functionalized particles with biosensing applications such as ssDNA-, biotin-PEG- and streptavidin-coated particles stick stronger to PLL-g-PEG coated glass slides. In contrast, minimal non-specific interactions are found between these functionalized particles and glass slides coated with BRT-ES40, demonstrating the usefulness of BRT-ES40 as a blocker of non-specific particle-surface interactions.

Table 2.2: Fraction of differently modified particles stuck to differently modified silica surfaces (%), as obtained from a particle mobility assay.

	glass modification	
particle type, modification	polypeptide	PLL-g-PEG
silica, polypeptide	1.3 ± 0.6	3.8 ± 0.9
silica, PLl-g-PEG	1.9 ± 0.6	2.5 ± 0.2
polystyrene, ssDNA	1.0 ± 0.7	25.0 ± 14.6
polystyrene, biotin-PEG	1.7 ± 0.8	12.6 ± 6.0
polystyrene, streptavidin	3.2 ± 1.0	80.1 ± 13.0

We have found that at least for some cases, such as in blocking non-specific interactions of functionalized particles with glass surfaces, BRT-ES40 performs very well. Nonetheless, further testing is necessary to evaluate the anti-fouling properties of this polymer brush compared to PLL-g-PEG. Since binding peptides have been investigated for many types of surfaces, such as plastics, metals and other oxides, the polypeptide approach also appears to be easier to generalize than the synthetic adsorbing bottle-brush systems.

3

FREE PARTICLE MOTION SENSING FOR CONTINUOUS BIOMARKER MONITORING

3.1 INTRODUCTION

Technologies that enable continuous monitoring of biomolecular concentrations in dynamic biological systems offer exciting opportunities, for applications in fundamental research, studies on organs-on-a-chip, monitoring of patients in critical care, and monitoring of industrial processes and bioreactors as well as ecological systems.[20,56,57] However, it is fundamentally difficult to develop measurement technologies that are not only sensitive and specific, but also allow monitoring over long time spans. Technologies such as ELISA and flow cytometry are sensitive, but also consume reagents such as antibodies, fluorophores and enzymes in every assay. The repeated use of reagents complicates monitoring applications over long periods. On the other hand, sensing technologies like surface plasmon resonance[58], redox cycling[12,59] and quartz crystal microbalance can operate without consuming reagents, but have not been designed for monitoring biomolecules at very low concentrations.

A sensing technology that combines high sensitivity with continuous measurements is biomarker monitoring using particles coupled to a surface via a flexible DNA-based tether. Target molecules facilitate the formation of reversible single-molecular bonds between the particle and the substrate, leading to changes in the Brownian motion of the tethered particle. By recording binding and unbinding events, DNA and protein biomarkers can be monitored with pico- to nanomolar sensitivity.[33,35] However, the tether is an essential element in the assay configuration, so

Parts of this Chapter are included in manuscript: Buskermolen, A., Lin, Y., van Smeden, L., et al; to be submitted. (A.B., Y.L. and L.S. are equally contributing first authors.)

tether breakage or detachment leads to a loss of sensor functionality. Furthermore, the presence of a tether restricts the rotation of the particle and the range of angles that the particle can assume. This implies that only a small fraction of the particle surface interacts with the substrate, which can limit the achievable sensitivity and precision.[60]

Here, we demonstrate a biomarker monitoring methodology that is based on free diffusion of particles near a surface, which we refer to as free-diffusion-based biosensing by particle mobility (f-BPM). The proximity of particles to the surface is not imposed by a molecular tether but by gravitational force, which facilitates free translational and rotational motion of the particles. The particles are tracked over long periods of time, reversible single-molecular interactions are probed with high motion contrast, and the total surfaces of particles and sensing substrate are used.

In this chapter, we describe the basic concepts of the f-BPM sensing methodology and demonstrate it for the continuous monitoring of oligonucleotides in a competition assay format, with biomarker concentrations across the nanomolar and micromolar range. We demonstrate the versatility of the technology by comparing different sample matrices, and data analysis methods. In the next chapter, we present a cartridge preparation method for long-term storage and immediate use of the f-BPM sensors.

3.2 BASIC CONCEPT

3.2.1 *Continuous biomarker monitoring based on measuring free diffusional motion of particles*

The molecular monitoring concept proposed in this chapter is based on the continuous tracking of the free Brownian motion of biofunctionalized particles near a sensor surface, in order to monitor time-dependent fluctuations of analyte concentrations in solution. We refer to the methodology as free-diffusion-based biosensing by particle mobility (f-BPM). To perform a sandwich assay, the particles and the sensor surface are functionalized with affinity binders specific to the target molecule, and particles are tracked over time using video microscopy. When target molecules are absent, the particles exhibit free Brownian motion. At higher target concentrations, target-induced sandwich complexes are reversibly formed between the particle and the sensor surface, restricting the particle motion intermittently to a confined area. All affinity-based interactions are designed to be reversible, so that over time target molecules bind and unbind, and sandwich complexes associate and dissociate. In the case of a sandwich assay, the activity is low for low target concentration and increases with higher target concentrations.

Sandwich assays are suitable for measuring analytes that have two spatially separate binding sites. In this Chapter, our focus is on measuring molecules with only one binding site, by implementing a competition assay format. Figure 3.1a describes the measurement concept for a competition assay configuration. Here, the particles functionalized with initial biotinylated oligos (grey) diffuse in the vicinity of a substrate functionalized with substrate-side binders (green). During the activation process, particle-side binders (orange) were captured by the initial biotinylated oligos. The particle binder has 20 bp complementarity to the initial biotinylated oligo and 9 bp complementarity to the ssDNA analogue on the substrate (substrate binder). The particle binder hybridizes and de-hybridizes to the substrate binder with a bound state lifetime of around 5 seconds due to 9bp DNA hybridization and causes transient binding of the particles. When the 11 nt ssDNA analyte (blue) is present, it competes

with the substrate binder (ssDNA analogue) by hybridizing to the 9 bp binding region on particle binders. Therefore, it hinders the particle to switch from unbound states to bound states. At a higher concentration of 11 nt ssDNA analyte, the binding sites on all particle binders are blocked and cannot bind to the ssDNA analogue again, until the analyte molecule dissociates. Therefore, the competition assay format of the f-BPM biosensor shows high switching activity and high bound fraction at low analyte concentration.

To distinguish the two characteristic motion types, that is free Brownian motion and confined Brownian motion, and extract the bound fraction and switching activity, the movement of particles was tracked over time using video microscopy. Particle trajectories are reconstructed by determining the particle center positions in every recorded video frame. The effective diffusion coefficient of each particle is determined as a function of time via the mean squared displacement (MSD). Significant changes in the diffusion coefficient (D) of the particle are assigned as binding or unbinding events. Timespans with high D (0.15 $\mu m^2/s$) relate to free Brownian motion (unbound state) and periods with low D (0.03 $\mu m^2/s$) to confined Brownian motion (bound state). Subsequent state attributions define single-molecule binding and unbinding events at transitions between high and low D of particles (Figure 3.1b). In a DNA competition assay, sandwich complexes are reversibly formed between the particle and the sensor surface after adding the particle binders (activators), restricting intermittently the particle motion to a confined area with a significant decrease in the diffusion coefficient of particles. In the presence of target, the target binds to the particle binders and competes with the analogue. Thus, particles switch to free Brownian motion with a higher diffusion coefficient at high target concentrations.

The switching activity, defined as the average number of binding and unbinding events per particle per unit of time, depends on the target concentration: the switching activity is high for low target concentration and is low for high target concentration. Typically, between 500 and 1000 particles are imaged and tracked simultaneously in one field of view. Due to the large statistics, the distributions of diffusion coefficients measured in the unbound states and the bound states show bell-shaped curves with

a Gaussian-like distribution, as discussed later in Section 3.3.2. In the absence of target, the fraction of low diffusion coefficients increases due to higher frequency of binding. With increasing target concentration, the target competes with the analogues and results in a larger fraction of unbound particles. Both the switching activity and bound fraction can be used as output parameters in the f-BPM system.

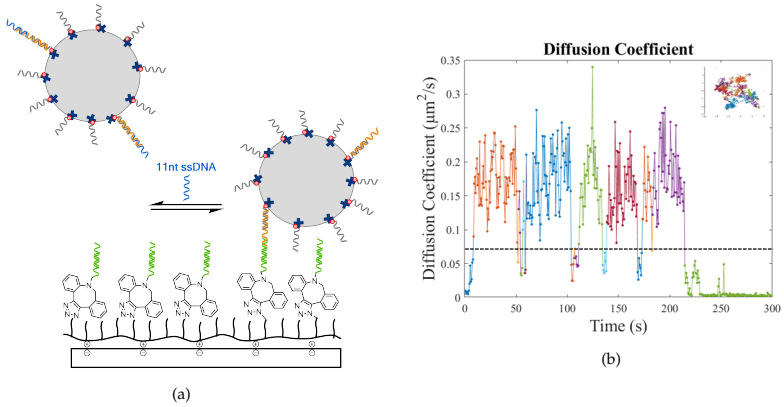

Figure 3.1: Basic principle of continuous biomarker monitoring based on measuring free long-range diffusional motion of biofunctionalized particles having reversible molecular binding with a substrate, exemplified for a ssDNA competition assay format. (a) Microparticles are functionalized with initial biotinylated oligos (grey) and particle-side binders (orange). The particles diffuse in the vicinity of a substrate functionalized with substrate-side binders (green). The particle binder (orange) has 20 bp complementarity to the initial biotinylated oligo and 9 bp complementarity to the ssDNA analogue on the substrate (substrate binder). The particle binder hybridizes and de-hybridizes to the substrate binder with a bound state lifetime of around 5 seconds due to 9bp DNA hybridization, causing transient binding of the particles. When the 11 nt ssDNA analyte (blue) is added, it competes with the substrate binder (ssDNA analogue) by hybridizing to the 9 bp binding region on particle binders. Therefore, it hinders the particle to switch from unbound states to bound states. At a higher concentration of 11 nt ssDNA analyte, the binding sites on all particle binders are blocked and cannot bind to the ssDNA analogue again, until the analyte molecule dissociates. Therefore, the f-BPM biosensor shows high bound fraction at low analyte concentration. (b) The diffusion coefficient of one particle as a function of time for a competition system with oligonucleotide binders and target. In the presence of low concentrations of analyte, particles show transitions from unbound to bound states. The inset shows the corresponding trajectory of the particle. State transitions can be detected by setting a threshold between the two states (dashed line).

Single-molecule binding and unbinding events can be identified in the data due to significant changes in the diffusion coefficient. The time between two consecutive events corresponds

to the lifetime of the bound and unbound states, as indicated in Figure 3.1b. In the absence of target, the unbound state lifetimes relate to the effective association rate of particles, which depends on the densities of particle binders (activators) and substrate binders (analogues), and on the hit-rate between particle and substrate. The hit-rate is determined by the average distance between particle and substrate. The average distance is given by the barometric height distribution, with a mean of approximately 1 μm for the 1 μm particles. At proper activator concentrations, most particles are bound via a single interaction with the surface (single-molecular bonds). In this case, the corresponding mean bound state lifetimes are independent of activator concentrations, as expected for single-molecular bonds. Upon the addition of targets, the targets compete with the analogues and block the binding region on the activators, which results in a transition from bound states to unbound states.

3.3 RESULTS AND DISCUSSION

3.3.1 *Monitoring DNA target with f-BPM sensors in PBS and in filtered blood plasma*

The competition assay design is shown in the inset of Figure 3.2b. The DBCO-tagged substrate-side binders (orange) function as analogues. These are coupled to the PLL-g-PEG layer (grey) via the integrated azide groups using click chemistry. The particle-side binders (blue) are coupled to 1 μm particles via biotin-streptavidin bonds and DNA hybridization. The reversible 9 bp hybridization between substrate binders (analogues) and particle binders results in particle switching between unbound and bound states. Hence, at zero analyte concentration, the particles show a high switching activity. In the presence of the 11-nt analyte (green), the binding region on particle binders is blocked, causing a decrease in the particle switching rate. For a detailed explanation of the functionalization approach, see Section 3.5.2.

Figure 3.2 shows the sensor response in buffer for monitoring ssDNA with a competition assay format. Here, the analytes compete with the analogues giving the fBPM sensor an inverted response comparing to the sandwich assay format: higher analyte concentration leads to lower switching activity and bound fraction. The switching activity, fraction of bound particles, and the unbound state lifetime dynamically respond to different analyte concentrations. Figure 3.2a shows the dose-response curves for 11-nt analyte in terms of the bound fraction and the switching activity (inset), as a function of the applied target concentration. Two profiles (red, blue data) of gradually increased target concentration were consecutively applied. The two dose-response curves plotted in terms of the bound fraction were fitted with a Hill equation with EC50 values of 79 $\pm$ 22 nM and 100 $\pm$ 33 nM respectively. The inset shows the dose-responses plotted with switching activity. The fitted EC50 values are 110 $\pm$ 78 nM and 127 $\pm$ 58 nM. The EC50 values of the red and blue curves are similar, showing that the molecular functionality is consistent over time.

The characteristic bound state lifetimes and unbound state lifetimes as a function of target concentration are shown in Figure

3.2b with logarithmic-logarithmic scales. In the ssDNA competition assay, the characteristic bound state lifetimes (triangles) remain unchanged, indicating that the affinity of the binding interactions is independent of the target concentration. The unbound state lifetimes represent the characteristic of the switching caused by the binding of analytes with a certain association rate.

At a low concentration region, the unbound state lifetimes are higher than the theoretical values. The main cause is the contribution of inactive or less-active particles. The corresponding bound fraction shown in Figure 3.2a at low concentration region does not reach 100%, which means that there is a small fraction of particles that show less switching or get loose once in a while due to reversible binding. The above origins cause the unbound state lifetime to reach a plateau of approximately 70 seconds at a low concentration region. At a high concentration region, the unbound state lifetimes becomes longer than the measurement time and therefore it only levels up to 850 seconds and reaches the second plateau. The bound fraction also shows a plateau at 15%, potentially caused by non-specific interactions between the particles and the substrate. These bindings also lead to a decrease in the unbound state lifetimes. The influence of non-specific interactions and the bias caused by the finite measurement length is reflected in the sigmoidal shape of the dose-response. Fitting the unbound state lifetimes with a sigmoidal curve yields an EC50 of 421 ± 130 nM. The EC50 obtained via the unbound state lifetimes is higher than the values extracted in panel a. Since we discarded the incomplete lifetimes measured at the beginning and the end of the measurements, the unbound state lifetime might be underestimated especially when particles are exhibiting less switching, which is the concentration region corresponding to a bound fraction lower than 50%. Hence, the EC50 values extracted by different output parameters, i.e. the switching activity, bound fraction and unbound state lifetimes, can be different.

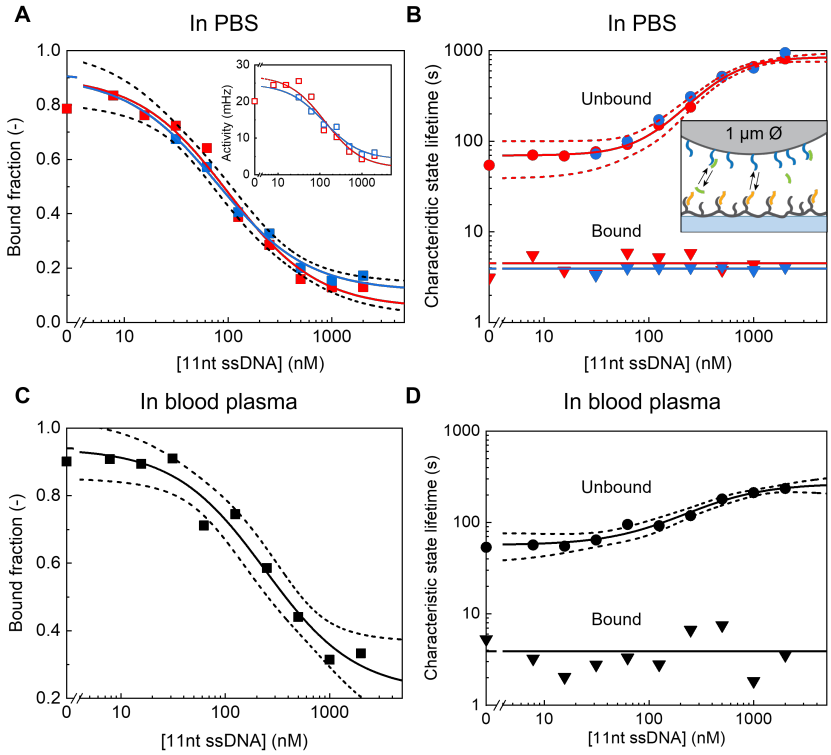

Figure 3.2: Dynamic response to target concentration of an f-BPM sensor with 1 μm particles, for a DNA competition assay in PBS and in filtered undiluted blood plasma. (a) The bound fraction as a function of target concentration. The red and blue squares represent two consecutive dose-responses with decreasing concentration series. The EC50 of the two dose-response curves fitted with a Hill equation are 79 $\pm$ 22 nM and 100 $\pm$ 33 nM respectively. The inset shows the dose-responses plotted in terms of switching activity. The fitted EC50 values are 110 $\pm$ 78 nM and 127 $\pm$ 58 nM. (b) Characteristic unbound state lifetimes are dependent on the target concentration in a range of 10 to 2000 nM. Fitting a sigmoidal curve yields an EC50 of 461 $\pm$ 41 nM. The bound state lifetimes (triangles) are independent of the target concentration, with an average of 5 seconds (solid horizontal lines). The inset shows 1 μm particles functionalized with particle binders (blue) via biotin-streptavidin interactions and DNA hybridization. DBCO-tagged substrate binders (orange) are coupled to the PLL-g-PEG polymer (grey) via the integrated azide groups, using second generation click chemistry. The reversible 9 bp hybridization between substrate binders and particle binders results in transient binding of particles to the substrate. In the presence of the 11-nt target (green), the binding region on particle binders is blocked, causing a decrease in switching events. (c) Switching activity measured for the ssDNA target in 50 kDa spin-filtered bovine blood plasma. Dashed lines indicate the 95% confidence interval of the Hill equation fit. (d) Characteristic unbound and bound state lifetimes measured in filtered bovine blood plasma. Fitting the unbound state lifetimes with a sigmoidal curve yields an EC50 of 421 $\pm$ 130 nM.

To demonstrate the capability of detecting analytes in biologically relevant media, we performed the ssDNA competition assay in filtered undiluted blood plasma. The dose-response curves are shown for the bound fraction and unbound state lifetime (figure 3.2c, d). The EC50 values measured in plasma and in buffer show good correspondence, proving that ssDNA analyte can be dynamically monitored in a filtered biological matrix. The background signal observed in plasma is generally higher than in PBS. The non-specific interactions between the particles and the surface result in a higher bound fraction and lower unbound state lifetime at a high concentration region, causing a decrease in the contrast and the sensitivity of the system.

Compared to the ssDNA sandwich assay, several interesting differences are seen. First, in the competition-based f-BPM sensor, the density of particle binders is about 1000 times lower compared to the sandwich-based f-BPM sensor, to avoid irreversible multivalent bonds. Second, the ssDNA competition assay responds within minutes, which is much shorter than the ssDNA sandwich assay. The fast response can be attributed to the higher concentration of the target molecules. Third, the signal drift observed over time is higher in the ssDNA sandwich assay. Possibly the observed signal drift in the sandwich assay originates from irreversible multivalent bonds between particles and substrate.

3.3.2 *Single-binding events and multivalent interactions*

In a competition assay format, the average mobility of particles reaches the lowest level right after the activation process is done, i.e. when the particle-side binders are supplied. Upon the addition of analytes (competitors), the particles become more mobile. As shown in Figure 3.3, if one single activator molecule (particle-side binder) captured by the particle binds to the substrate, the particle moves within a confined region with a circular motion pattern. If two particle binders captured by the same particle simultaneously bind to the substrate, two bonds between the particle and the substrate can be formed, leading to a double-bound state. The motion of the double bound state is either a stripe-like or a dot-like pattern.

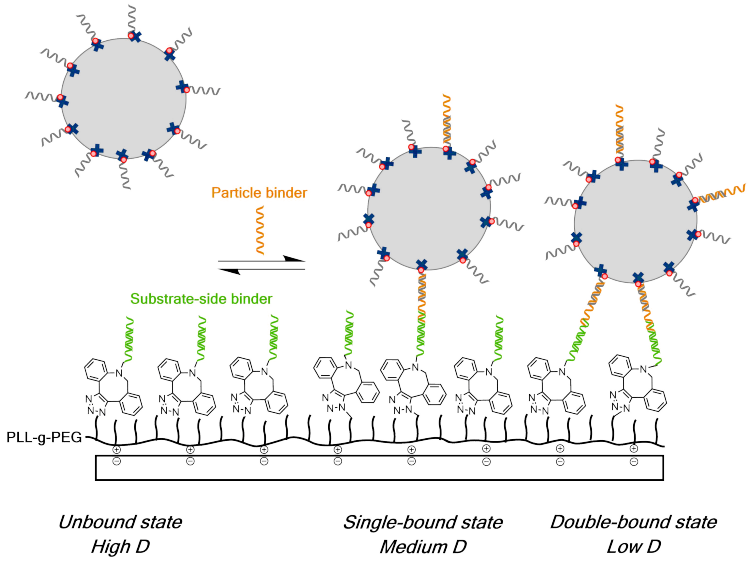

Figure 3.3: Schematic representation of the unbound, single-bound, and double-bound states of particles. Both the particles and the substrate are functionalized with binder molecules, which are able to bind to the particle-side binders (activators, orange). In its unbound state, the particle moves freely in the bulk solution with a Brownian motion. Upon addition of particle-side binders, the binder-induced sandwich bond can be formed, resulting in reduced mobility of the particle. When two bonds are formed between the particle and surface, the particle shows a more confined motion, referred to as a double-bound state.

The three main possible states, i.e. free Brownian motion, circular-motion and stripe-like motion, of the particles can be determined by analyzing the motion pattern and the corresponding diffusion coefficient of the particles over time. In Figure 3.4a, an example of a particle switched between unbound states and single-bound states is shown. The right panel indicates the trajectory of the particle reconstructed over a 20-minutes measurement. The different colors represent every switch between unbound states and single-bound states. In Figure 3.4b, another example of a particle switched between unbound states, single-bound states and double-bound states is shown. The corresponding motion of the particle switched between single-bound states and double-bound states is plotted in the inset of Figure 3.4b. Additionally, unbound state lifetimes and single-bound state lifetimes can be extracted based on simply setting a threshold or by using deep learning algorithm (See Section 3.5.4). The thresholding-based

event detection utilizes the differences in the diffusion coefficient of particles encountering the unbound states and single-bound states. To obtain the diffusion coefficient of the particles at each time frame, we use the mean squared displacement calculated with a sliding window. The unbound state lifetime is defined as the time-span of a particle showing free Brownian motion (D>0.1 $\mu m^2/s$), which is dependent on the analyte concentration. The lifetimes of the single-bound states and double-bound states are defined as the time-span of a particle showing circular motion (0.025<D<0.1 $\mu m^2/s$) and stripe-like pattern (D<0.025 $\mu m^2/s$) respectively, as shown in figure 3.4b.

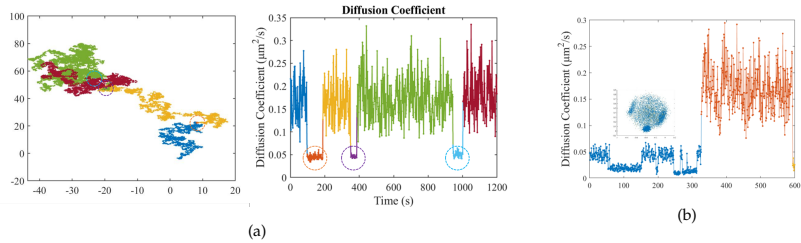

Figure 3.4: (a) Left: Trajectories of a single particle in presence of binders that can simultaneously bind to the particle and the substrate. The dashed circles indicate bound states caused by single-molecular bonds. Right: The D calculated as a function of time based on the displacements derived from the particle trajectories. Particles show transitions from unbound to single-bound states. (b) The diffusion coefficient traces of a particle switched between unbound states, single-bound states and double-bound states. The inset shows the corresponding trajectory when the particle mainly switched between single-bound states and double-bound states. The particle exhibits a circular motion pattern at single-bound state and shows stripe-like or dot-like motions at multivalently-bound states.

The major disadvantage of using a threshold is that it is less suitable for distinguishing the single-bound and double-bound states. Since the contrast between the diffusion coefficient of the single-bound and double-bound states is lower compared to the fluctuations of the diffusion coefficient, as shown in Figure 3.4b, false-positive events are detected and thereby lead to an overestimated switching activity. A deep-learning model developed by Petrus Bult was used to separate the single-bound and double-bound states.[61] As shown in Figure 3.5, the diffusion coefficients of the detected unbound, single-bound, and double-bound states are plotted in the histogram. The overlapping region between the single-bound and double-bound states which cannot be distin-

guished by setting a threshold is successfully separated via the deep-learning algorithm.

Brownian motion of a particle is a stochastic process and the corresponding diffusion coefficient depends on the size of the particle and its environment. The width of the curves represents the variability in calculated diffusion coefficients due to particles diffusing at various distances from the surface. When a particle approaches the surface, the diffusion coefficient decreases because of drag forces acting on the particle. In the absence of particle binders, most particles diffuse freely (prominent purple curve in the left panel), with some non-specific interactions occurring (small red and green curves in the left panel). With increasing concentration of particle binder, the fraction of low diffusion coefficients i.e. bound states increases (more prominent purple curve compared to low binder concentration), because more molecular sandwich complexes are formed by the binding of particle binders, which restrict the diffusion of the particles. In conclusion, the three main peaks separated by the deep learning algorithm show clear transitions between unbound, single-bound and double-bound states. The diffusion coefficient distributions are clearly different for the three states, allowing for state assignments based on measured diffusion coefficient values.

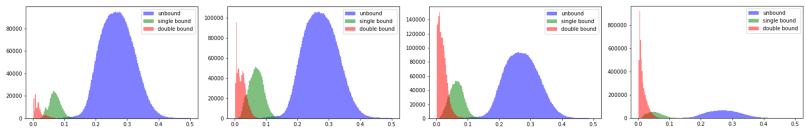

Figure 3.5: Distributions of measured D of 700 particles showing unbound state (purple), single-bound state (green), and double-bound state (red) populations dependent on the concentration of particle binders. The three states were determined by the deep-learning algorithm. The concentrations of the particle binders (from the left panel to the right panel) are 0, 50, 100, and 200 pM.

3.3.3 *Regenerating f-BPM sensors for achieving continuous monitoring of ssDNA over weeks*

The functionality of f-BPM biosensors can decay due to dissociation of functionalized biomolecules, non-specific interactions, or aggregation of particles for example. Regeneration refers to procedures to recover the functionality of a biosensor that has

been used for some time. In this section we study the feasibility of two regeneration methods, namely the regeneration of the sensor surface and the regeneration of the particles.

The first regeneration of f-BPM biosensors was done by directly adding more particle binders (activators), which we refer to as the reactivation process. The loss of biosensor response due to dissociation of substrate-side binders or particle binders can then be compensated. A drawback of this reactivation process is that it is difficult to control the final surface coverage of the particle binders and the sensor response after the reactivation process. Moreover, the loss of statistics over time due to non-specific binding of particles is still a problem. The second regeneration process is based on removing all particles and replacing them with freshly prepared particles. By employing an air-water interface, approximately 90% of the non-specifically bound or multivalently bound particles can be dragged away. The advantage of this method is that we can re-do the same particle activation process as in the beginning and therefore it's easier to control the signal after the reactivation.

Here we study the use of both regeneration methods in order to achieve a 2-week operational lifetime of the f-BPM sensor. As shown in Figure 3.6, the particles and surface remain functional in approximately 48 hours without the need of applying any regeneration process. After 48 hours, the system becomes less responsive because of the dissociation of particle-side binders. The particle-side binders (activators) are coupled to the particles via biotin-streptavidin interactions and 20bp DNA hybridization. As discussed in Section 2.2.1, the dissociation rate of biotin-streptavidin is about $(5.5 \pm 2.2) \times 10^{-6} s^{-1}$,[45] which is the weakest bond in the system. For an operational lifetime shorter than a week, reactivating the system by adding more particle binders is generally enough. However, the non-specifically bound particles cannot be regenerated by the reactivation process. Though the system is still capable of responding to the analyte within one week, we observed a clear drop in the unbound fraction over time, which is possibly caused by non-specific binding or multivalent interactions.

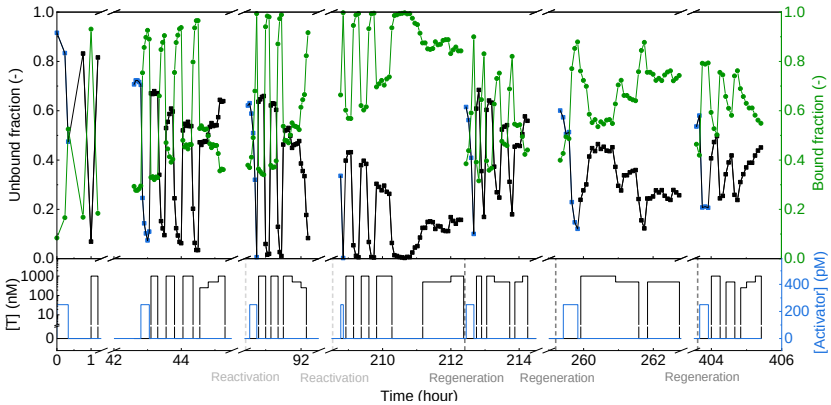

Figure 3.6: Continuous monitoring of single-stranded DNA target with competition assay format over two weeks. The top panel shows the fraction of unbound particles measured during the activation and sensing process. Blue data points represent the unbound fraction measured over the activation process. Black data points show the sensor response when adding alternating high and zero analyte concentrations. The corresponding bound fraction is shown with green circles. Lines are guides to the eyes. The bottom panel shows the applied 11nt ssDNA target and the activator concentration profiles. The reactivation process (light grey, dashed lines) was done by directly adding particle binders. The regeneration process (dark grey, dashed lines) is based on removing inactive particles with an air-water interface and replacing them with freshly prepared particles and particle binders. The applied time points of the two processes are indicated with dashed lines in the bottom panel.

After approximately one week, most of the particle probes are not functional anymore due to non-specific binding or multivalent interactions. In addition, the continuous flushing of analytes and buffers also gradually washed the particles out of the measurement chamber. In this case, replacing the old particles with freshly prepared particles is necessary. By applying an air-water interface, the non-specifically bound particles were removed and new particles were supplied. The lost signal caused by non-specific interactions was also recovered by the regeneration process. The same activation process (blue data points) was done to ensure the similarity of the signal. As shown in Figure 3.6, the regenerated f-BPM biosensor responds to the addition of particle binders and different concentrations of analytes. Hence, it is demonstrated that the oligonucleotide-functionalized PLL-g-PEG surface is functional for over two weeks.

3.4 CONCLUSION

There is a demand in fields of fundamental and ecological research, patient care, and industry for measurement technologies that are sensitive, specific, and also allow for the monitoring of biomolecular concentrations over long time spans. Here, we described a methodology referred to as free-diffusion-based biosensing by particle mobility (f-BPM), which combines continuous monitoring and single-molecule resolution with wide dynamic range (nM to μM). The DNA competition assay was used to demonstrate the capability and applicability of this approach.

Continuous monitoring was shown of oligonucleotides in PBS and in filtered blood plasma. Due to the reversible binding-based sensing principle, the system can provide single-molecule kinetics. On single slides, biosensing data was recorded over several days. The molecular architecture of the f-BPM biosensor is less complex than the t-BPM system demonstrated in Chapter 2, because the f-BPM sensor uses free-diffusing particles instead of tethered particles. Tether breakage or detachment in the t-BPM system can lead to a loss of sensor functionality. Furthermore, the f-BPM biosensor gives higher contrast, which helps to e.g. distinguish mono-, and multivalent bonds. A larger area-probing of the sensing surfaces is achieved with the f-BPM sensor due to the freely rotating particles. This may reduce sensitivities to intra-particle heterogeneities, because interactions are recorded from the total particle surface area. The sensing principle of f-BPM technique is based on affinity binding events of target molecules, allowing quite general applications for measuring a broad range of detection molecules. Together this can realize continuous monitoring for applications in fundamental research, for studies on organs on a chip, for the monitoring of patients in critical care, and for the monitoring of industrial processes and bioreactors as well as ecological systems.

3.5 MATERIALS AND METHODS

3.5.1 *Materials*

Custom-made fluid cell stickers were obtained from Grace Biolabs (USA). PBS tablets, and NaCl were purchased from Sigma-Aldrich. Dynabeads MyOne Streptavidin C1 were purchased from ThermoFisher Scientific. Poly(l-lysine)-grafted poly(ethylene glycol) was purchased from SuSoS (Switzerland) with a grafting ratio of 3.5. The molecular weight of the PLL backbone and PEG side chains are 20 kDa and 2 kDa respectively. Azide functionalized PLL-g-PEG (Nanosoft Biotechnology LLC, USA) is composed of a 15 kDa PLL backbone and 2 kDa PEG chain with a grafting ratio of 3.5. The ssDNA oligonucleotides (standard desalting and HPLC purification for chemically modified DNA) used in the study were purchased from IDT (Integrated DNA Technologies).

3.5.2 *Surface functionalization and particle preparation*

Preparation of biofunctionalized surfaces

Glass slides (25 x 75 mm, #5, Menzel-Gläser) were pre-cleaned by 40 minutes of sonication in isopropanol (VWR, absolute) and 30 minutes of sonication in MilliQ. After the substrate was dried with a nitrogen stream, 1 minute of oxygen plasma was applied to the slides to plasma-oxidize the surface. PLL-g-PEG and PLL-g-PEG-N_3 were pre-mixed in MilliQ with the ratio of 9:1 by weight at a final concentration of 0.45 mg/mL and 0.05 mg/mL respectively. Custom-made fluid cell stickers (Grace Biolabs) with an approximate volume of 20 μL were then attached to the substrate and the PLL-g-PEG/PLL-g-PEG-N_3 polymer mixture was immediately injected to the flow chamber and incubated for two hours. After the polymer self-assembled onto the negatively charged substrate, the unbound or loosely bound polymers were removed by withdrawing the solution out of the chamber.

The substrate-side binder is a partially double stranded DNA consisting of two complementary oligos, namely a 31nt oligo (3 ' C ATT ATT ACA AGC TAA GCT CTT GCA CTG ACG 5 ') and a DBCO functionalized oligo (5 ' CGA TTC GAG AAC GTG ACT

GCT TTT T 3 ′ DBCO). The 100 μM 31nt oligo was pre-hybridized with 100 μM DBCO functionalized oligo at a volume ratio of four to one. After removing the unbound or loosely bound PLL-g-PEG and PLL-g-PEG-N_3, the partially double stranded DNA was diluted to 1 μM with 500 mM NaCl in PBS (130 mM NaCl, 7 mM Na_2HPO_4, 3 mM NaH_2PO_4 at pH 7.4) and injected into the flow cell, followed by 72 hours of incubation at room temperature.

Preparation of particles

1 μL of Dynabeads MyOne Streptavidin C1 (Invitrogen) was mixed with 1 μL of 10 μM biotinylated particle binder and 4 μL PBS. The mixture was incubated for 1 hour at room temperature (RT) on a rotating fin (VWR, The Netherlands). Subsequently, 1 μL of 100 μM polyT was added and the mixture was incubated for 15 minutes at RT on the rotating fin. The particle mixture was washed with 0.05 vol.-% Tween-20 (Sigma-Aldrich) in PBS and reconstituted in 4000 μL of PBS. Right before injecting particles into flow cells, the particle solution was sonicated with 10 pulses at 70% with 0.5 duty cycle (Hielscher, Ultrasound Technology).

3.5.3 *Dose-response experiments for the ssDNA competition assay in PBS and undiluted filtered blood plasma*

The flow cell was washed with 40 μL of PBS, followed by the injection 40 μL of particles. After 15 minutes of incubation, the particle-side binders were added to the flow cell. The particle-side binder has 20 bp complementarity to the 20 nt ssDNA on the particle and 9 bp complementarity to the substrate-side binder on the surface. When the bound fraction of the f-BPM sensor reached the baseline signal, the unbound particle-side binder was removed and ssDNA analyte was injected into the flow cell chamber.

DNA competition assay in PBS

For each target concentration, 40 μL of 11nt ssDNA (5 ′ TCA TTA TTA CGA AAA 3 ′) analyte in PBS was injected into the flow cell chamber, after which the particle motion was recorded for 5 min in the absence of flow.

DNA competition assay in filtered blood plasma

Bovine plasma (P4639-10ML, Sigma Aldrich) was reconstituted in MilliQ and then filtered with 50-kDa molecular weight cut-off

centrifugal filter (UFC905008, Millipore). The ssDNA target (5 ′ TCG TAC CGT GTG TAA TAA TGC G 3 ′) in plasma filtrate was injected into the flow cell chamber with a total volume of 40 μL, after which the particle motion was recorded for 5 min in the absence of flow.

3.5.4 *Analysis of particle mobility*

Particle tracking by phasor localization

The 5 min particle motion measurements in the absence of flow, were recorded on a Leica DMI5000M microscope (Dark field microscopy, Leica Microsystems GmbH, Germany). The position of the particles was recorded in a field of view of 883 $\times$ 552 μm^2 for 5 minutes at a frame rate of 60 Hz with an integration time of 5 ms. By analyzing the intensity of pixels around the particle with a phasor-based localization method,[54] the center of every particle can be determined over each time frame.

State detection based on deep learning algorithm

Simulations are performed to generate motion resembling particles in the f-BPM system by modeling the overdamped Langevin equation. During a simulation run, bonds can form and dissociate between the particle surface and points distributed in a square lattice on the substrate. Up to two bonds can be formed between the particle surface and substrate. The particle is modeled as a sphere with several protrusions, representing roughness on the particle surface. These protrusions are not allowed to overlap with the substrate, confining the particle's motion, resulting in various motion patterns. The simulated data are used to train a deep learning model for processing the experimental data.[62]

Analysis of switching activity, lifetimes, and bound fraction

The position of every particle at each frame is localized with an accuracy of about 20 nm. The particle trajectories over time are reconstructed based on a phasor based localization. By analyzing the position of particles over time with the deep learning model, freely moving particles and particles at single-binding state and multiple-binding state are distinguished. For each particle, a diffusion coefficient D is determined from the mean squared displacement. The diffusion coefficients corresponding

to the detected three main states, i.e. unbound, single-bound and double-bound, are plotted in a histogram, as shown in Figure 3.5. The switching activity, defined as the average number of binding and unbinding events per particle per unit of time, is extracted based on the detected changes in different states. The state lifetimes correspond to the timespan of the detected states. The percentages of bound particles (single-binding and multiple-binding) are obtained as an output parameter "bound fraction".

Calculation of the diffusion coefficient

The calculation of the diffusive properties of particles in the f-BPM assay is based on analyzing the mean squared displacement of consecutive intervals of measured particle motion. The particle trajectory within the measurement window can be used to calculate the corresponding mean squared displacement over the time step. The corresponding measured diffusion coefficient is determined via a weighted average. When measuring free motion, the mean squared displacement is linear in time. In this case, the diffusion coefficient (parallel) can be calculated by linear fitting of the mean squared displacement curve.[61,62]

3.6 APPENDIX

3.6.1 *The reversibility of the f-BPM biosensor*

The reversibility of the f-BPM biosensor is demonstrated by recording the bound fraction as a function of time. For a competition assay, the bound fraction rises with decreasing target concentration and goes down with increasing target concentration. Figure 3.7 shows the applied 11nt target concentration profile and the measured bound fraction as a function of time. The target concentration was first decreased in a step-wise fashion (red squares), and thereafter the target was removed. Due to the law of mass action, the competition assay system shows a faster response comparing to the sandwich assay. The second dose-response (blue squares) was measured with a similar concentration series. It is expected that the substrate-side binders on the surface should not dissociate over time, resulting in a stable baseline signal. As shown in Figure 3.7, similar level of bound fraction was measured at zero target concentration over a measurement time of approximately 8 hours.

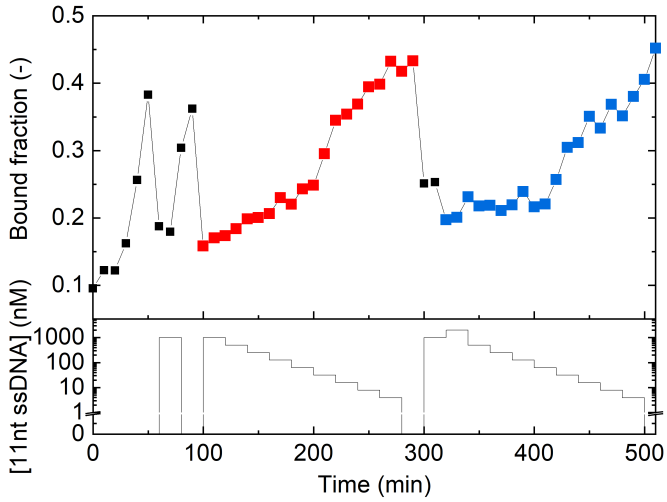

Figure 3.7: The top panel shows the bound fraction measured over time and the bottom panel shows the applied 11nt target concentration profile. The red and blue data points represent two consecutive dose-responses with equal decreasing concentration series applied in a stepwise fashion. The reversibility of the f-BPM biosensor is demonstrated by recording the bound fraction as a function of time before and after the removal of targets.

3.6.2 *Continuous monitoring of femtomolar ssDNA target with sandwich assay format*

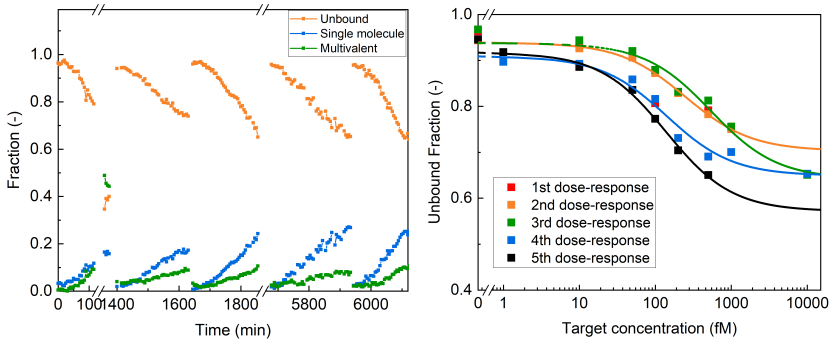

Figure 3.8: Continuous monitoring of femtomolar single-stranded DNA target with sandwich assay format. Particles and substrate are functionalized with ssDNA binders such that a 49 nt ssDNA target can bind to either side. The binders have 40 nt (particle-side) and 9 nt (substrate-side) complementarity with the target molecule. (a) The orange, blue, and green data points represent the fraction of unbound particles, single-bound particles, and multivalently-bound particles respectively. The dynamic range of the f-BPM sensor is tuned to femtomolar region by increasing the affinity of particle-side binders. Five does-responses were measured and regeneration processes were done in between. Continuous monitoring of target in a concentration range of 1 fM to 10000 fM was achieved with an operational lifetime of approximately 4 days. (b) The dose-response curves measured over time. The fitted EC50 values are 248 ± 39 fM (orange), 539 ± 180 fM (green), 141 ± 50 fM (blue), and 139 ± 44 fM (black).

Particles and substrate are functionalized with ssDNA strands as binders such that a 49 nt ssDNA target can bind to either side. The binders have 40 nt (particle-side) and 9 nt (substrate-side) complementarity with the target molecule. Upon the addition of target, the target-induced sandwich bond can be formed, resulting in a decrease in the particle mobility. Figure **??** shows the dynamic response of the f-BPM biosensor to ssDNA targets. The orange, blue, and green data points represent the fraction of unbound particles, single-bound particles, and multivalently-bound particles respectively. With increasing target concentrations, the bound fraction (single-bound, multivalently-bound) becomes larger. Because of the high affinity of the binder molecules (particle-side), the operational range is tuned to femtomolar region. However, since the particle-side binders cannot dissociate due to the high

affinity, the system needs to be regenerated by the regeneration process described in Section 3.3.3. Old particles were removed by an air-water interface, and thereafter the flow cell was supplied with new particles. Continuous monitoring of target in a concentration range of 1 fM to 10000 fM was achieved with an operational lifetime of approximately 4 days.

3.6.3 *Particle trajectories and the corresponding diffusion coefficients*

Examples of single particle trajectory and the corresponding diffusion coefficients are shown in Figure 3.9 and Figure 3.10. In Figure 3.9, single-stranded DNA target with a concentration of 10 pM was added to perform the DNA sandwich assay, while in Figure 3.10, 50 pM of ssDNA target was added. The position of particles were tracked over a duration of 10 minutes and particle trajectories (inset graphs) can be reconstructed. The diffusion coefficient of every particle is calculated as a function of time and the binding/unbinding events are digitally detected in parallel for all of the particles in the field of view. At low target concentration, as shown in Figure 3.9, particles mainly switched between unbound states and single-binding states.

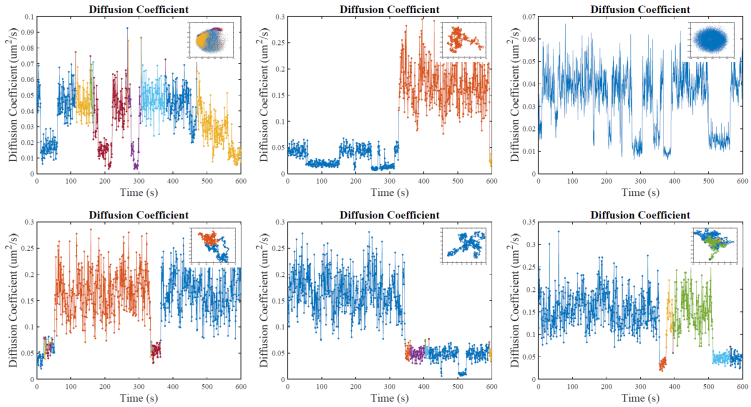

Figure 3.9: Single particle trajectory and the corresponding diffusion coefficients. Single-stranded DNA target with a concentration of 10 pM was added to perform the DNA sandwich assay. At low target concentration, particles mainly switched between unbound states and single-binding states.

In Figure 3.10, particles switched between single-binding states and multiple-binding states. Time traces with the two bound

states is shown, corresponding to the time-span marked by different color in the insets. In general, particles move freely on the substrate with Brownian motion when exhibiting unbound states. When the analyte binds to the binders, particles show circular motion patterns in a single bound state and stripe-like motion patterns at double-bound states.

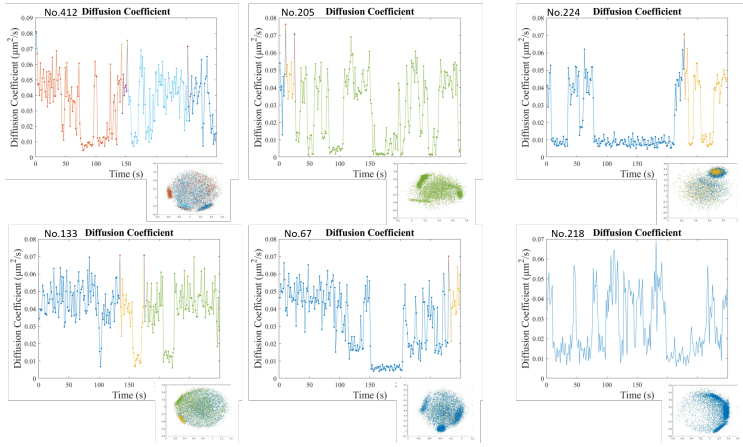

Figure 3.10: Single particle trajectory and the corresponding diffusion coefficients. Single-stranded DNA target with a concentration of 50 pM was added to perform the DNA sandwich assay. At higher target concentration, particles mainly switched between single-binding states and multiple-binding states.

3.6.4 *The flow rate effect on different-sized particles*

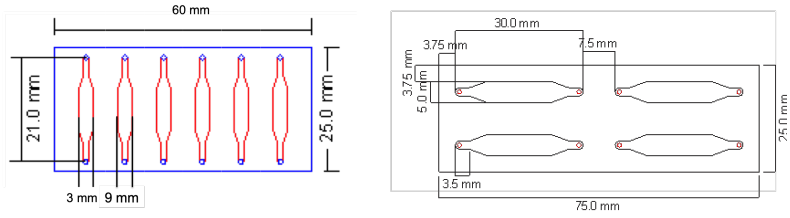

Figure 3.11: The dimensions of the flow cells. (a) A small flow cell with a total volume of 20 μL per cell. (b) A large flow cell with a total volume of 60 μL per cell.

Since the proximity of particles to the surface is not imposed by a molecular tether but by gravitational force, particles can be flushed out of the chamber if the flow rate is too high. To study

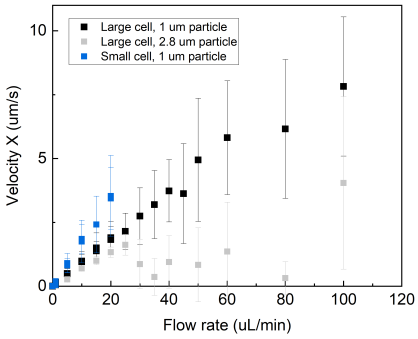

Figure 3.12: Two different size of particles (1 μm and 2.8 μm) and flow cells (20 μL and 60 μL) were used to study the flow effect on the f-BPM biosensor. The average velocity of the different-sized particles in the two flow cells is plotted as a function of the applied flow rates.

the flow effect on the f-BPM biosensor for further continuous monitoring applications in flow cell systems, two different size of particles (1 μm and 2.8 μm) and flow cells (20 μL and 60 μL) were used. The dimensions and design of the flow cells are shown in Figure 3.11. If the direction of the applied flow remains the same, the total residence time of a particle approximately equals to the total length of the flow cell chamber divided by the average particle velocity. We observed that larger and heavier particles can withstand a higher flow rate.

Figure 3.12 shows the average velocity of the different-sized particles as a function of the applied flow rates, measured in two different flow cells. A linear correlation between the particle velocity and the flow rate was observed for 1 μm particles in both small and large flow cells, indicating that the higher the flow rates are, the shorter the particles can remain in the flow cell. A linear correlation with a steeper slope was observed for 1 μm particles. As for larger particles, the average slope of the correlation is much smaller. Upon a continuous flow injection with a flow rate of 20 μL/min, the residence time of a 1 μm particle in a 20 μL flow cell is around 125 minutes, while the residence time of a 2.8 μm particle in a 20 μL is approximately 250 minutes, indicating the possibility of continuous monitoring in a flow cell system. Further extension of particle residence time can be achieved by applying a flow switch, i.e. by reversing the flow direction.

4

DEVELOPMENT OF READY-TO-USE F-BPM BIOSENSOR

In this chapter, we study the ability to prepare an f-BPM biosensor in dry form for the development of ready-to-use cartridges. We present a simple and cost-effective drying method for preserving the oligonucleotides functionalized PLL-g-PEG surface and the particle probes for at least three weeks. To protect the functionalized surface during dry storage, it is dried in the presence of a sugar mixture. Upon drying, a thin sugar coating is formed, which preserves the functionality of the biomolecules and the particles. Here, we describe a set of sugars including a combination of trehalose, sucrose, glucose, fructose, and pullulan, and a method for using them that allows long-term dry storage of the f-BPM biosensor, demonstrated with a DNA competition assay.

The first part deals with the preservation of a biofunctionalized surface during dry storage. The sensor surface was treated with different sugar mixtures and vacuum dried for 48 hours, while the particles were freshly prepared. After providing the rehydrated surface with fresh particles, the responsiveness of the integrated biosensor and the functionality of the surface were determined. The second part of this chapter focuses on drying both the biofunctionalized surfaces and particles. The f-BPM biosensors in dried form were kept under vacuum for a long period (48 hours, 1 week, and 3 weeks), thereafter rehydrated and tested for their responsiveness and concentration-dependent behavior.

Parts of this Chapter are included in manuscript: Buskermolen, A., Lin, Y. T., Smeden, L., et al; to be submitted. (A.B., Y.L. and L.S. are equally contributing first authors.)

4.1 INTRODUCTION

To develop ready-to-use biosensors that meet the demands for practical applications, various techniques to preserve biomolecules and biofunctionalized surfaces have been reported, including freeze-drying, vacuum drying, and immobilization in biocompatible polymers of organic or inorganic origin.[63] Specifically, several dehydration methods in the presence of protectants are widely used to facilitate the industrial chain supply, reduce storage associated costs, and increase the product shelf-life.[64]

In Section 2.5.2, we reported the successful long-term storage of the biofunctionalized PLL-g-PEG surface in wet form for three months at room temperature. The covalently functionalized oligonucleotides and PLL-g-PEG surfaces have been proven to stay functional. However, for BPM biosensors, both biofunctionalized surfaces as well as particles need to be preserved for extended periods. The possible instability factors are particle aggregation, dissociation of biomolecules, loss of bioactivity, and non-specific interactions over time. An effective conservation method should preserve the functionality of biomolecules as well as the analytical performance of the biosensor as a whole, ideally under room temperature and without the demands of strict storage conditions or complicated sample handling.

Freeze-drying is a commonly used method for the preservation of oligonucleotides, proteins, bacteria and cells. Briefly, freeze-drying (lyophilization) is a three-step process that produces a structurally intact and easily reconstituted end product. Initial freezing is performed with the usage of a cryoprotective in such a fashion that the amounts and sizes of ice crystals are kept to a minimum. When the temperature is controlled to be below the highly critical collapse temperature, free water present in the sample is subsequently removed by direct vaporization of ice under vacuum. The remaining bound water is forced out in the secondary drying step by gradually increasing the process temperature. The resulting product can normally be stored under vacuum conditions for long term with good activity upon rehydration.[63]

The usage of cryoprotectant additives for the maintenance of viability of cells or bacteria and bioactivity of biomolecules through

freeze-drying has been extensively studied. Studies have shown the protective effects of non-sugar additives through the freeze-drying of bacteria.[65] However, the disadvantages of freeze-drying based preservation methods are the time-consuming process, the complexity of the techniques and the associated costs due to strict storage conditions. These are major concerns when developing biosensors for on-site applications outside of the laboratory.

Vacuum-drying is an alternative to freeze-drying and is especially effective for the preservation of sensitive biomolecules or complicated molecular systems that can be damaged due to freezing. Carbohydrates are commonly used as protectants during dehydration and storage of biomolecules, with sucrose and trehalose being the most extensively employed. One of the survival strategies that desiccation-tolerant organisms seem to have in common is the accumulation of high concentrations of small carbohydrates, such as trehalose, sucrose, maltose, or raffinose prior to drying.[66] There are several hypotheses of how sugars play a role in the protection mechanism of cellular and macromolecular structure in anhydrobiotes. Firstly, sugar can replace the water that is normally hydrogen-bonded to polar residues.[66] Secondly, sugars are involved in the formation of a glassy matrix in the cytoplasm. In a glassy state, molecules are randomly distributed (like liquid) with low molecular mobility (like solid).

Here, we present a simple and cost-effective sugar-based vacuum drying method for preserving biofunctionalized PLL-g-PEG surfaces and particle probes. The dried f-BPM biosensors can be stored in a vacuum chamber for at least 3 weeks. The measured dose-response curves are comparable to freshly prepared f-BPM biosensors. The rehydrated f-BPM biosensors are capable of detecting analytes in buffer and in filtered blood plasma. The functionality of biomolecules on particles and PLL-g-PEG surfaces were assessed in terms of activity and state lifetimes using the f-BPM technique. In conclusion, we are able to achieve long-term dry storage of ready-to-use f-BPM biosensors. The results support the role of sucrose and trehalose as protective compounds during the vacuum-drying process. This approach holds promise for the future application of preserved biofunctionalized surfaces and particles.

4.2 THEORY

Drying of cells generally leads to massive damage to cellular membranes which eventually leads to cell death. The removal of water molecules in cells causes drastic changes in inter- and intra-molecular interactions. In the presence of bulk water, intracellular proteins and membranes are surrounded and bound with water molecules by hydrogen bonds and normally would not directly interact with other biomolecules. During the dehydration process, these proteins and membranes compensate for the loss of hydrogen bonding with water by hydrogen bonding with other molecules, causing protein-protein interaction, aggregation, and denaturation. Therefore, the dehydration process can cause structural damages (conformational changes) of the biomolecules, and destabilization of other internal structures such as nucleic acids.[67]

However, some organisms are able to survive almost complete dehydration,[66] a phenomenon known as anhydrobiosis. A common theme in these organisms is the accumulation of large amounts of disaccharides, especially sucrose and trehalose.[68] In general, sugars such as disaccharides and polysaccharides have the ability to form high viscosity and low mobility films, leading to the increased stability of the preserved material. Besides the formation of such films, a direct interaction between the sugar and polar group in proteins appears to be essential for stabilizing biomaterials of various composition during air drying or freeze drying. Methods for stabilizing proteins in dry form using sugars and sugar alcohols are widely used in the pharmaceutical industry.[69] Studies have shown that disaccharides, such as sucrose, lactose, and trehalose, have been widely used as protectants and stabilizers during dehydration.[67]

Monosaccharides such as D-glucose and D-fructose are reducing agents which can react with amino compounds on proteins. This chemical reaction between amino acids and reducing sugars is called the Maillard reaction.[70] Sucrose is a disaccharide of D-glucose and D-fructose. During dehydration of proteins, sucrose can stabilize proteins by replacing the hydrogen bonds, which are broken when water evaporates (known as the water replacement hypothesis), preventing protein denaturation.[71,72]

Trehalose, a nonreducing disaccharide, can stabilize proteins and is the most effective carbohydrate in preserving the structure and function of biological systems during dehydration and subsequent storage. Crowe et al. first presented the so-called water replacement hypothesis,[66] asserting that the hydrogen bonding between sugars and the polar headgroups of the lipids that constitute biomembranes, contribute to preserving the integrity of biological structures. As the systems are dried and frozen, these interactions replace those of hydration water at the membrane-fluid interface.[68] In addition, a compact structure will be formed in the presence of trehalose during drying due to its high solubility in water, which makes it more difficult to fully dehydrate a sample.

Pullulan is a highly soluble polysaccharide composed of maltotriose units. It has a molecular weight ranging from 45 kDa to 600 kDa. Furthermore, it is highly soluble, due to its ability to form many intermolecular hydrogen bonds and its notable hydrophilicity.[73–75] When drying a 5-10% pullulan solution onto a smooth surface, it can form transparent films that exhibit exquisite mechanical properties.[73]

Sugars have been used a lot for medical purposes, for example, to stabilize therapeutics or vaccines. However, there are not many examples where sugar drying is used in preserving biosensors. An example that relates to this research is a biosensor based on actuated magnetic particles that use a sugar solution for dry storage.[76]This technology, like BPM, uses magnetic nanoparticles. In this research, both the sensor surface and the nanoparticles were dried. Another example is a paper sensor for bacterial detection which can be stored for 6 months at ambient temperature.[77] A third example is a microfluidic immunoassay where antibody-gold conjugates were dried with sucrose and trehalose (5% w/v each). After 60 days of storage at elevated temperature, the sensor still retained 80-96% activity.[78]

4.3 RESULTS AND DISCUSSION

The shelf-life of the oligonucleotide functionalized PLL-g-PEG surface in wet state was proven to be at least three months in Section 2.5.2. The fact that f-BPM is based on freely moving particles makes it particularly suitable for the fabrication of a ready-to-use sensor. The storage lifetime of biosensors depends on the retention of the biological activity of the used molecular components. This may vary, depending on the coupling chemistry, the storage conditions and the intrinsic stability of the biomolecules. The challenges for the f-BPM sensor are to preserve the functionality of biomolecules during dry storage and to prevent particles from getting stuck or becoming aggregated. A known strategy is to preserve biomolecules by embedding them in a sugar matrix. The effects of various sugar mixtures, i.e., sucrose/trehalose, glucose/fructose and pullulan/trehalose, on the preservation of the biofunctionalized particles and surfaces were investigated.[79]

The first step is to study the functionality of the oligonucleotide functionalized PLL-g-PEG surface after drying in the selected three sugar mixtures, dried under vacuum for 48 hours. The oligonucleotide functionalized particles were freshly prepared in buffer and added to the rehydrated surface. The biological activity was tested by a DNA competition assay with the f-BPM sensing technique. Three different sugar conditions, including sucrose/trehalose, glucose/fructose and pullulan, were tested and analyzed for their response in terms of the switching activity and the unbound fraction when different analyte concentrations were applied. (Detailed information of the rehydration and activation processes are described in Section 4.5.3)

4.3.1 *Drying and rehydration of oligonucleotide modified PLL-g-PEG surface with sugar mixtures*

The illustration of the preservation procedure of the biofunctionalized surface is shown in Figure 4.1. Our first goal is to study the effect of different sugar drying methods on the preservation of surfaces functionalized with oligonucleotides and PLL-g-PEG polymers. The efficiency of this drying process is evaluated by measuring the signal of the f-BPM biosensors when different con-

centrations of ssDNA targets are present. There are two simple output parameters for f-BPM biosensors, i.e., the bound fraction and the switching activity. The switching activity is defined as the average number of binding and unbinding events per particle per unit of time, which depends on the target concentration. Particles that stay bound over the measurement time are classified as inactive or non-specifically bound particles and were eventually excluded in the data processing.

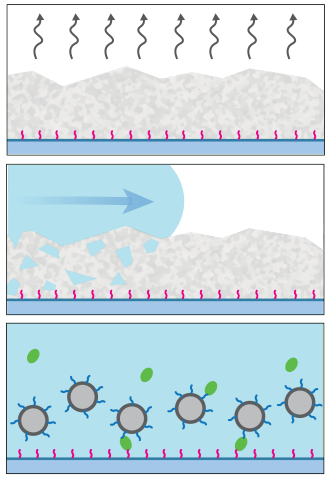

Figure 4.1: Schematic overview of the dehydration and rehydration processes of oligonucleotide-functionalized PLL-g-PEG surface. The gray layer represents the sugar mixtures (sucrose/trehalose, pullulan/trehalose, glucose/fructose). In the top panel, the sugars present in high concentrations stabilize the biomolecules and their structures by forming a high viscosity layer, leading to a reduced possibility of non-specific interactions or rupture of the bonds. The surface covered with sugars was stored in a vacuum chamber and gradually dehydrated. As shown in the middle panel, after 48 hours of dry storage, the sugars were dissolved and removed from the measurement chamber by several times washing with PBS. In the bottom panel, the freshly prepared 1μm particles functionalized with particle binders (blue) were provided to the preserved PLL-g-PEG surface coated with substrate binders, whereas the DNA competition assay can be performed. The activation process is described in Appendix 4.6.1. Finally, the target was added and could reversibly bind to the particle binders and substrate binders.

The sensing principle for the ssDNA competition assay is the competition for binding between analogues and analytes. The particle binder (5 ′ GTA GAC ATC CAA CCT GAC TAC GTG AGT AAT AAT GCG 3 ′) has 20 bp complementarity to the initial biotinylated oligo (Biotin 3 ′ CAT CTG TAG GTT GGA CTG

AT 5 ′) coupled on particles, and 9 bp complementarity to the ssDNA analogue on the substrate (substrate binder). Due to the high affinity of the 20bp DNA hybridization, when a particle binder binds to the initial biotinylated oligo, it doesn't dissociate within a time scale of hours. However, on the other side, the particle binder hybridizes and de-hybridizes to the substrate binder with a bound state lifetime of around 10-20 seconds due to 9bp DNA hybridization and causes transient binding of the particles. Therefore, the addition of particle binder is defined as the activation process.

Figure 4.2 shows that the switching activity rises with the gradual increase of particle binder concentrations. When enough switching events were observed, i.e., the bound fraction reached 40-50%, the activation process was terminated by washing away the unbound binders. The density of particle binders is controlled to be 5000 times lower than in sandwich assays. This is essential in order to achieve reversible monovalent bonds and avoid irreversible multivalent bonds between the particles and the substrate.

When the 11 nt ssDNA analyte is added, it competes with the substrate binder (ssDNA analogue) by hybridizing to the 9 bp binding region on particle binders. Therefore, it hinders the particle to switch from unbound states to bound states. At a higher concentration of 11 nt ssDNA analyte, the binding sites on all particle binders are blocked and cannot bind to the ssDNA analogue again, until the analyte molecule dissociates. Therefore, the f-BPM biosensor shows high switching activity and high bound fraction at low analyte concentration and vice versa.

To ensure the quality of different batches of biofunctionalized slides, at least one sample from each batch was tested first without going through any drying process. After confirming that the biofunctionalized surface is functional, the rest of the slides were dried with the same procedure but in different sugar mixtures. The goal is to prove that the drying process effectively maintains the functionality of the oligonucleotides and PLL-g-PEG polymers on the surface, and the oligonucleotides still have the ability to capture the complementary ssDNA target after dehydration, dry storage and rehydration process.

The switching activity signal in Figure 4.2 shows that the oligonucleotides functionalized PLL-g-PEG surface is still functional. Both bound fraction and switching activity increased during the activation process. The crossover point where the bound fraction continued to increase while the switching activity started to decrease indicates the dominance of multivalent interactions. Due to the finite measurement time, there is a maximum number of switching events that can occur per particle within each measurement, influenced by kinetic parameters such as state lifetimes. When multivalent interactions or re-binding occurs, the switching activity becomes lower while the bound fraction can still increase until 100% of particles are bound.

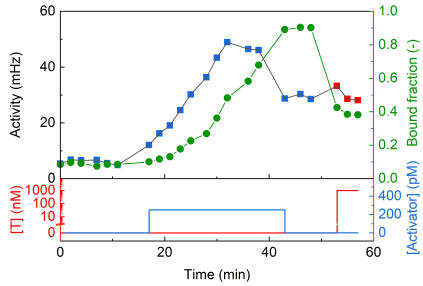

Figure 4.2: Response of a f-BPM biosensor after drying the surface with pullulan. The top panel shows the switching activity measured during activation (blue) and sensing (red) process. The corresponding bound fraction is shown with green circles. Lines are guides to the eyes. The bottom panel represents the concentration profile of the 11nt ssDNA target (red) and the activator (blue). In the activation process, the switching activity increased in the beginning and dropped afterwards, while the bound fraction continued to increase. Upon the addition of targets, the bound fraction decreased significantly, showing that the system responds to the presence of targets.[79]

Upon addition of 1 μM ssDNA analyte, the bound fraction significantly reduced, indicating the competition between the analytes and the analogues. However, the corresponding switching activity remains similar before and after adding 1 μM of ssDNA analyte. The activity measured at the end of the activation process dropped due to the transition from single bond to multivalent interactions. When reaching the over-activation stage with re-binding of analytes occurring, long bound state lifetimes were observed and the number of switching events per particle decreased. However, the activity signal is still lower than the maximum activity. The result demonstrated the functionality of

the oligonucleotides functionalized PLL-g-PEG after drying and rehydration.

Figure 4.3a and 4.3b show the sensor response of the f-BPM biosensor dried with glucose/fructose and with sucrose/trehalose respectively. After washing away the sugar mixtures, the system was first activated and exposed to a sequence of different concentrations of competing ssDNA analyte. The bottom panel shows the sequence of corresponding analyte concentrations with alternating high and zero analyte concentrations. The top panel includes both the switching activity and the bound fraction as the output signal, which dynamically respond to both increasing and decreasing analyte concentrations. Similar over-activation and re-binding events were observed in both cases.

Though the bound fraction data in Figure 4.3a and 4.3b show good correspondence in time response, the baseline switching activity measured at zero analyte concentrations appears to be more stable when using a sucrose/trehalose sugar mixture. It is expected that the particle binders on the particles should not dissociate over a time scale of hours, causing the system to show a stable baseline switching activity at zero analyte concentration. One possible reason for the fluctuating signal at zero analyte concentrations observed in Figure 4.3a is the incomplete fluid exchange. The signal at zero analyte concentration, measured right after the supply of higher concentrations (500 nM and 1 μM) of analyte, was often lower than the baseline switching activity. This reduction of baseline switching activity is attributed to the remaining analyte in the system due to incomplete fluid exchange, which happens when washing away high concentrations of analytes. In conclusion, among the tested sugar mixtures, 25% w/w sucrose with 10 mM trehalose and 0.05% v/v Tween20 show the most robust and consistent response.

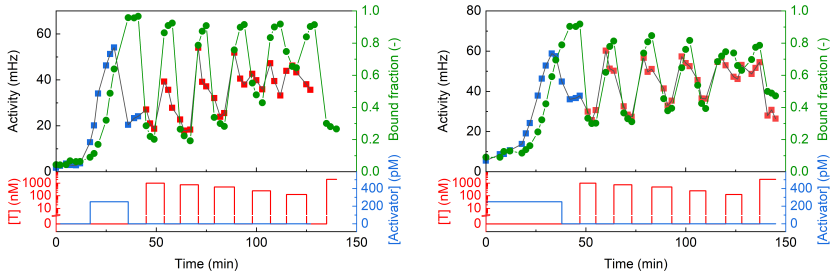

Figure 4.3: Dynamic response to the target concentration of an fBPM sensor, for a DNA competition assay in PBS. The top panel shows the switching activity measured during the activation and sensing process. Blue data points represent the switching activity measured over the activation process. Red data points show the sensor response when adding alternating high and zero analyte concentrations. The corresponding bound fraction is shown with green circles. Lines are guides to the eyes. The bottom panel shows the applied 11nt ssDNA target and the activator concentration profiles. (a) Response of an f-BPM DNA competition assay after drying the surface with glucose/fructose. (b) Response of an f-BPM DNA competition assay after drying the surface with sucrose/trehalose.[79]

4.3.2 *Development of a ready-to-use f-BPM biosensor*

The three sugar conditions were tested for drying both biofunctionalized particles and PLL-g-PEG surfaces. The freshly prepared particles functionalized with oligonucleotides were first re-suspended in the three sugar mixtures and added separately to the sensor surfaces. Then the sensors were dried under vacuum for around 48 hours and 3 weeks. The drying and rehydration procedure of the ready-to-use f-BPM biosensors is shown in Figure 4.4. The biosensor surface and particles were homogeneously exposed to air and then vacuum dried with uniform conditions.

The dynamic response of an f-BPM biosensor vacuum-dried in pullulan/trehalose with the procedure described in Figure 4.4 for approximately 48 hours are shown in Appendix 4.6.3. We observed that the pullulan/trehalose mixture cannot easily be washed away. It takes approximately one hour of flushing with PBS to fully release the particles and to achieve a bound fraction lower than 10%. The reproducibility of the analytical performance of the ready-to-use biosensors stored in pullulan/trehalose is relatively low.

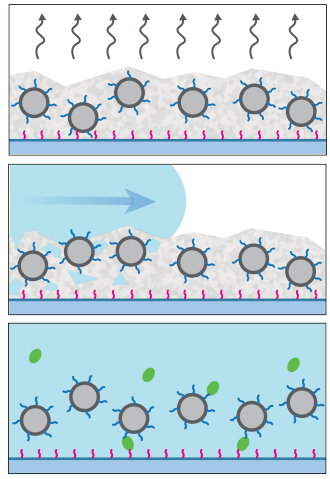

Figure 4.4: Schematic representation of the dehydration and rehydration processes for ready-to-use f-BPM biosensors. The gray layer represents the sugar mixtures. The 1 μm particles functionalized with particle binders (blue) were added to PLL-g-PEG surface coated with substrate binders (red). In the top panel, the sugars present in high concentrations hinder the diffusion of particles by forming a high viscosity layer, leading to a reduced possibility of non-specific interactions or aggregation. The system was stored in a vacuum chamber and gradually dehydrated. After a certain dry storage period (two days, one week, and three weeks), the disaccharide molecules were dissolved and removed from the measurement chamber by several times of washing with PBS, as shown in the middle panel. The activation process is described in Section 4.5.3. In the bottom panel, the target was added and can reversibly bind to the particle binders and substrate binders.

The dose-response and time-response results of an f-BPM biosensor vacuum-dried in glucose/fructose with the procedure described in Figure 4.4 for approximately 48 hours are shown in Appendix 4.6.3. The rehydration process was still longer than expected. One hour of incubation and washing steps in between are needed to reach a low bound fraction of approximately 10%. The output signal including the switching activity and bound fraction both respond to the addition of activators and different concentrations of competitors. However, the reproducibility of the response of these glucose/fructose-based dry cartridges is also limited. Some samples show good preservation of anti-fouling properties but lose the capability of responding to analytes.

In Section 4.3.1, the sucrose/trehalose mixture was proved to be relatively suitable for preserving oligonucleotides functionalized PLL-g-PEG surface. To test the capability of drying both the particle probes and biofunctionalized surface in a glassy matrix,

the same sucrose/trehalose mixture was used. The whole f-BPM biosensor was dried in sucrose/trehalose with similar procedures and conditions described in Figure 4.4. After the rehydration process, bright field video microscopy shows that the particles immediately became mobile, indicating that the sucrose/trehalose mixture dissolved quickly in PBS. The bound fraction was reduced to 10% after around 20 minutes of incubation with three washing steps in between. The biosensor responds to both the addition of activators and different 11nt ssDNA analyte concentrations ranging from 4 nM to 2 μM. Duplicate experiments were performed, showing that the results are robust and reproducible. Hence, the sucrose/trehalose mixture was selected as the protectant for further studying on different storage times and comparison of sensor response in PBS and in filtered blood plasma.

Figure 4.5a shows two dose-response curves measured over three hours to study the performance of the dried and rehydrated f-BPM biosensors. The dose-responses expressed in the bound fraction give EC50 values of 28 ± 4 nM (red) and 17 ± 3 nM (blue). The EC50 of the two curves were comparable and the results show relatively good consistency. The characteristic bound state lifetimes shown in Figure 4.5b remain unchanged, indicating that the affinity of the binding interactions is independent of the target concentration. Furthermore, the bound state lifetime is similar to what we observed in the t-BPM biosensors, since the intrinsic dynamics of analyte molecules do not change while using different systems. The unbound state lifetimes curve has a sigmoidal shape. Fitting the characteristic unbound state lifetime with a sigmoidal curve gives EC50 values of 691 ± 538 nM (red) and 393 ± 85 nM (blue). At low target concentrations, the rate of particle-substrate binding is governed by the density of binder molecules, giving the plateau of mean unbound state lifetime at 80 seconds. At higher concentrations, the targets occupy part of the binder molecules causing the mean unbound state lifetime to increase. At concentrations above 1μM, the unbound state lifetimes become longer than the measurement time and therefore a plateau is reached at 600 seconds.

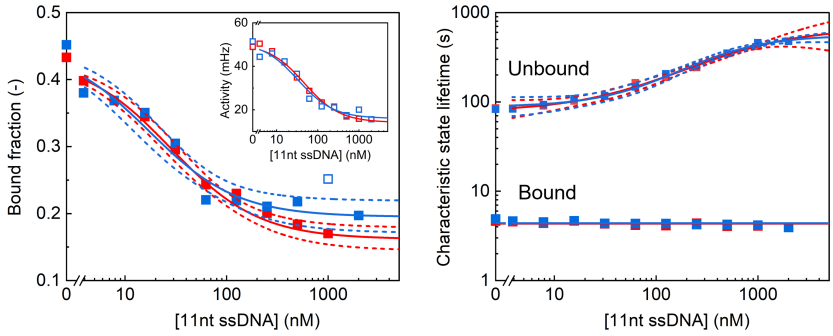

Figure 4.5: Dose–response curves measured with sugar-matrix sensors that were stored in a sucrose/trehalose matrix for dry storage of 3 weeks (measured in duplicate). The red and blue data represent two consecutive dose-responses with decreasing concentration series. (a) The bound fraction versus the applied 11nt ssDNA target concentration. The corresponding EC50 of the two dose-response curves are 28 $\pm$ 4 nM (red) and 17 $\pm$ 3 nM (blue). The inset shows the dose-response plotted in terms of the switching activity. (b) Characteristic unbound and bound state lifetimes measured with a sugar-matrix sensor stored for 3 weeks. Fitting the characteristic unbound state lifetime with a sigmoidal curve gives EC50 values of 691 $\pm$ 538 nM (red) and 393 $\pm$ 85 nM (blue). Characteristic unbound state lifetimes are dependent on the target concentration in a range of 4 to 2000 nM. The characteristic bound state lifetime shows independent behavior with an average of 5 seconds.

4.3.3 *The performance of ready-to-use f-BPM biosensors for different storage times.*

In Section 4.3.2, a simple fabrication process for making ready-to-use fBPM cartridges has been designed and executed as shown in Figure 4.4. In order to test the shelf life of the sugar-dried f-BPM biosensors under laboratory conditions, we prepared and dried three cartridges by the same procedure but with different storage time (2 days, 1 week and 3 weeks) in the vacuum chamber. The cartridges composed of particle probes and functionalized surfaces were vacuum-dried homogeneously and thereafter followed by the reassembling of flow cells and rehydration processes including washing steps. (See Appendix 4.6.1) Once the particle probes became mobile again and the bound fraction was reduced to 10% or lower, the system was activated by applying activators.

The time-dependent responses of the rehydrated f-BPM biosensors stored for one week and three weeks are shown in Figure 4.6a and 4.6b, respectively. The blue concentration profile in the

two bottom panels indicates the activation process, while the blue squares in the top panels show the corresponding switching activity. The activation process was terminated after the bound fraction reached 50%. As shown in the red concentration profiles in the bottom panels, the target concentration was first returned from 1μM to zero in a single step, followed by gradual decreases in small steps. The switching activity (red squares) responds inversely to the ssDNA analyte concentrations, as it should be for competition assays. Upon adding activators or competitors, the bound fraction, as the second output parameter, shows similar trends compared to the switching activity in both cases.

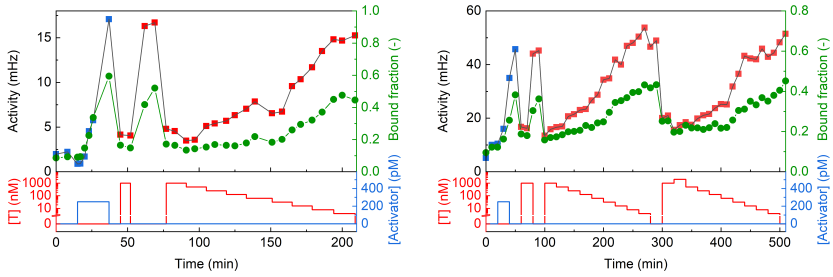

(a) 1 week of storage

(b) 3 week of storage

Figure 4.6: The top panel shows the switching activity measured during the activation and sensing process. Blue data points represent the switching activity measured over the activation process. Red data points show the sensor response when adding alternating high and zero analyte concentrations. The corresponding bound fraction is shown with green circles. Lines are guides to the eyes. The bottom panel shows the applied 11nt target concentration profile (red) and the concentration of activators (blue) used in the activation process. (a) The performance of an f-BPM biosensor after 1 week of dry storage in sucrose/trehalose mixtures. (b) The performance of an f-BPM biosensor after 3 weeks of dry storage in sucrose/trehalose mixtures.

In Figure 4.7a and 4.7b, we evaluate the effects of sugar-drying and subsequent storage by comparing the dose–response curves of the f-BPM biosensors stored for different periods. As a reference, the results (orange squares) obtained by a freshly prepared f-BPM biosensor are also plotted. After 2 days (green squares), one week (black squares) and three weeks (red squares) of dry storage at room temperature in a vacuum chamber, the f-BPM biosensors are capable of responding to different target concentrations in a similar dose-dependent manner compared to the freshly prepared sample.

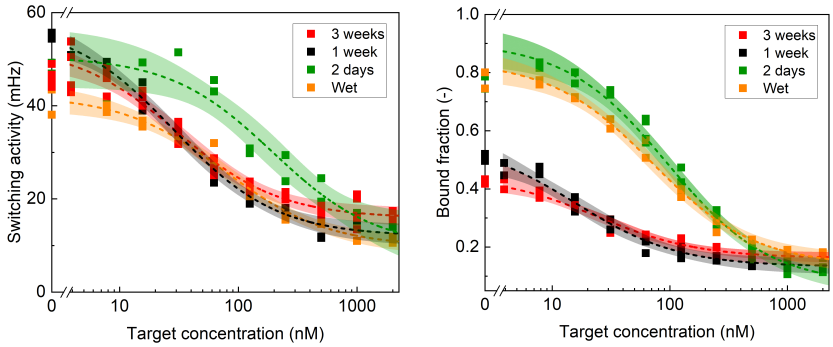

(a) (b)

Figure 4.7: Effect of dry storage period on the performance of the f-BPM biosensor with DNA competition assay. The control sample (wet, orange squares) was without any preservatives or dehydration processes. (a) Dose-response curves plotted with switching activity. The corresponding EC50 values measured with cartridges stored for different periods are 77 ± 15 nM (wet, orange), 195 ± 72 nM (2 days, green), 29 ± 5 nM (1 week, black) and 30 ± 6 nM (3 weeks, red). The shades indicate the 95% confidence range of the fit. (b) The bound fraction versus the applied 11nt ssDNA target concentration. The fitted EC50 values are 24 ± 6 nM (wet, orange), 95 ± 15 nM (2 days, green), 16 ± 5 nM (1 week, black) and 71 ± 11 nM (3 weeks, red).

The rehydrated biosensors after dry storage respond to target concentrations ranging from 4 nM to 2 μM. The corresponding dose-response curves demonstrated in Figure 4.7a and 4.7b were performed with two replicates for each ssDNA concentration, showing that the results are robust and reproducible. The dose-response obtained by the cartridge stored for 2 days deviates from the other three curves. The possible causes are due to different activation conditions and density of binders. Dose-response curves plotted with switching activity give EC50 values of 77 ± 15 nM (wet, orange), 195 ± 72 nM (2 days, green), 29 ± 5 nM (1 week, black) and 30 ± 6 nM (3 weeks, red), which are within estimates of error. The contrast of the signal is slightly different, but the EC50 values and dynamic range are similar, indicating the preservation of the particle probe and functionalized surfaces does not lead to significant changes in the molecular systems nor the functionality of biomolecules such as oligonucleotides or streptavidins. It is interesting to note that the rehydrated system was even showing a higher contrast than their freshly prepared counterparts.

The results showed that the f-BPM biosensor, with appropriate materials and conditions, can give reproducible DNA competition assay results for different periods of dry storage. In conclusion, the rehydrated f-BPM biosensor has an operational life span of several hours and the tested shelf-life is at least three weeks when stored in a vacuum chamber. Further testing is required to evaluate the suitability of this approach for immunosensor applications.

Figure 4.8a and 4.8b demonstrate the capability of detecting analytes in biologically relevant media, we performed the ssDNA competition assay in 50kDa-filtered undiluted blood plasma with a ready-to-use f-BPM biosensor after 3 weeks of dry storage in the sucrose/trehalose mixture. The two output parameters including switching activity and bound fraction are measured over time as shown in Figure 4.8b. In comparison, the results performed by a freshly prepared f-BPM biosensor in 50kDa-filtered undiluted blood plasma is shown in Figure 4.8a. The PEG side chains of the PLL-g-PEG polymer are expected to function as a low-fouling layer that resists protein adsorption. In general, the results in the beginning are similar to the reference sample and the system can still respond to different target concentrations, proving that the ssDNA target can be dynamically monitored in a more complex environment even with the rehydrated f-BPM biosensor.

However, when performing a DNA competition assay in 50kDa-filtered bovine blood plasma for over several hours, the total number of active particles in a fixed-size of the field of view decreased dramatically compared to measurements in PBS. Stuck particles and aggregated particles are assigned to inactive particles and were filtered out via data processing, therefore causing lower statistics and higher signal fluctuations. In comparison, for the tethered-BPM system, it has been shown in different molecular systems[33,80] that non-specific interactions were lower in the 50kDa-filtered plasma. This may be due to the limited range of motion restricted by the tether and the antifouling properties. A hypothesis is that particles are exploring a much larger area in f-BPM systems. Therefore, the probability of particles interacting with proteins, other particles or biomolecules suspended in the solution is much higher.

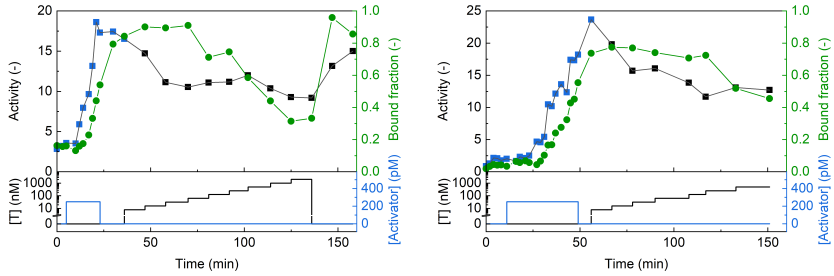

Figure 4.8: Comparison of the sensor response in 50kDa-filtered undiluted blood plasma with freshly prepared sensor and rehydrated sensor. The top panel shows the switching activity measured during the activation and sensing process. Blue data points represent the switching activity measured over the activation process. Black data points show the sensor response when adding alternating high and zero analyte concentrations. The corresponding bound fraction is shown with green squares. Lines are guides to the eyes. The bottom panel shows the applied 11nt target concentration profile (black) and the concentration of activators (blue) used in the activation process. (a) A freshly prepared f-BPM biosensor was used to perform DNA competition assay in 50kDa filtered bovine blood plasma (b) An f-BPM biosensor vacuum dried for 48 hours in presence of sucrose and trehalose was used to perform DNA competition assay in 50kDa filtered bovine blood plasma.

4.4 CONCLUSION

The lifetime of biosensors depends on the retention of the biological activity of all the biocomponents included in the biosensor. This may vary from hours, days, weeks to months, depending on the coupling chemistry, the storage conditions and the intrinsic stability of the biomolecules. In general, fast and simple on-site sample-handling steps are key for developing ready-to-use biosensors, especially for portable biosensing, for both healthcare and industry and for speeding up translation to real-life applications.

Carbohydrates were investigated for their potential use as multifunctional protectants and stabilizers during drying for biomolecules such as proteins and oligonucleotides. Based on the efficient protective properties for disaccharides reported in other drying tests, three different sugar mixtures, including sucrose/trehalose, pullulan/trehalose, and glucose/fructose, were selected and tested as stabilizers for the long-term storage of oligonucleotides, PLL-g-PEG and particles.

Firstly, a simple and effective method for the drying of oligonucleotides functionalized PLL-g-PEG surface to be used directly in a biosensor is reported. Oligonucleotides and PLL-g-PEG were vacuum dried in the presence of the three aforementioned sugar mixtures. The biosensor's performance was experimentally evaluated based on its dynamic response and EC_{50} values. For all three conditions, the biofunctionalized PLL-g-PEG surfaces were successfully preserved for two days and still showed good antifouling properties after adding freshly prepared particles. The integrated system responds to the addition and removal of the target, proving that the functionality of the dried and rehydrated oligonucleotides is preserved.

Secondly, the dried biofunctionalized surface and particles were used directly after rehydration and activation as the essential elements of a biosensor for determining the concentration of ssDNA target. The sucrose/trehalose mixture rehydrates easily, gave few stuck particles and the best uniformity. With a vacuum drying procedure, the glassy layer containing sucrose/trehalose has a consistent thickness throughout the cartridge, which minimizes heterogeneities. In conclusion, sucrose and trehalose

rendered good results, whereas other sugars, such as glucose and pullulan were less effective. Reproducible and consistent results were obtained with cartridges stored for a prolonged period and the biofunctionalized surface exhibited nearly no loss of bioactivity. The f-BPM biosensors dried for 2 days, 1 week and 3 weeks exhibited similar dose-response curves, indicating that the drying and rehydration processes do not significantly affect the sensor performance.

The results show that the sensor is highly suited for long-term storage in sugar matrices and for immediate use upon rehydration, both related to the fact that the sensor is based on freely diffusing particles. This study highlighted the development of a ready-to-use f-BPM biosensor based on dehydration with commonly used carbohydrate protectants. The long-term dry storage results showed that the f-BPM biosensor was stable in the presence of sucrose and trehalose for at least 3 weeks at ambient temperature in a vacuum chamber.

4.5 MATERIALS AND METHODS

Sugar mixtures with different mixing ratios have been tested for dry storage of the f-BPM sensor: (i) 25% w/w sucrose, 10 mM trehalose and 0.05% v/v Tween20 in Milli-Q (ii) 276 mM D-fructose, 184 mM D-glucose and 0.05% v/v Tween20 in Milli-Q (iii) 100 mg/mL Pullulan, 250 mM Trehalose and 0.05% v/v Tween20 in Milli-Q.

4.5.1 *Materials*

Custom-made fluid cell stickers were obtained from Grace Biolabs (USA). D-glucose, D-fructose, sucrose, trehalose, pullulan, PBS tablets, and NaCl were purchased from Sigma-Aldrich. Dynabeads MyOne Streptavidin C1 were purchased from ThermoFisher Scientific. Poly(l-lysine)-grafted poly(ethylene glycol) was purchased from SuSoS (Switzerland) with a grafting ratio of 3.5. The molecular weight of the PLL backbone and PEG side chains are 20 kDa and 2 kDa respectively. Azide functionalized PLL-g-PEG (Nanosoft Biotechnology LLC, USA) is composed of a 15 kDa PLL backbone and 2 kDa PEG chain with a grafting ratio of 3.5. The ssDNA oligonucleotides (standard desalting and HPLC purification for chemically modified DNA) used in the study were purchased from IDT (Integrated DNA Technologies).

Table 4.1: Composition of sugar mixtures for dry storage of the biocomponents

Sucrose/trehalose	25% w/w sucrose	10 mM trehalose	0.05% Tween20
Glucose/fructose	276 mM D-fructose	184 mM D-glucose	0.05% Tween20
Pullulan/trehalose	100 mg/mL pullulan	250mM trehalose	0.05% Tween20

4.5.2 *Preparation of biofunctionalized surfaces*

Glass slides (25 x 75 mm, #5, Menzel-Gläser) were pre-cleaned by 40 minutes of sonication in isopropanol (VWR, absolute) and 30 minutes of sonication in MilliQ. After the substrate was dried with a nitrogen stream, 1 minute of oxygen plasma was applied to the slides to plasma-oxidize the surface. PLL-g-PEG and PLL-g-

PEG-N_3 were pre-mixed in MilliQ with the ratio of 9:1 by weight at a final concentration of 0.45 mg/mL and 0.05 mg/mL respectively. Custom-made fluid cell stickers (Grace Biolabs) with an approximate volume of 20 μL were then attached to the substrate and the PLL-g-PEG/PLL-g-PEG-N_3 polymer mixture was immediately injected to the flow chamber and incubated for two hours. After the polymer self-assembled onto the negatively charged substrate, the unbound or loosely bound polymers were removed by withdrawing the solution out of the chamber.

The substrate-side binder is a partially double stranded DNA consisting of two complementary oligos, namely a 31nt oligo (3 ' C ATT ATT ACA AGC TAA GCT CTT GCA CTG ACG 5 ') and a DBCO functionalized oligo (5 ' CGA TTC GAG AAC GTG ACT GCT TTT T 3 ' DBCO). The 100 μM 31nt oligo was pre-hybridized with 100 μM DBCO functionalized oligo at a volume ratio of four to one. After removing the unbound or loosely bound PLL-g-PEG and PLL-g-PEG-N_3, the partially double stranded DNA was diluted to 1 μM with 500 mM NaCl in PBS (130 mM NaCl, 7 mM Na_2HPO_4, 3 mM NaH_2PO_4 at pH 7.4) and injected into the flow cell, followed by 72 hours of incubation at room temperature.

4.5.3 *The processes to dry and rehydrate the particles and the bio-functionalized surface*

Drying of bio-functionalized surface

The flow cell was washed with 20 μL of PBS, followed by the injection of 20 μL of the three sugar solutions. After 5 minutes of incubation, the top layer of the flow cell sticker was carefully removed. The exposed bio-functionalized surface was dried for 2 days in a vacuum chamber at room temperature.

Preparation of particles

1 μL of Dynabeads MyOne Streptavidin C1 (Invitrogen) was mixed with 1 μL of 10 μM biotinylated particle binder and 4 μL PBS. The mixture was incubated for 1 hour at room temperature (RT) on a rotating fin (VWR, The Netherlands). Subsequently, 1 μL of 100 μM polyT was added and the mixture was incubated for 15 minutes at RT on the rotating fin. Then the Eppendorf, containing the particle mix, was placed in a magnetic rack and 0.05% Tween20 in PBS was added to the height of the magnet, to

let the beads settle. Once the beads were settled, 0.05% Tween20 in PBS was added up to 1 mL. The beads were washed by turning the Eppendorf a few times in the magnetic rack. After the beads were settled again, the solution was removed and 1 mL of fresh PBS was added. Then, the solution was sonicated 10 times using a sonic finger (Amplitude 70 and Cycle 0.4; Hielscher, Ultrasound Technology). The solution was vortexed and diluted 3 times in fresh PBS. The solution was kept at RT on a rotating fin.

Drying of particles onto the surface

To prepare the particles the same procedure described in the previous section was executed until washing with 0.05% Tween20 in PBS. Subsequently, the washing solution was replaced with 250 μL PBS. The particles were vortexed shortly and 80 μL was added to a new Eppendorf. This Eppendorf was placed in the magnetic rack to let the beads settle. Once settled, the PBS was removed and 240 μL of sugar mix was added and the solution was sonicated with the sonic finger 10 times (Amplitude 70 and Cycle 0.4). Then, the particles were thoroughly vortexed. Subsequently, they were diluted 4 times to achieve a 3000-times dilution. This mixture was sonicated in the sonic bath for 20 seconds.

The chamber was gently washed with PBS (3x chamber volume). Then 20 μL of the particles in sugar solution was added. After 5 minutes the top layer of the flow cell was carefully removed and 10 μL of corresponding sugar mix was added. The slides were kept under vacuum for 2 days.

4.5.4 *Analysis of particle mobility*

Particle tracking was performed based on phasor localization, as described in Section 3.5.4. Event detection based on deep learning algorithm and analysis of switching activity, lifetimes, and bound fraction are described in Section 3.5.4.

4.6 APPENDIX

4.6.1 *The integration of the ready-to-use cartridges*

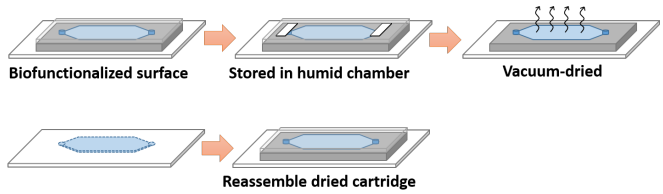

Figure 4.9: The integration process of the ready-to-use cartridges. The surface was first functionalized with low-fouling PLL-g-PEG layer and substrate-side ssDNA binders, and the particles was coupled with particle-side binders. After replacing the buffer with sugar mixtures, the top side of the chamber was removed and the whole surface was homogeneously exposed to air. The dehydration process was performed in a vacuum chamber, with the whole surface drying under similar conditions. When the dry storage was terminated, the flow cell sticker was removed. A new flow cell sticker was assembled onto the glass slide. Further rehydration process was done, followed by the activation process and the continuous monitoring of 11nt ssDNA targets.

Figure 4.9 shows the entire integration process for making the ready-to-use cartridges. The surface was first functionalized with low-fouling PLL-g-PEG layer and substrate-side ssDNA binders, and the particles were coupled with particle-side binders. After replacing the buffer with sugar mixtures, the whole sensor surface was dried. As shown in the third panel of Figure 4.9, the whole surface was homogeneously exposed to air and dried under similar conditions since we removed the top side of the chamber. When the dry storage was terminated, the flow cell sticker was removed, leaving a transparent film on the glass slide. A new flow cell sticker was assembled onto the transparent film. Further rehydration processes were done, followed by the activation process and the continuous monitoring of 11nt ssDNA targets. The particles show free Brownian motion after the rehydration process, leading to a low switching activity and bound fraction. During activation, an activator was present and particles can bind to the surface, resulting in an increased bound fraction. Furthermore, the interactions between the substrate binder and the activator are reversible, thus binding and unbinding events can take place. Once the activation process is terminated, the

bound fraction and switching activity should remain constant, since the free activators are washed away and no further binding can take place. Upon addition of an excess of competitors, the bound fraction and switching activity decrease.

4.6.2 *State lifetime analysis of ready-to-use f-BPM biosensors*

The dose-response curves for 11-nt analyte in terms of three output signals, i.e., the measured switching activity, bound fraction and unbound state lifetime, as a function of the applied target concentration are shown in Figure 4.10. The correspondence between the data points in panel a-c is highlighted by their colors. The four colors (orange, green, black, red) represent the wet sample, the ready-to-go cartridges with a dry storage period of 2 days, 1 week and 3 weeks respectively. The EC50 values extracted based on switching activity and bound fraction show a high similarity. However, the EC50 values are much higher for all data in panel c. The possible origins might be caused by the influence of multivalent binding and re-binding processes. The unbound lifetimes are significantly increased only when most of the particles are exhibiting transitions between single-binding states and unbound states.

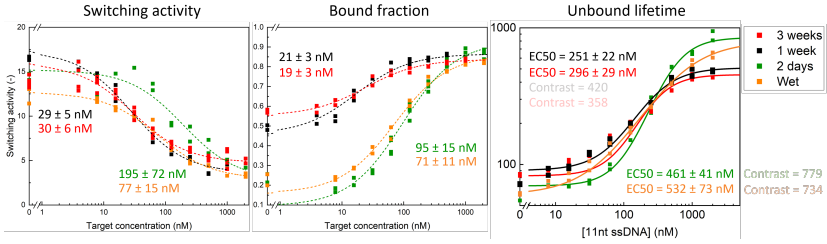

Figure 4.10: The dose-response curves for 11-nt analyte in terms of switching activity, bound fraction and unbound state lifetime. The correspondence between the data points in panel a-c is highlighted by their colors. The four colors (orange, green, black, red) represent the wet sample, the ready-to-go cartridges with a dry storage period of 2 days, 1 week and 3 weeks respectively.

4.6.3 *Sugar-based drying with glucose/fructose and pullulan/trehalose mixtures*

To prove that the sugar-based drying with the glucose/fructose mixture preserves the functionality of the oligonucleotides and PLL-g-PEG polymers on the surface, the biofunctionalized surface was dried with the procedure illustrated in Figure 4.1. The total dry storage time of the surface is 2 days. The particles were prepared separately without going through the dehydration and rehydration processes. The bound fraction and switching activity signal in Figure 4.11 shows that the system is capable of responding to activators and analytes. Both the bound fraction and switching activity increased during the activation process. The oligonucleotides are proven to be able to capture the complementary ssDNA after the dehydration and rehydration processes, and the low-fouling properties of PLL-g-PEG polymers are also preserved. Upon the addition of 1 μM ssDNA analyte, the bound fraction significantly reduced, indicating the competition between the analytes and the analogues. However, the corresponding switching activity remains similar before and after adding 1 μM of ssDNA analyte. The possible reason is that the activity dropped due to multivalent interactions.

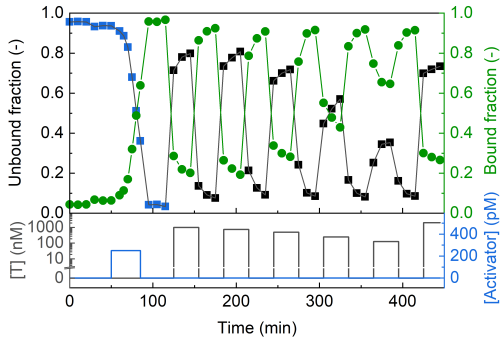

Figure 4.11: Response of a f-BPM biosensor after drying the surface with glucose/fructose. The top panel shows the unbound fraction measured during activation (blue) and sensing (red) process. The bound fraction is shown with green circles. Lines are guides to the eyes. The bottom panel represents the concentration profile of the 11nt ssDNA target (red) and the activator (blue). In the activation process, the bound fraction increased due to the higher switching frequency. Upon the addition of targets, the bound fraction decreased significantly, showing that the system responds to the presence of targets.

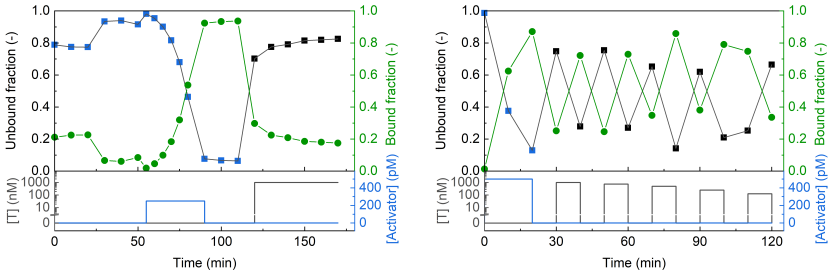

Figure 4.12: Response of a f-BPM biosensor after drying both the particles and the surface with the glucose/fructose and pullulan/trehalose mixtures. The top panel shows the unbound fraction measured during activation (blue) and sensing (red) process. The bound fraction is shown with green circles. Lines are guides to the eyes. The bottom panel represents the concentration profile of the 11nt ssDNA target (red) and the activator (blue). During the activation process, the bound fraction increased. Upon the addition of targets, the bound fraction decreased significantly. (a) The response of a f-BPM biosensor stored in the pullulan/trehalose mixture for two days. (b) The response of a f-BPM biosensor stored in the glucose/fructose mixture for two days.

Figure 4.12 shows the response of the f-BPM biosensors dried with the glucose/fructose and pullulan/trehalose mixtures respectively. The dehydration and rehydration procedures are illustrated in Figure 4.4. After two days of dry storage, the sugars were removed and the functionality of the f-BPM biosensors was tested by adding 250 pM activators and 1 μM analytes. The top panel indicates the bound fraction measured over time, while the bottom panel shows the switching activity as a function of time. Both the bound fraction and switching activity increased during the activation process. Upon the addition of 1 μM ssDNA analyte, the bound fraction significantly reduced, indicating the competition between the analytes and the analogues. The corresponding switching activity remained at a similar level due to multivalent interactions. In conclusion, glucose/fructose and pullulan/trehalose are both capable of preserving the functionality of biofuncitonalized particles and surfaces. The rehydrated f-BPM biosensors dynamically responded to the addition of activators and analytes. However, in comparison to glucose/fructose and pullulan/trehalose, the sucrose/trehalose mixture rehydrates easily and gave few stuck particles and the best uniformity. When the sucrose/trehalose layer starts to dissolve in PBS, the average mobility of particles increases and 90% of the particles release within

20 minutes. As for the glucose/fructose and pullulan/trehalose mixtures, the average time needed to reach 90% of unbound fraction is around 1 hour. Therefore, the sucrose/trehalose mixture is more suitable for developing a ready-to-use f-BPM biosensor.

4.6.4 *Rehydration process visualized by bright field microscopy*

In theory, even if the particles and substrates are coated with low-fouling materials such as PEG or oligonucleotides, freely-moving particles could still aggregate or non-specifically interact with the substrate or other non-relevant proteins over a longer time period, which is the main challenge for the long-term continuous monitoring by particle-based biosensors. When measuring in 50 kDa filtered blood plasma, we observed more particle aggregations compared to the tethered BPM system (t-BPM), as shown in Figure 4.13. This is mainly due to the higher probability of freely-moving particles getting into contact with each other. If too many particles are aggregated, the total statistics become low since the particle tracking software based on phasor localization can not recognize nor localize particle aggregates. Further studies are required to improve the anti-fouling properties of particle surfaces and substrate surfaces.

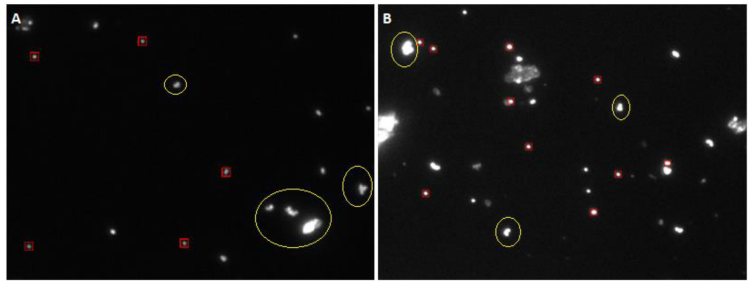

Figure 4.13: Particle aggregations observed in the presence of 50 kDa filter blood plasma. The yellow circles indicate that the aggregated particles cannot be tracked with phasor localization. The red squares label the properly tracked particles.

5

ORIENTED IMMOBILIZATION OF PCT ANTIBODIES ON ANTI-FOULING POLYELECTROLYTES

5.1 INTRODUCTION

Sepsis is a severe systemic inflammatory response syndrome of a human body against infection, usually caused by bacteria, and has lead to millions of global deaths every year.[81] The mortality rate in sepsis remains high (up to 30%)[82] and delayed diagnosis or inappropriate treatments may contribute to prolonged intensive care unit (ICU) stay.[83] In the last decades, various biomarkers such as acute-phase proteins and cytokines were investigated for the early diagnosis of sepsis. Among all, procalcitonin (PCT), C-reactive protein (CRP), interleukin (IL)-6, IL-8, and tumor necrosis factor-alpha (TNF-α) appear to show a positive correlation to sepsis.[84]

After exposure to bacterial products, levels of IL-6 and TNF-α have been shown to rise sharply within one hour, even before the onset of fever.[85,86] The very short half-life of IL-6 and TNF-α makes these biomarkers undetectable 24 hours after the onset of illness.[87,88] The level of CRP increases within 6–8 hours after tissue damages or infections and its half-life is 19 hours. Comparatively, CRP rises late following inflammation and since it can be elevated in both infectious and noninfectious states, it is generally recognized not to be specific for sepsis or infection.[89] PCT is significantly elevated (up to 5000-fold) within 2-4 hours in systemic inflammation or bacterial infections, and the level persists with a half-life of approximately 24 hours, making PCT an acute phase biomarker for diagnosis purposes.[90] PCT is generally detectable ($> 1\mu g/L$) in the plasma for 6-8 hours after infections, reaches a plateau after 12 hours, and then decreases to normal levels after 2 to 3 days.[87]

Procalcitonin, a small protein composed of 116 amino acids with a molecular weight of 13 kDa, is considered to be the main

biomarker of disorders that are accompanied by systemic inflammation and sepsis.[91] Serum PCT is more sensitive and specific than other serum biomarkers such as lactate, CRP, and IL-6.[92] PCT is expressed in multiple organ tissues.[92] In healthy individuals, serum PCT is intracellularly cleaved to calcitonin, and therefore the levels of PCT are normally below 0.01 μg/L. In severe bacterial infections and sepsis, serum PCT levels increase above 100 μg/L and decrease when patients are treated with proper antibiotics.[91] PCT levels correlate with the severity of bacterial infections and are usually low in viral infections, chronic inflammation, or post-surgical states. Hence, monitoring PCT levels in real-time can help detect the course of bacterial, fungal, or parasitic infections and assess the effectiveness of the therapeutic intervention as well.[93] PCT measurements in clinical practice can optimize the risk stratification and therapeutic decision-making when guiding the duration of antibiotic treatment.[94]

In recent years, various certified methods such as enzyme-linked immunosorbent assay (ELISA) and fluorescent immunoassays have been developed and broadly used for PCT detection in clinical applications. However, these diagnostic testings rely on centralized clinical laboratories, which takes typically a day. Since sepsis develops rapidly with a survival rate of 79.9% from the first hour and a sharp drop of 7.6% per hour, real-time detection and rapid diagnosis of PCT levels are needed to improve treatment outcomes and reduce mortality rates.[95] A platform with continuous sampling (e.g. via a catheter) that allows automatic continuous monitoring of acute-phase biomarkers is therefore a future direction for research to suit clinical needs.

In this study, the f-BPM sensing technique described in Section 3.2 is used to study the feasibility of rapid PCT detection, where we focus on the immobilization of anti-PCT antibodies on the biosensing substrate. Site-directed chemistry for antibody immobilization is helpful to maximize the performance of immunosensors. We aim at developing functionalization strategies in combination with anti-fouling polymer surfaces in order to preserve the binding potential of PCT antibodies. Among various methods, DNA-directed immobilization of antibodies has the advantage that it minimizes the risk of antibody denaturation during immobilization procedures.[96] To achieve DNA-directed immobilization

of PCT antibodies on oligonucleotide-functionalized PLL-g-PEG surfaces, we employed a novel glycan remodeling technique for DNA attachment on the Fc region of PCT antibodies.[97] To demonstrate the potential of the new strategy, detection of PCT molecules is performed through a sandwich assay using the f-BPM technique, where the PCT analyte simultaneously binds to the anti-PCT antibody coupled on the particles and another type of anti-PCT antibody immobilized on the surface. We have achieved a limit of detection of 10 pM, dynamic range of 10-1000 pM, and total detection time of 5 min for monitoring PCT. A comparative study was performed in order to evaluate the differences in the antibody orientation among physisorption and site-specific immobilization strategies.

5.2 COUPLING STRATEGY

5.2.1 *Glycan antibody remodeling technique*

A simple and robust strategy based on the remodeling of N-glycans for site-specific conjugation of a drug to an antibody was reported by van Geel et al.[97] Glycans are sugar groups that are attached to proteins in post-translational modification steps. For further modification purposes, the glycan can be remodeled to contain a functional group. Glycan remodeling strategies are suitable for all human antibodies because they all have a glycosylation site, which is at asparagine (Asn) located approximately at the 300^{th} amino acid in the Fc region of the antibodies. Approximately 20% of human antibodies also have a glycosylation site at Asn 88 of the heavy chain. In this case, the glycosylation site is located in the Fab region.[97] Hence, antibodies with only the glycosylation site at the Fc region such as the PCT antibody 13B9 are selected to ensure the site-specific modification of the Fc region only.

As shown in Figure 5.1, the glycan remodeling technique is a three-step approach. Most of the glycan is trimmed using Endoglycosidase S, leaving one N-acetylglucosamine at each side of the Fc region. Then a designed sugar (UDP-GlcNAc-N_3) can be tagged to the remaining N-acetylglucosamine on the antibody by endo-β-N-acetylglucosaminidase, an enzyme catalyzed by manganese (II) chloride. The enzymatic connection enables the splitting of the GlcNAc-N_3 and the phosphates, followed by the glycosylation of GlcNAc-N_3 onto the remaining N-acetylglucosamine. The azide (N_3) group creates an anchor point for conjugating various drugs or biomolecules via second-generation copper-free click chemistry.[97]

DBCO-tagged single-stranded DNA can be attached to the azide groups on the Fc region of the antibody, forming an ssDNA-antibody conjugate. In order to achieve DNA-directed immobilization of antibodies, another ssDNA with complementary sequences needs to be coupled to the surface. Therefore, the glass substrate was first functionalized with PLL-g-PEG/PLL-g-PEG-azide polymer mixtures by physisorption based on electrostatic interactions. DBCO-tagged ssDNA was coupled to the azide

groups on the PLL-g-PEG surface via click chemistry. Next, two ssDNA were hybridized to the ssDNA on the surface for capturing the ssDNA-antibody conjugates. Finally, the ssDNA attached to the antibody was hybridized with the overhang connected to the surface. The result would be an antibody immobilized on the surface with exposed Fab parts, which are accessible for epitopes.

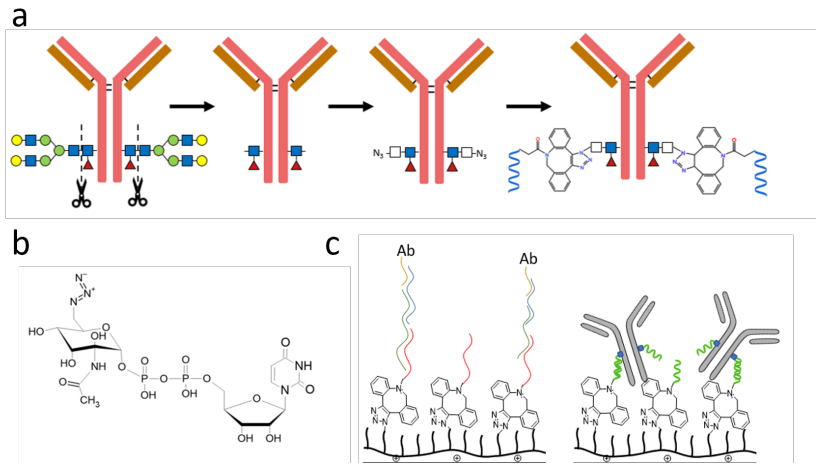

Figure 5.1: Oriented immobilization of PCT antibodies. (a) Schematic overview of glycan remodeling procedure followed by DNA conjugations. First, the glycans were removed from the antibody by Endoglycosidase S, which splits the glycans between the two N-acetylglucosamines (blue squares). The sugar UDP-GlcNAc-N_3 (white square) was then attached to the glycosylation site by endo-β-N-acetylglucosaminidase. Finally, DBCO-tagged ssDNA was attached to the azide group by copper-free click chemistry.[98] (b) Detailed molecular structure of the sugar UDP-GlcNAc-N_3. (c) Immobilization of the ssDNA-antibody conjugates on PLL-g-PEG surfaces. The glass substrate was first functionalized with PLL-g-PEG/PLL-g-PEG-azide polymer mixtures by physisorption based on electrostatic interactions. DBCO-tagged ssDNA with complementary sequences was coupled to the azide groups on the PLL-g-PEG surface. The left image shows two complementary ssDNA strands sequentially hybridized to the ssDNA on the surface, with the ssDNA-antibody conjugates bound to the last ssDNA strand. The right image is a simplification that shows how the antibody is bound to the PLL-g-PEG surface.

5.3 RESULTS AND DISCUSSION

Two critical steps in the development of the immunoassay for PCT detection are the conjugation and characterization of antibody-oligonucleotide conjugates. We started with a very robust antibody, trastuzumab, for testing the conjugation and characterization protocols. Having proven that the oligonucleotides can be coupled to the Fc region of trastuzumab, further modification of PCT antibody 13B9 was then executed (see Section 5.3.2).

5.3.1 *Trastuzumab remodeling*

Modification of Trastuzumab

The glycan remodeling copper-free click strategy developed by Synaffix is based on a three-stage process: (i) trimming of all glycan isoforms on the antibodies with an endoglycosidase to liberate the GlcNAc on the Fc region; (ii) enzymatic transfer of a galactose residue utilizing a glycosyl transferase for attaching the azido-modified GalNAc analogue; and (iii) copper-free click conjugation of BCN or DBCO modified molecules, which is DBCO-modified ssDNA in our case.

Gel electrophoresis of Trastuzumab-ssDNA conjugates

The glycan remodeling technique was first performed on trastuzumab as a model system. The excess of the unreacted sugars and enzymes were removed by 10 kDa molecular weight cut-off spin columns. Since there are three steps in the glycan remodeling strategy, the mass of the reduced antibody samples before and after each step was characterized by gel electrophoresis and was used to confirm the modification and conjugation yield. Figure 5.2 shows the gel electrophoresis results of the reduced Trastuzumab, the modified Trastuzumab, and the Trastuzumab-ssDNA conjugates. Since the intact antibody mass is much larger than the mass of the ssDNA, the antibody samples were reduced by dithiothreitol (DTT) prior to the gel electrophoresis to be able to see a clearer difference of the mass changes. DTT is a reducing reagent that can cleave the disulfide bridges connecting the heavy chains and light chains of the antibodies. The reduced antibody samples were separated by sodium dodecyl sulfate-polyacrylamide gel electrophoresis (SDS-PAGE) using a

10% polyacrylamide separation gel. The protein standard was loaded in lanes 1, 7, and 11 of the gel as a reference for the estimation of mass. The gel was also stained with SYBR gold for visualizing the presence of ssDNA. (See Appendix 5.6.1)

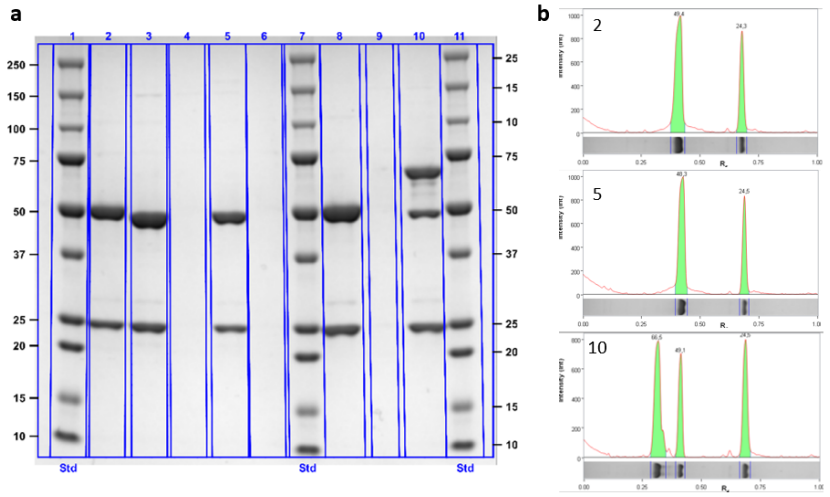

Figure 5.2: Protein gel of different states of reduced modified Trastuzumab stained with Coomassie Brilliant Blue. (a) Lane 1: Protein standard; lane 2: Trastuzumab; lane 3: Glycan trimmed Trastuzumab; lane 4: Enzymes for glycan trimming; lane 5: Azido-modified Trastuzumab; lane 6: Materials for azide modification; lane 7: Protein standard; lane 8: Negative control sample (non-modified Trastuzumab incubated with DBCO-ssDNA); lane 9: DBCO-ssDNA; 10: ssDNA-Trastuzumab conjugates; lane 11: Protein standard. (b) The intensity profiles of the detectable bands in lanes 2, 5, and 10.

The mass of the heavy chains and light chains are approximately 50 kDa and 25 kDa respectively. The total mass of an antibody, which is composed of two light chains and two heavy chains, is 150 kDa. The mass changes caused by the trimming of glycan on the Fc region of the heavy chains can be seen by comparing lane 2 (unmodified Trastuzumab) and lane 3 (trimmed Trastuzumab) in Figure 5.2. There is a shift of mass for the band near 50 kDa, representing the mass changes of the heavy chains. The band at 25 kDa remains unchanged, indicating that there is no mass difference in the light chains before and after the glycan trimming process. We conclude that the trimmed glycans occurred only on the heavy chains. To further characterize the mass changes with higher accuracy, we measured the antibody samples with LC-MS and the results can be found in the

Master thesis of Maud Linssen.[98] It can be concluded based on the LC-MS results that the trimming of glycans by Endoglycosidase S is fully completed. The coupling of the azido-modified GalNAc analogue to the antibodies can also be seen when comparing lane 3 (trimmed Trastuzumab) and lane 5 (azido-modified Trastuzumab) in Figure 5.2. A slight increase in the mass only occurred for the heavy chains, while the band representing the light chains remained unchanged.

After modifying the Fc region of Trastuzumab with clickable azide groups, the DBCO-tagged ssDNA was covalently coupled to the heavy chains. As described in the previous paragraph, gel electrophoresis results are not capable of determining the modification efficiency due to low mass changes caused by the attached azide. However, the mass of the attached DBCO-ssDNA is large enough to cause a clear separation in the band of those unconjugated heavy chains and the conjugated ones. Hence, gel electrophoresis was used to confirm the conjugation of DBCO-ssDNA and to estimate the conjugation efficiency. As shown in lane 10 of Figure 5.2, two main bands were detected at 49.1 kDa and 66.5 kDa. The band at 49.1 kDa in lane 10 (ssDNA-Trastuzumab conjugates) is at approximately the same relative migration distance as the band representing heavy chains in lane 5 (Modified Trastuzumab), indicating that there are a fraction of heavy chains without ssDNA. The second band at 66.5 kDa is 17.4 kDa heavier than the original heavy chain (50 kDa) of the azido-modified Trastuzumab. In theory, the attachment of ssDNA onto the heavy chain should cause an increase of approximately 11.8 kDa in the mass. The observed mass changes in the second band are larger than expected. The possible origin is due to the different structures of DNA and proteins. Since we utilize protein gels to run the samples containing DNA, different migration behaviors can occur when running the gel. Therefore, the actual mass changes caused by the attachment of DBCO-ssDNA can not be accurately quantified by the observed relative migration distances in protein gels. The standard protein ladder can not be used as a reference to estimate the mass of samples containing DNA. However, by staining the same protein gel with SYBR gold (See Appendix 5.6.1), we are able to confirm that the mass changes of 17.4 kDa observed in lane 10 at 66.5 kDa were indeed

caused by the presence of ssDNA since the band at 66.5 kDa shows high fluorescence.

The fraction of heavy chains containing ssDNA can be estimated by calculating the relative quantity of the heavy chains with and without ssDNA. The intensity of the band representing non-conjugated heavy chains at 49.1 kDa in lane 2 of Figure 5.2 was set to 1 as a reference quantity. The intensity of the band at 49.1 kDa in lanes 3, 5, and 10 can be compared to that of lane 2 by using Image Lab software. The conjugation efficiency was calculated by the intensity ratio of the band at 66.5 kDa (Heavy chain-ssDNA conjugates) and the band at 49.1 kDa (non-conjugated heavy chains) in lane 10 of Figure 5.2. In conclusion, the yield of the heavy chains containing ssDNA is approximately 65%.

Optimization of the conjugation efficiency of the Trastuzumab-ssDNA conjugates

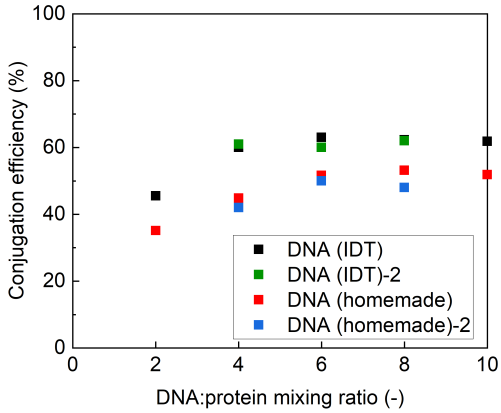

Figure 5.3: Optimization for the conjugation yields of homemade DBCO-ssDNA (red and blue) and DBCO-ssDNA purchased from IDT (black and green). The azido-modified Trastuzumab was incubated with DBCO-ssDNA's. The y-axis represents the antibody to DBCO-ssDNA ratios used in the conjugation process.

The conjugation protocol for ssDNA-Trastuzumab complexes was tested by mixing different ratios of DBCO-ssDNA and azido-modified Trastuzumab. Our goal was to use the minimum amount of DBCO-ssDNA for achieving the highest conjugation efficiency. The amount of unbound DBCO-ssDNA should be as little as possible since they can also hybridize with the

substrate-side binders and eventually decrease the density of ssDNA-antibody conjugates used in the assay, causing interferences in the assay performance. Two different DBCO-ssDNA's were tested with different mixing ratios to the antibodies for achieving a higher conjugation efficiency. The two oligos were obtained by either direct purchase from IDT or by attaching DBCO-PEG4-NHS ester to amine-modified ssDNA via amine coupling. The modification protocol and the sequence are described in Section 5.5.3. Figure 5.3 demonstrates the conjugation efficiency of the two DBCO-ssDNA with the specified mixing equivalents in the x-axis. The corresponding gel results used to estimate the conjugation efficiency of different DBCO-ssDNA's with different mixing ratios are shown in Figure 5.4 and 5.5.

As shown in Figure 5.3, the conjugation efficiency increases with increasing mixing equivalent of DBCO-ssDNA. In general, the conjugation efficiency of the DBCO-ssDNA purchased from IDT is approximately 10% higher for all mixing ratios compared to that of the homemade DBCO-PEG4-ssDNA. The lower conjugation efficiency observed in the homemade DBCO-PEG4-ssDNA might be caused by the steric hindrance of PEG4, making it more difficult for the DBCO-PEG4-ssDNA to interact with the azide groups on the Trastuzumab.

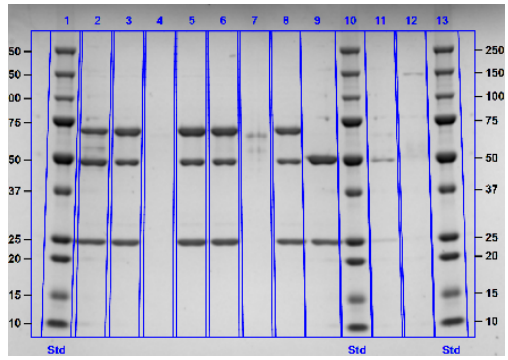

Figure 5.4: Protein gel of modified Trastuzumab incubated with different ratios of DBCO-ssDNA purchased from IDT. The lanes 1 to 13 were loaded with the following samples respectively: Protein standard; Trastuzumab conjugated with ratio 1:1.3; Trastuzumab conjugated with ratio 1:2.6; Conjugation blank; Trastuzumab conjugated with ratio 1:3.9; Trastuzumab conjugated with ratio 1:5.1; Conjugation blank; Trastuzumab conjugated with ratio 1:6.4; Trastuzumab; Protein standard; Modified Trastuzumab; Modification blank; Protein standard.

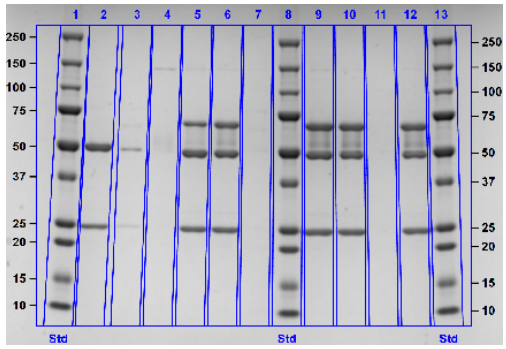

Figure 5.5: Protein gel of modified Trastuzumab incubated with different ratios of homemade DBCO-ssDNA based on amine coupling. The lanes 1 to 13 were loaded with the following samples respectively: Protein standard; Trastuzumab; Modified Trastuzumab; Modification blank; Trastuzumab conjugated with ratio 1:1.3; Trastuzumab conjugated with ratio 1:2.6; Conjugation blank; Protein standard; Trastuzumab conjugated with ratio 1:3.9; Trastuzumab conjugated with ratio 1:5.1; Conjugation blank; Trastuzumab conjugated with ratio 1:6.4; Protein standard.

5.3.2 *PCT antibody remodeling*

Based on the modification protocol and conjugation protocol tested for trastuzumab, we continued with the modification of PCT antibodies and further biomedical applications of the ssDNA-PCT antibody conjugates. The PCT antibody 13B9 was chosen based on their weaker affinities to PCT molecules. The modification and conjugation processes used in this section are the same as described in Section 5.3.1. The characterization of the ssDNA-PCT antibody conjugates was executed by both LC-MS and gel electrophoresis. The detailed results and deconvoluted mass spectra of the heavy chains of PCT antibody 13B9, glycan trimmed 13B9, and the modified 13B9 can be found in the Master thesis of Maud Linssen.[98] In conclusion, the conjugation efficiency of the ssDNA-13B9 was approximately 53.5%. The conjugation efficiency was lower than ssDNA-Trastuzumab, which is 65%.

For the conjugation of oligonucleotides to PLL-g-PEG surfaces, we applied the same covalent coupling strategy as described in Section 2.2.1, which is based on the second generation of click chemistry. Thereafter, the antibody-oligonucleotide conjugates were attached to the PLL-g-PEG surface via DNA hybridizations.

5.3.3 *Immobilization of PCT antibodies on anti-fouling polyelectrolytes and sensing functionality*

The functionality of the ssDNA-13B9 conjugates was tested with the f-BPM biosensors described in Section 3.2. The binding ability of the ssDNA fragment and the antibody 13B9 were tested by DNA hybridization of the ssDNA-13B9 conjugates and by PCT sandwich assays respectively. To prove that the ssDNA conjugated onto the 13B9 antibody is functional, we first coupled the ssDNA-13B9 conjugates onto particles functionalized with complementary ssDNA. Thereafter, we performed the PCT sandwich assay with the ssDNA-13B9 functionalized particles and 27A3 physisorbed glass. The functionality of ssDNA fragments on the conjugates can be proved by the attachment of antibodies on the particles and the binding of PCT molecules.

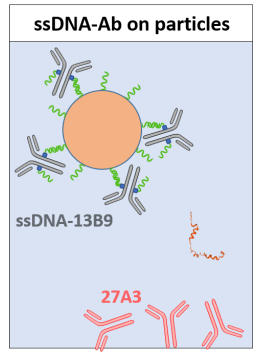

Figure 5.6: The schematic overview of the molecular system with ssDNA-13B9 conjugates immobilized on particles for performing the PCT sandwich assay. The 27A3 antibodies (pink) were physisorbed onto a glass surface. The streptavidin-coated 1μm particles were functionalized with initial biotinylated oligos (green) based on biotin-avidin interactions. The ssDNA-13B9 conjugates (grey) were coupled to the initial biotinylated oligos on the particles via DNA hybridization. The PCT molecules (red) can simultaneously bind to ssDNA-13B9 on the particles and 27A3 on the surface, forming a target-induced sandwich bond. The presence of PCT molecules was detected by analyzing the mobility changes of particles. In a PCT sandwich assay, higher concentrations of PCT lead to a higher bound fraction.

The molecular design of the PCT sandwich assay is shown in Figure 5.6. The 27A3 antibodies were physisorbed onto a glass surface and the surface was blocked with 1% BSA. The streptavidin-coated 1μm particles were functionalized with initial biotinylated oligos based on biotin-avidin interactions. The

ssDNA-13B9 conjugates were coupled to the initial biotinylated oligos on the particles via DNA hybridization. After providing the 27A3 coated surface with the 13B9 functionalized particles, the PCT molecules were added from low concentrations to high concentrations. The applied concentration range was 50 pM to 10 nM. The experiment was performed twice with two assay buffers (PBS or 0.1% BSA in PBS).

The free-diffusion-based biosensing by particle mobility (f-BPM) described in Chapter 3 was utilized to perform PCT sandwich assays. To perform a sandwich assay, the particles and the sensor surface are functionalized with affinity binders (PCT antibodies) specific to the target molecule (PCT), and particles are tracked over time using video microscopy. When target molecules are absent, the particles exhibit free Brownian motion. At higher target concentrations, target-induced sandwich complexes are formed between the particle and the sensor surface, restricting the particle motion intermittently to a confined area. In the case of a PCT sandwich assay, the bound fraction is low for low target concentration and increases with higher target concentrations.

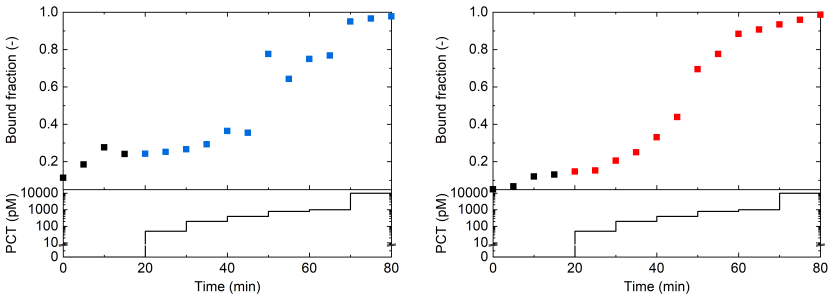

Figure 5.7: Dynamic response to target concentration of an f-BPM sensor with 1 μm particles, for a PCT sandwich assay in PBS and in 0.1% BSA. The particles are functionalized with ssDNA-13B9 conjugates via DNA hybridizations, while the surface is modified with physisorbed 27A3 antibodies. The top panels show the bound fraction measured over time. The bottom panels show the applied concentration profiles of PCT. (a) The bound fraction was measured over time with different PCT concentrations in PBS buffer. The black data points represent the background signal without the presence of PCT molecules. The blue data points represent the signal measured in the presence of PCT. (b) The bound fraction was measured over time with different PCT concentrations in 0.1% BSA. The black data points represent the background signal without the presence of PCT molecules. The red data points represent the signal measured in the presence of PCT.

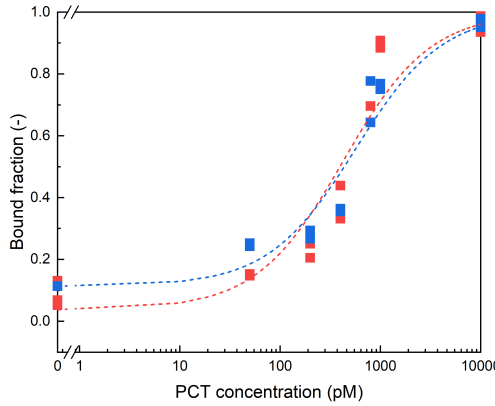

Figure 5.8: Dose-response curves of PCT sandwich assay performed in 0.1%BSA (red) and PBS (blue), with EC50 values of 502 ± 110 pM and 625 ±118 pM respectively.

The bound fractions measured over time with gradually increasing PCT concentrations are plotted in Figure 5.7a and 5.7b. The two bottom panels show the sequence of corresponding PCT concentrations applied over time. The results in Figure 5.7a were measured in PBS, while the data in Figure 5.7b were performed in 0.1% BSA. Both results show a clear response to different PCT concentrations, indicating that the ssDNA-13B9 conjugates were successfully coupled onto the particles and the antibody activity was retained. Please note that the binding affinity of the antibody pair 13B9-27A3 is much stronger compared to the oligonucleotide-based system described in Section 3.3.1. Since normal washing steps cannot release the PCT molecules, we only measured with increasing analyte concentrations.

The two dose-response curves measured in 0.1% BSA and PBS are comparable, as shown in Figure 5.8. The EC50 values for the two dose-response curves were determined by Hill equation fits. The EC50 values were 502 ± 110 pM and 625 ± 118 pM for 0.1% BSA and PBS respectively. Despite that the EC50 values and dynamic range observed in the two assay buffers are similar, it is recommended to use 0.1% BSA as the assay buffer since the background signal is lower and the fluctuations in the signal are smaller. The hypothesis is that the presence of 0.1% BSA might stabilize proteins and antibodies, leading to a lower degree of non-specific interactions.

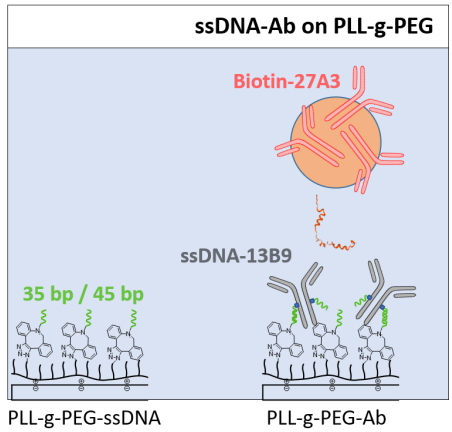

Figure 5.9: The schematic overview of the molecular system with ssDNA-13B9 conjugates immobilized on PLL-g-PEG surfaces for performing the PCT sandwich assay. The biotinylated 27A3 antibodies were coupled to streptavidin-coated 1μm particles via biotin-avidin interactions and the ssDNA-13B9 conjugates were immobilized onto oligonucleotides functionalized PLL-g-PEG surface via DNA hybridizations. The PCT molecule (red) can simultaneously bind to 27A3 (pink) on the particles and ssDNA-13B9 (grey) on the surface, forming a target-induced sandwich bond. The restricted motion of particles can be optically detected.

Having proven that the ssDNA-13B9 conjugates are still functional and the ssDNA fragments can bind to complementary DNA, the next step is to immobilize the ssDNA-13B9 conjugates onto the anti-fouling PLL-g-PEG surface. The schematic illustration of the molecular system is shown in Figure 5.9. The biotinylated 27A3 antibodies were coupled to streptavidin-coated 1μm particles via biotin-avidin interactions and the ssDNA-13B9 conjugates were immobilized onto oligonucleotides functionalized PLL-g-PEG surface via DNA hybridizations. Two different sequences of oligonucleotides (green) were tested as shown in Figure 5.10a and 5.10b. The number of nucleotides of the longest DNA sequence used in the hybridization is 13 base pairs (Figure 5.10a) and 20 base pairs (Figure 5.10b). The detailed sequences of all the DNA strands are shown in the Methods section 5.5.3. The PCT molecules (red) can simultaneously bind to 27A3 (pink) on the particles and ssDNA-13B9 (grey) on the surface, forming a target-induced sandwich bond. The presence of PCT molecules causes a decrease in the mobility of particles. Therefore, higher concentrations of PCT lead to a higher bound fraction.

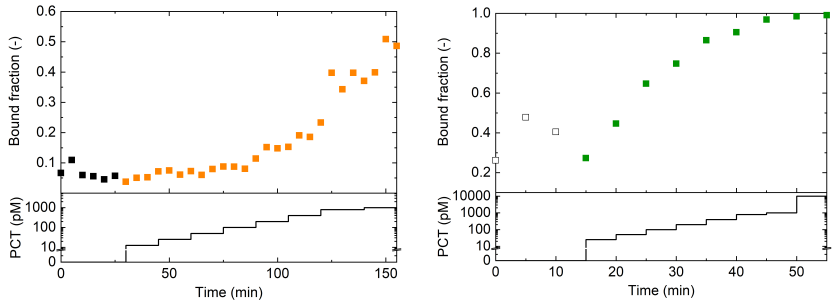

Figure 5.10: Dynamic response to target concentration of an f-BPM sensor with 1 μm particles, for a PCT sandwich assay in 0.1% BSA. The biotinylated 27A3 antibodies were coupled to the particles and the ssDNA-13B9 conjugates were immobilized onto the PLL-g-PEG surface. The top panels represent the measured bound fraction, while the bottom panels show the concentration profiles of PCT. (a) The bound fraction was measured over time with different PCT concentrations by the molecular system utilizing hybridization of 13 base pairs. The black data points represent the background signal without the presence of PCT molecules. The orange data points represent the signal measured in the presence of PCT. (b) The bound fraction was measured over time by the molecular system utilizing hybridization of 20 base pairs. The green data points represent the signal measured in the presence of PCT. The hollow squares are the data points measured at zero PCT concentration. The observed fluctuations in the signal measured at zero PCT concentration might be due to non-specific interactions or the inhomogeneity on the surface.

For both systems employing different sequences of DNA hybridization, an increase in the bound fraction was observed with gradually increasing PCT concentrations, indicating that the ssDNA-13B9 can be conjugated onto the PLL-g-PEG surface with different designs of capturing oligonucleotides. In theory, if the utilized DNA hybridization for capturing the ssDNA-13B9 is stronger, the dissociation and detachment of the conjugates should occur less and therefore the system becomes more stable. Since the 13 base pairs of DNA hybridization is relatively weaker and the 20 base pairs of DNA hybridization is more stable, we expect the 20 base pair system to respond to the addition of PCT molecules in a lower concentration region. The results shown in Figure 5.10b indicate that the bound fraction appears to have a significant increase at approximately 100 pM. In comparison, the 13 base pair system started to respond to the addition of analyte at the concentration region of 500 pM.

The EC50 values were found to be 132 ± 26 pM and 1236 ± 124 pM for the 20 and 13 base pair systems respectively. The EC50 values extracted from the 13 base pair system are larger than the EC50 of the 20 base pair system due to the weaker DNA hybridization for capturing the ssDNA-13B9 conjugates onto the PLL-g-PEG surface. The thermal dissociation rate at which the dissociation of the shortest hybridized DNA occurs is calculated in Appendix 5.6.2. The weakest hybridization of the 20 base pair system is much stronger compared to that of the 13 base pair system. Therefore, It is expected that the hybridized DNA dissociated over time in the 13 base pair system during the measurements, causing a gradual decrease in the number and density of 13B9 antibodies immobilized on the surface. Furthermore, most of the dissociated ssDNA-13B9 conjugates cannot re-bind to the PLL-g-PEG surface because of the continuous flow of fluid.

The EC50 values of all experiments shown in Figure 5.7a, 5.7b, 5.10a, and 5.10b are listed and compared in Table 5.1 to assess the sensitivity of the different molecular systems. As a reference, the dose-response curve measured with the molecular system shown in Figure 5.11a performed by Khulan Seregelen is also included. The non-directional coupling-based system utilizes the physical adsorption of 13B9 on the surface and the non-directional binding of 27A3 on particles via biotin-avidin interactions. The dose-response curve (black) measured with the non-directional coupling-based system is shown in Figure 5.11b as a reference.

As shown in Table 5.1, the systems including physical adsorption of antibodies on glass surfaces give similar EC50 values, which is approximately 500-650 pM, indicating the sensitivity and dynamic range do not show a clear difference while changing the coupling strategy employed on the particles. However, since we used a lower concentration of the ssDNA-13B9 conjugates for modifying particles in comparison with the non-directional system, it is not clear whether the directional coupling of antibodies on particles improves the stability or binding capacity or not. Further quantification of antibodies on both particle-side and substrate-side is needed.

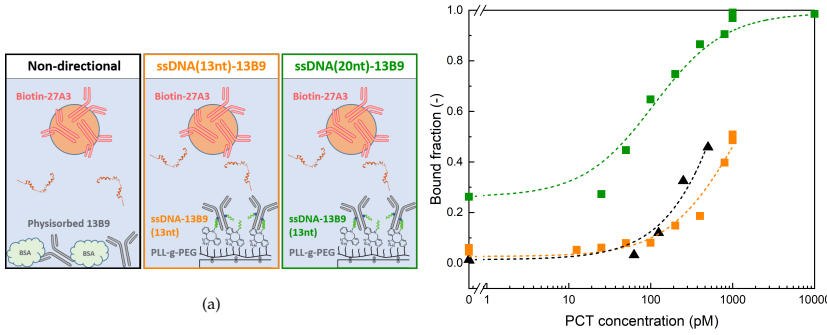

Figure 5.11: (a) The schematic overview of the particle and surface fictionalizations based on non-directional coupling and directional coupling. The left panel (black) represents the system utilizing physical adsorption of 13B9 on the surface and non-directional coupling of biotinylated 27A3 on particles. The middle panel (orange, 13nt) and right panel (green, 20nt) represent the systems utilizing directional coupling of 13B9 on PLL-g-PEG surfaces based on different sequences of complementary DNA hybridization. (b) The dose-response results were obtained with directionally coupled and non-directionally coupled antibodies for comparative studies. Green data points represent the molecular system utilizing hybridization of 20 base pairs, while orange data points represent the 13 base pairs system. The fitted EC50 values are 132 $\pm$ 26 pM (green), 1236 $\pm$124 pM (orange), and 657 $\pm$ 90 (black).

The PCT sandwich assay results obtained by the system using oriented immobilization of ssDNA-13B9 conjugates on the PLL-g-PEG surface showed a significantly lower EC50 value in comparison with the rest of the EC50 values, indicating that the system shows a higher sensitivity. The quantification of antibodies on surfaces is still critical. The antibody coverage on different surfaces was not measured, but it can be theoretically estimated. The density of antibodies based on physical adsorption is approximately 1.5 mg/m^2.[99] In the click-based PLL-g-PEG system, the theoretical antibody coverage is approximately 1.5×10^{-6} mg/m^2. Therefore, the observed improvement in the sensitivity of the biosensor can be caused by; (i) the fraction of functional 13B9 antibodies immobilized on the surface is larger, causing a higher probability of forming a sandwich bond (ii) the oriented immobilization of the ssDNA-13B9 conjugates leads to a higher binding capacity due to more exposed Fab sites available for the binding of PCT molecules, or (iii) the covalent coupling and strong DNA hybridization of 13B9 antibodies on the surface lead to a slower dissociation and detachment of antibodies.

Table 5.1: The EC50 values were measured with the listed systems, involving different types of antibodies, antibody orientations, particle and substrate functionalizations, coupling strategies, and assay buffers. The surface of particles and substrates was either functionalized with physisorbed antibodies or directionally coupled antibodies. The physisorbed antibodies were blocked with BSA. The two assay buffers are 0.1% BSA and PBS.

Surface functionalization	**Particle functionalization**	**Assay buffer**	**EC50 (pM)**
Physisorbed 13B9 on glass	Biotinylated 27A3	0.1% BSA	657 $\pm$ 90*
Physisorbed 27A3 on glass	ssDNA-13B9 immobilized on particles	PBS	502 $\pm$ 110
Physisorbed 27A3 on glass	ssDNA-13B9 immobilized on particles	0.1% BSA	625 $\pm$ 118
ssDNA-13B9 immobilized on PLL-g-PEG (13 bp)	Biotinylated 27A3	0.1% BSA	132 $\pm$ 26
ssDNA-13B9 immobilized on PLL-g-PEG (20 bp)	Biotinylated 27A3	0.1% BSA	1236 $\pm$124*

5.4 CONCLUSION

We have studied a sensor surface suitable for continuous monitoring of PCT molecules. We have employed the glycan remodeling technique and explored the methodology for immobilizing anti-PCT antibodies on the sensor surface and on the particles with a specific orientation. The Fc region of the anti-PCT antibodies was enzymatically modified to enable covalent attachment of single-stranded DNA via copper-free click chemistry. Based on the mass spectrometry results, the glycan modification efficiency of Trastuzumab and PCT antibody 13B9 was estimated to be 77% and 54% respectively. When coupling ssDNA onto the Fc of antibodies, four equivalents of DBCO-ssDNA is needed to achieve an optimal conjugation efficiency, which is approximately 80% measured using SDS-PAGE.

The functionality of the ssDNA-antibody conjugates immobilized on either the particle surface or the substrate surface was tested via the f-BPM technique. The approach involves particles coated with one type of anti-PCT antibody and a surface functionalized with another type of detection anti-PCT antibody, allowing the particles to switch from unbound state to bound state once the PCT analyte simultaneously binds to the two antibodies. Based on this PCT sandwich assay, the fraction of bound particles rises in response to increasing PCT concentrations. PCT concentrations were detectable within a range of 10 pM-1000 pM with a detection time of 5 min. When immobilizing anti-PCT antibody 13B9 to a PLL-g-PEG surface with a specific orientation, the EC_{50} extracted from the dose-response curve was lower compared to physisorbed antibodies, indicating a higher sensitivity. Since the theoretical coverage of the antibodies on the PLL-g-PEG surface is lower than the physisorbed antibodies, we conclude that possibly the loss of antibody activity due to misorientation has been reduced for antibodies on the PLL-g-PEG surface and more binding sites on the antibodies remain functional and accessible.

Given the specificity and clinical relevance of PCT antibodies and the anti-fouling properties of PLL-g-PEG surfaces, we believe the development of the anti-PCT antibody functionalized PLL-g-PEG surface with specific orientation is of importance for

future development of diagnostic platforms for sepsis without having to rely on centralized clinical laboratories. The f-BPM biosensors were used as a model system to indicate the feasibility of continuous monitoring of PCT molecules. However, further tests on studying the reproducibility and specificity of this assay and the reversibility of the antibody-antigen binding are needed to meet the requirements of clinical detection.

5.5 MATERIALS AND METHODS

5.5.1 *Materials*

All chemicals were purchased at Sigma Aldrich unless stated otherwise. The enzymes endoglycosidase S, endo-β-N-acetylglucosaminidase, trastuzumab, manganese (II) chloride, and UDP sugar (UDP-GlcNAc-N_3) were provided by Synnafix. PCT antibodies type 13B9 and 27A3 were provided by HyTest. Tris, glycine, SDS running buffer, Laemmli loading buffer, Coomassie brilliant blue R-250, and Precision plus protein standard were purchased from Bio-Rad. Novex wedge well 4-20% tris glycine gels were purchased from Invitrogen. SYBR gold and Dynabeads MyOne streptavidin C1 were purchased from Thermo Fischer Scientific. Oligonucleotides were purchased from Integrated DNA Technologies (IDT).

5.5.2 *Glycan remodeling technique*

Glycan remodeling technique developed by Synaffix

Antibodies were pre-concentrated to a concentration of approximately 15 mg/mL using Amicon® Ultra 0.5 mL Ultracel 10K spin filters. Thereafter, the protein concentration was estimated by UV absorbance using a NanoDrop spectrophotometer 2000 (Thermo Fisher Scientific) with the A280 mode. 20 μg Endoglycosidase S and two micromole manganese (II) chloride were added to 100 μL concentrated antibodies for deglycosylation.

The deglycosylation process was executed overnight on a shaker at 30°C. After the deglycosylation, 90 μg of Glycosyltransferase and 0.3 micromoles of UDP-GlcNAc-N_3 were added. The attachment of UDP-GlcNAc-N_3 proceeded for 9 hours on a shaker at 30°C. Unbound UDP-GlcNAc-N_3 was filtered out using Amicon® Ultra 0.5 mL Ultracel 10K spin filters.

5.5.3 *Characterization of the ssDNA-antibody conjugates*

Conjugation of ssDNA

Two types of DBCO-ssDNA, including the one purchased from IDT (5 ′ CGA TTC GAG AAC GTG ACT GCT TTT T 3 ′-DBCO)

and the other homemade DNA (5 ′ GTC TGT AGA CAG TTT CAT CGG TGA C 3 ′ -PEG4-DBCO) were coupled to the azido-modified 13B9 antibodies respectively. The homemade DBCO tagged ssDNA (5 ′ GTC TGT AGA CAG TTT CAT CGG TGA C 3 ′ -PEG4-DBCO) was prepared by labeling amine-modified oligo (5 ′ GTC TGT AGA CAG TTT CAT CGG TGA C -3 ′ amine) with Dibenzocyclooctyne-PEG4-N-hydroxysuccinimidyl ester (Sigma-Aldrich). The DBCO-PEG4-NHS Ester was dissolved in DMSO at a final concentration of 10 mM. Then, amine-modified oligo (5 ′ GTC TGT AGA CAG TTT CAT CGG TGA C -3 ′ amine) at a final concentration of 100 μM was added to the DBCO-PEG4-NHS Ester solution and incubated at room temperature for 2 hours. The oligonucleotides were purified via ethanol precipitation and stored in PBS. The modified antibody was incubated overnight at 30°C with 2 to 10 equivalents of the DBCO-ssDNA from IDT and the homemade DBCO-ssDNA.

Characterization of the ssDNA-antibody conjugates

Samples were taken in between every modification step and conjugation step for gel electrophoresis analysis and liquid chromatography-mass spectrometry (LC-MS). The LC-MS measurements are described in the Master thesis of Maud.[98]

Samples taken in between modification steps and conjugation steps were diluted to a final protein concentration of 0.5 mg/mL using PBS buffer. Intact antibodies were reduced to heavy and light chains using dithiothreitol (DTT) with equal amounts. The antibodies were incubated with DTT for 30 minutes on a shaker at 56°C. Thereafter, all samples were denatured by equal amounts of Laemmli loading buffer at 95°C for 10 minutes. For each sample, approximately 2 μg of proteins were loaded onto a 4-20% tris-glycine gel. At least two lanes in each gel were filled with the precision plus protein standard as a reference. Electrophoresis was performed for 90 minutes at 150 V, using a tris/glycine/SDS running buffer. Before the protein staining procedure, the staining of ssDNA was performed by incubating the gel for 15 minutes in MilliQ and 5 μL SybrGold, followed by three washes of MilliQ. The gel was imaged using the Gel Doc EZ Imager with an excitation wavelength of 302 nm. The gels were then incubated for 30 minutes in Coomassie brilliant blue R-250 for staining. The gels were de-stained in MilliQ for at least overnight. Thereafter,

the gels were imaged using a Gel Doc EZ Imager (Bio-Rad) and analyzed with Gel Image lab software (Bio-Rad).

5.5.4 *PCT sandwich assay*

Directional and non-directional immobilization of PCT antibodies onto glass substrates are described in the following sections. Directional coupling is based on the DNA-directed immobilization of the modified ssDNA-antibody conjugates, while non-directional immobilization is based on the physical adsorption of unmodified PCT antibodies.

Directional binding of antibodies

Glass slides (25 x 75 mm, #5, Menzel-Gläser) were pre-cleaned by 30 minutes of sonication in isopropanol (VWR, absolute) and 10 minutes of sonication in MilliQ. After the substrate was dried with a nitrogen stream, 1 minute of oxygen plasma was applied to the slides to plasma-oxidize the surface. PLL(20)-g[3.5]-PEG(2) and PLL(15)-g[3.5]-PEG(2)-N_3 were pre-mixed in MilliQ with the ratio of 9:1 by weight at a final concentration of 0.45 mg/mL and 0.05 mg/mL respectively. Custom-made fluid cell stickers (Grace Biolabs) with a volume of 20 μL were then attached to the substrate and the PLL-g-PEG/PLL-g-PEG-N_3 polymer mixture was immediately injected into the flow chamber and incubated for two hours. After the polymer self-assembled onto the negatively charged substrate, the unbound or loosely bound polymers were removed by withdrawing the solution out of the chamber.

The substrate-side binder is a partially double-stranded DNA consisting of two complementary oligos, namely a 31nt oligo (3 ′ C ATT ATT ACA AGC TAA GCT CTT GCA CTG ACG 5 ′) and a DBCO functionalized oligo (5 ′ CGA TTC GAG AAC GTG ACT GCT TTT T 3 ′ DBCO). The 100 μM 31nt oligo was pre-hybridized with 100 μM DBCO functionalized oligo at a volume ratio of four to one. After removing the unbound or loosely bound PLL-g-PEG and PLL-g-PEG-N_3, the partially double-stranded DNA was diluted to 1 μM with 500 mM NaCl in PBS (130 mM NaCl, 7 mM Na2HPO4, 3 mM NaH2PO4 at pH 7.4) and injected into the flow cell, followed by 72 hours of incubation at room temperature. Unbound DNA was washed away from the flow cell using 500

mM NaCl in PBS. The capture DNA (35nt or 45nt) was added into the flow cell at a final concentration of 10 μM and the hybridization was done for 30 minutes. Next, unbound DNA (35nt or 45nt) was washed away from the flow cell using PBS.

The DBCO-DNA purchased from IDT and the homemade DBCO-DNA both were mixed with the modified antibodies with a ratio of 1:4. The ssDNA-antibody conjugates were then added to the flow cell at a final concentration of 0.25 μM in PBS. The hybridization of the complementary DNA sequences was done by one hour of incubation in a humid chamber. Finally, the flow cell was blocked by incubating 1% of bovine serum albumin (BSA) in PBS for one hour.

Physical adsorption of antibodies

Glass slides were cleaned by 15 minutes of sonication in methanol. The slides were dried using a nitrogen gun. A flow-cell sticker was attached to the slide and immediately filled with PBS. 20 μL of 100 nM antibodies were added and the incubation proceeded at room temperature for one hour. Thereafter, the surface was blocked for one hour using 1% BSA in PBS.

Particle preparation for directional coupling

Dynabeads MyOne streptavidin C1 particles and 10 μM of biotin-DNA (5 ′ AAA AAG CAG TCA CGT TCT CGA ATC G 3 ′ - Biotin) were mixed with a 1:2 ratio and incubated for 30 minutes on a rotating fin. One equivalent of modified antibodies with a final concentration of 0.25 nM was added to the particles and the mixture was incubated for 30 minutes. Unbound biotin-DNA and antibodies were separated from the particles by using a magnetic rack. After the supernatant was removed, the particles were re-suspended in 1% BSA in PBS for blocking. The incubation proceeded on a rotating fin for one hour. After blocking, the particles were sonicated using a sonic finger (Hielscher) for 10 pulses with amplitude 70 and cycle 0.4. The particles were further diluted 4000 times in 0.1% BSA in PBS.

Particle preparation for non-directional coupling

Biotinylated antibodies were produced using the ChromaLink Biotinylation (SoluLink) kit. Two μL of Dynabeads MyOne streptavidin C1 particles were mixed with two μL of 100 nm biotinylated antibodies and incubated for 45 minutes on a rotating fin. Ten μL of 10 mM biotin-PEG was added to the particles to block

all accessible streptavidin. The particles were incubated for 10 minutes on a rotating fin at RT. Unbound antibodies and biotin-PEG were washed three times with PBS on a magnetic rack. The particles were re-suspended in 1% BSA in PBS for blocking and incubated on a rotating fin for one hour. After blocking, the particles were sonicated using a sonic finger (Hielscher) for 10 pulses with amplitude 70 and cycle 0.4. The particles were further diluted 4000 times in 0.1% BSA in PBS.

PCT sandwich assay

The flow cell was washed three times using assay buffer (0.1% BSA in PBS). Thereafter, 20 μL of particles were added to the flow cell and were incubated for 15 minutes. The 5 min particle motion measurements in the absence of flow, were recorded on a Leica DMI5000M microscope (Darkfield microscopy, Leica Microsystems GmbH, Germany). The position of the particles was recorded in a field of view of 883×552 μm^2 for 5 minutes at a frame rate of 60 Hz with an integration time of 5 ms. By analyzing the intensity of pixels around the particle with a phasor-based localization method,[54] the center of every particle can be determined over each time frame.

The background signals were measured in the absence of analytes (PCT). After obtaining a stable baseline, PCT was added to the flow cell with a step-wise increasing concentration series, ranging from 4 to 800 pM. For each concentration, particles were tracked for five minutes in either one or three different fields of view.

5.5.5 *Analysis of particle mobility*

Particle tracking was performed based on phasor localization, as described in Section 3.5.4. Event detection based on deep learning algorithm and the analysis of switching activity, lifetimes, and bound fraction is described in Section 3.5.4.

5.6 APPENDIX

5.6.1 *Gel electrophoresis results stained with SYBR-gold*

The protein gel shown in Figure 5.2 was also stained with SYBR gold to confirm that the mass changes were indeed caused by the presence of ssDNA. Figure 5.12 shows the imaged bands of samples listed in Table 5.2. However, we also observed a fluorescent band in the Trastuzumab sample. Since the observed intensities for the fluorescence of the proteins are very low, it is expected that this is caused by either fluorescence from phenylalanine, tryptophan, and tyrosine, or from non-specific binding of the SYBR-gold to the antibody. For the band containing DNA, the observed intensity of the fluorescence is much higher. Therefore, it is confirmed that the conjugates indeed contain ssDNA strands.

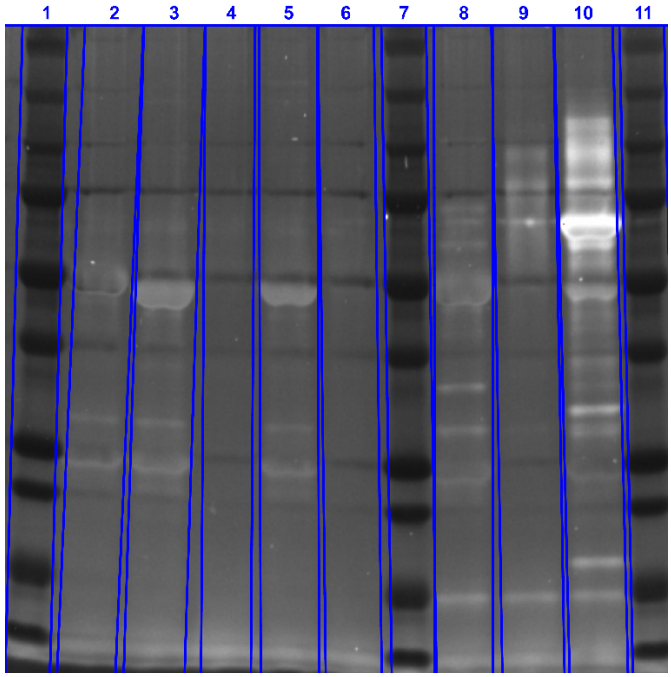

Figure 5.12: Protein gel of the listed samples including plain trastuzumab and modified Trastuzumab stained with SYBR-gold. The different lanes were loaded with the following orders. Lane 1: Protein standard; 2: Trastuzumab; 3: Glycan trimmed Trastuzumab; 4: Blank glycan trimming; 5: Modified Trastuzumab; 6: Modification blank; 7: Protein standard; 8: Non-modified Trastuzumab incubated with DBCO-ssDNA; 9: Conjugation blank; 10: Conjugated Trastuzumab; 11: Protein standard.

Table 5.2: Molecular weight and relative quantities of the heavy chain (approximately 50 kDa) and light chain (approximately 25 kDa) bands of the listed samples.

Sample	**Molecular weight of bands**	**Relative quantity**
Trastuzumab	49.4	1
(Lane 2)	24.3	0.5
Trimmed Trastuzumab	46.9	1.2
(Lane 3)	24	0.65
Modified Trastuzumab	48.3	0.81
(Lane 5)	24.5	0.41
Trastuzumab + DBCO-ssDNA	49.6	1.35
(Lane 8)	24.6	0.68
Conjugated Trastuzumab (Lane 10)	66.5	0.8
	49.1	0.43
	24.5	0.58

5.6.2 *Thermal dissociation rate*

The shortest hybridization lengths of the two systems described in Section 5.3.3 are 13nt and 21nt respectively. The thermal dissociation rate, the rate at which dissociation of hybridized DNA strains occurs, for DNA decreases with $10^{8-0.5n}s^{-1}$, in which n is the number of nucleotides of one ssDNA strand contributing to the hybridization.[100] This means that the hybridization of 20nt has an estimated 10,000 times stronger binding than the hybridization of 13nt.

6

CONCLUSION AND OUTLOOK

The goal of this thesis was to develop a robust molecular architecture and coupling process to immobilize biomolecules on anti-fouling surfaces for continuous monitoring biosensors. The thesis focused on three main topics, namely (1) the development of a biofunctionalization strategy and its role in the enhancement of analytical performances of continuous monitoring biosensors, (2) the development of a continuous monitoring principle based on particles that diffuse over a biofunctionalized surface, and (3) the development of biosensors for out-of-the-lab use, for long-term use, and biosensors with antibodies as binder molecules. The first topic was discussed in chapters 2 and 3, the second topic mainly in chapter 3, and the third topic in chapters 4 and 5. In this chapter, the main conclusions of this thesis are summarized and discussed, and an outlook is presented.

6.1 SUMMARY OF MAIN RESULTS

In **chapter two** we demonstrated a biofunctionalization strategy based on PLL-g-PEG that allows continuous measurements of biomolecules over long durations in a sensing technology with single-molecule resolution. The biofunctionalization involves covalent coupling by click chemistry to electrostatically grafted polymers. With this biofunctionalization strategy, we demonstrate the continuous monitoring of medically relevant analytes, in sandwich and competitive assays, in buffer and in filtered blood plasma, with picomolar, nanomolar, and micromolar analyte concentrations. Moreover, we quantified the enhancement of analytical performances of the biosensors in terms of stability and operational lifetime. Since the anti-fouling polymers are attached to the substrate by multivalent electrostatic interactions, the biofunctionalization scheme is suited for various substrates. The coupling process involving click chemistry and DNA-directed immobilization is suited for a variety of analytes and the im-

plementation of different assay formats. The biosensors give consistent and reversible responses with a long operational lifetime.

In **chapter three** we presented a biomarker monitoring methodology that is based on free diffusion of particles near a surface, in which the target-induced binding and unbinding are reflected in the changes of particle mobility to detect the presence of analyte molecules. The target-induced interactions are reversible and do not require the addition of reagents, which is advantageous for applications that require biomolecular measurements over long timespans or at remote locations where reagents are not easily supplied. The proximity of particles to the surface is imposed by gravitational force, enabling free translational and rotational motion of the particles. In comparison to the limited interaction area in tethered particle systems, the total surfaces of free particles and sensing substrate are used. In the free particle motion sensing technique, single-molecular interactions related to changes in the underlying molecular binding system are probed with high contrast, allowing the quantification of rates and lifetimes, and the extraction of multiple readout parameters. The biofunctionalization strategy presented in Chapter 2 was studied with the free particle motion sensing technique enabling measurements over several days.

In **chapter four** we investigated the effects of various sugar mixtures on the preservation of the biofunctionalized surfaces and particles, aiming at the manufacturing of ready-to-go cartridges. The storage lifetime of biosensors depends on the retention of the biological activity of the used molecular components, which vary depending on the coupling chemistry, the storage conditions, and the intrinsic stability of the biomolecules. The free particle motion sensing system is particularly suitable for the fabrication of a ready-to-use sensor. The biofunctionalization strategy involving polymers, and covalent coupling were used in a study of the dehydration process with sugars. Experimental results show the ability to preserve the biofunctionalized surfaces and particles for at least three weeks, without clear loss of responsive biomolecules or functional particles. Due to the high stability of the biofunctionalized surface described in Chapter 2, and the suitability of the sensing technique demonstrated in Chapter 3

for preparation with a sugar layer as described in Chapter 4, we believe that the ready-to-go cartridges can potentially benefit further developments of continuous monitoring sensors.

In **chapter five** we employed a glycan remodeling technique and explored the methodology for immobilizing antibodies on the sensor surface and on the particles with a specific orientation. The antibodies were site-specifically modified with enzymes, enabling covalent attachment of single-stranded DNA onto the fc region of antibodies via copper-free click chemistry. To quantify the modification and conjugation efficiency at each step, analytical tools such as mass spectrometry and SDS-PAGE were used. The biofunctionalization strategy described in Chapter 2 was combined with DNA-directed immobilization of the DNA-antibody conjugates. The free particle motion sensing proposed in Chapter 3 was used as a model system to demonstrate the feasibility of continuous monitoring of PCT, which is a biomarker for sepsis. A higher sensitivity was observed with the molecular system employing the directionally coupled antibodies compared to the physically adsorbed antibodies. Given the relevance of antibodies and the importance of anti-fouling properties, we believe that the development of the oriented immobilization technique will be important for further applications of the particle-based sensing techniques.

6.2 DISCUSSION AND OUTLOOK

This thesis has presented a biofunctionalization strategy and explored analytical performances of particle-based continuous monitoring biosensors with single-molecule resolution. The biofunctionalization strategy allows one to immobilize binders of interest on an anti-fouling surface with retention of bioactivity for achieving high stability and high reproducibility of the biosensor performance. Practical applications are discussed for the valorization of the general applicability of the biofunctionalization strategy.

In the particle mobility sensing, the ability to continuously monitor analyte concentrations at the picomolar to micromolar range and to extract single-molecular kinetics such as lifetimes and rates provides insights into both ensemble information and

single-molecule processes. The biofunctionalization strategy provides opportunities for continuous monitoring of analyte concentrations with a long operational lifetime and in complex environments. However, a deeper investigation of the aging mechanisms of the materials and the dissociation rates of the affinity-based anchoring points, including biotin-avidin bond and DNA hybridization, is required. We think that replacing these affinity-based interactions with covalent bonds can potentially further extend the operational lifetime.

The work in this thesis shows the benefits and strength of employing simple physisorption of anti-fouling polymers and strong covalent coupling of binder molecules. Quantitative analytical tools are essential for researchers to evaluate the conditions and reaction times of each modification process and to assess the functionality of the binders and materials involved in the sensor surface. To be able to tune the analytical performances such as the sensitivity and the dynamic range of the biosensor and to take the heterogeneity of the molecular system into account, it is necessary to quantify the number of functional binders and their distributions on the sensor surface for example using analytical tools with single-molecule resolution like DNA-PAINT. Moreover, the characterization of the biofunctionalized surface will allow researchers to study the causes of the degradation mechanisms and their consequences, and further gain insights into the direct influence caused by changes in buffer ionic strength, various substrate materials, or continuous flow, which is important for further studies and further applications of the sensing and biofunctionalization technologies.

The advantages of extracting both single-molecule information and ensemble readouts have been demonstrated in this thesis. The responses are in general similar when looking at the trends, but slight differences in the EC_{50} values and the plateaus were observed between the dose-response curves plotted with different parameters. Further studies on the relations between these parameters are recommended for developing a calibration method aiming at improving the accuracy and precision of the continuous monitoring biosensors. By combining simulations and post-processing data analysis algorithms, the false-positive and false-negative events and the biases caused by surface and

particle heterogeneity, and position to position variations can be minimized.

A preservation protocol was presented based on the dehydration of biomolecules in sugars for the fabrication of ready-to-go cartridges. However, the applicability of the methodology for preserving antibody functionality in immuno-sensors has not been proven. We think that further studies on the properties of sugar layers and the functionality of the rehydrated biomolecules will enable long-term dry storage of fully integrated immuno-sensors.

The feasibility of oriented immobilization of antibodies onto the novel biofunctionalized surface has been demonstrated in the thesis by showing the improvements in the sensitivity of the biosensors. However, comparative studies on other analytical performances such as reproducibility, reversibility, and stability have not yet been addressed. To be able to prove the added value of the oriented immobilized antibodies, future experiments should focus on the quantification and characterization of antibodies on the surface, the effect of variability in receptor functionality, and time-dependent sensor changes. Furthermore, investigations on the affinity and reversibility of the antigen-antibody interactions are needed to enable continuous monitoring in a wide variety of fields.

We believe that the biofunctionalization strategies and biosensing concept proposed in this thesis have the potential to open a broad range of applications in the field of continuous monitoring and single-molecule measurements. This can provide opportunities in understandings of clinically relevant biological processes, and developments in lab-on-a-chip, health care devices, and process and quality control in industrial applications.

BIBLIOGRAPHY

1. Coté, G. L., Lec, R. M. & Pishko, M. V. Emerging biomedical sensing technologies and their applications. *IEEE Sensors Journal* **3,** 251–266. ISSN: 1530437X (2003).
2. Kelley, S. O. What Are Clinically Relevant Levels of Cellular and Biomolecular Analytes? *ACS Sensors* **2,** 193–197. ISSN: 23793694 (2017).
3. Nahavandi, S., Baratchi, S., Soffe, R., Tang, S. Y., Nahavandi, S., Mitchell, A. & Khoshmanesh, K. Microfluidic platforms for biomarker analysis. *Lab on a Chip* **14,** 1496–1514. ISSN: 14730189 (2014).
4. Bandodkar, A. J. & Wang, J. Non-invasive wearable electrochemical sensors: A review. *Trends in Biotechnology* **32,** 363–371. ISSN: 18793096 (2014).
5. Silva, T. A., Moraes, F. C., Janegitz, B. C., Fatibello-Filho, O. & Ganta, D. Electrochemical biosensors based on nanostructured carbon black: A review. *Journal of Nanomaterials* **2017.** ISSN: 16874129 (2017).
6. Gil, E. d. S. & de Melo, G. R. Electrochemical biosensors in pharmaceutical analysis. *Brazilian Journal of Pharmaceutical Sciences* **46,** 375–391. ISSN: 21759790 (2010).
7. Naseri, M., Fotouhi, L. & Ehsani, A. Recent Progress in the Development of Conducting Polymer-Based Nanocomposites for Electrochemical Biosensors Applications: A Mini-Review. *Chemical Record* **18,** 599–618. ISSN: 15280691 (2018).
8. Madder, A. An Antica ff eine Antibody - Oligonucleotide Conjugate for DNA- Directed Immobilization in Environmental Immunoarrays (2018).
9. Schoukroun-Barnes, L. R., Macazo, F. C., Gutierrez, B., Lottermoser, J., Liu, J. & White, R. J. Reagentless, Structure-Switching, Electrochemical Aptamer-Based Sensors. *Annual Review of Analytical Chemistry* **9,** 163–181. ISSN: 19361335 (2016).
10. Schoukroun-Barnes, L. R., Wagan, S. & White, R. J. Enhancing the analytical performance of electrochemical RNA aptamer-based sensors for sensitive detection of aminoglycoside antibiotics. *Analytical Chemistry* **86,** 1131–1137. ISSN: 15206882 (2014).

11. Mage, P. L., Ferguson, B. S., Maliniak, D., Ploense, K. L., Kippin, T. E. & Soh, H. T. Closed-loop control of circulating drug levels in live animals. *Nature Biomedical Engineering* **1,** 1–10. ISSN: 2157846X (2017).

12. Parolo, C., Idili, A., Ortega, G., Csordas, A., Hsu, A., Yang, Q., Ferguson, B. S., Wang, J. & Plaxco, K. W. Real-Time Monitoring of a Protein Biomarker (2020).

13. Li, H., Dauphin-Ducharme, P., Arroyo-Currás, N., Tran, C. H., Vieira, P. A., Li, S., Shin, C., Somerson, J., Kippin, T. E. & Plaxco, K. W. A Biomimetic Phosphatidylcholine-Terminated Monolayer Greatly Improves the In Vivo Performance of Electrochemical Aptamer-Based Sensors. *Angewandte Chemie - International Edition* **56,** 7492–7495. ISSN: 15213773 (2017).

14. Akkilic, N. Biosensors and Bioelectronics Single-molecule biosensors : Recent advances and applications. **151** (2020).

15. Rissin, D. M. *et al.* letters Single-molecule enzyme-linked immunosorbent assay detects serum proteins at subfemtomolar concentrations. *Nature Biotechnology* **28,** 595–600. ISSN: 1087-0156 (2010).

16. Zhang, Y. & Nguyen, N. Magnetic digital microfluidics - a review. *Lab on a Chip* **17** (2017).

17. Lichtenberg, J. Y., Ling, Y. & Kim, S. Non-specific adsorption reduction methods in biosensing. *Sensors (Switzerland)* **19,** 1–17. ISSN: 14248220 (2019).

18. Blaszykowski, C., Sheikh, S. & Thompson, M. Surface chemistry to minimize fouling from blood-based fluids. *Chemical Society Reviews* **41,** 5599–5612. ISSN: 14604744 (2012).

19. Lin, P. H. & Li, B. R. Antifouling strategies in advanced electrochemical sensors and biosensors. *Analyst* **145,** 1110–1120. ISSN: 13645528 (2020).

20. Wang, F., Zhang, H., Yu, B., Wang, S., Shen, Y. & Cong, H. Review of the research on anti-protein fouling coatings materials. *Progress in Organic Coatings* **147,** 105860. ISSN: 03009440. https://doi.org/10.1016/j.porgcoat.2020.105860 (2020).

21. Liu, Y. & Yu, J. Oriented immobilization of proteins on solid supports for use in biosensors and biochips: a review. *Microchimica Acta* **183,** 1–19. ISSN: 14365073 (2016).

22. Gubala, V., Harris, L. F., Ricco, A. J., Tan, M. X. & Williams, D. E. Point of Care Diagnostics : Status and Future (2011).

23. Welch, N. G., Scoble, J. A., Muir, B. W. & Pigram, P. J. Orientation and characterization of immobilized antibodies for improved immunoassays (Review). *Biointerphases* **12,** 02D301. ISSN: 1934-8630 (2017).

24. Bonroy, K., Frederix, F., Reekmans, G., Dewolf, E., De Palma, R., Borghs, G., Declerck, P. & Goddeeris, B. Comparison of random and oriented immobilisation of antibody fragments on mixed self-assembled monolayers. *Journal of Immunological Methods* **312,** 167–181. ISSN: 00221759 (2006).

25. Wen, X., He, H. & Lee, L. J. Specific antibody immobilization with biotin-poly(l-lysine)-g-poly(ethylene glycol) and protein A on microfluidic chips. *Journal of Immunological Methods* **350,** 97–105. ISSN: 00221759. http://dx.doi.org/10.1016/j.jim.2009.07.011 (2009).

26. Bally, M., Bailey, K., Sugihara, K., Grieshaber, D., Vörös, J. & Städler, B. Liposome and lipid bilayer arrays towards biosensing applications. *Small* **6,** 2481–2497. ISSN: 16136829 (2010).

27. Young, M. A., Furr, D. P., McKeough, R. Q., Elliott, G. D. & Trammell, S. R. Light-assisted drying for anhydrous preservation of biological samples: optical characterization of the trehalose preservation matrix. *Biomedical Optics Express* **11,** 801. ISSN: 2156-7085 (2020).

28. Crowe, J. H. & Crowe, L. M. Preservation of mammalian cells - Learning nature's tricks. *Nature Biotechnology* **18,** 145–146. ISSN: 10870156 (2000).

29. Schleipen, J. J. H. B., Theije, F. K. D., Verschuren, C. A., Wijk, T. V. D., Zon, J. B. A. V., Dittmer, W. U., Immink, A. H. J., Nieuwenhuis, J. H. & Prins, M. W. J. Rapid integrated biosensor for multiplexed immunoassays based on actuated magnetic nanoparticles †, 3504–3510 (2009).

30. Jarrige, V. & Nieuwenhuis, J. H. A fast intraoperative PTH point-of-care assay on the Philips handheld magnotech system, 337–343 (2011).

31. Rodbard, D. Continuous Glucose Monitoring: A Review of Successes, Challenges, and Opportunities. *Diabetes Technology and Therapeutics* **18,** S23–S213. ISSN: 15578593 (2016).

32. Wasalathanthri, D. P. *et al.* Technology outlook for real-time quality attribute and process parameter monitoring in biopharmaceutical development—A review. *Biotechnology and Bioengineering*. ISSN: 10970290 (2020).

33. Visser, E. W. A., Yan, J., van IJzendoorn, L. J. & Prins, M. W. J. Continuous biomarker monitoring by particle mobility sensing with single molecule resolution. *Nature Communications* **9,** 1–10. ISSN: 20411723 (2018).

34. Lubken, R. M., de Jong, A. M. & Prins, M. W. J. Multiplexed Continuous Biosensing by Single-Molecule Encoded Nanoswitches. *Nano Letters* **20,** 2296–2302. ISSN: 15306992 (2020).

35. Yan, J., van Smeden, L., Merkx, M., Zijlstra, P. & Prins, M. W. J. Continuous Small-Molecule Monitoring with a Digital Single-Particle Switch. *ACS Sensors* **5,** 1168–1176. ISSN: 23793694 (2020).

36. Farka, Z., Mickert, M. J., Pastucha, M., Mikušová, Z., Skládal, P. & Gorris, H. H. Advances in Optical Single-Molecule Detection: En Route to Supersensitive Bioaffinity Assays. *Angewandte Chemie - International Edition* **59,** 10746–10773. ISSN: 15213773 (2020).

37. Vaisocherová, H., Brynda, E. & Homola, J. Functionalizable low-fouling coatings for label-free biosensing in complex biological media: advances and applications. *Analytical and Bioanalytical Chemistry* **407,** 3927–3953. ISSN: 16182650 (2015).

38. Kim, E. & Koo, H. Biomedical applications of copper-free click chemistry:: In vitro, in vivo, and ex vivo. *Chemical Science* **10,** 7835–7851. ISSN: 20416539 (2019).

39. Escorihuela, J., Marcelis, A. T. & Zuilhof, H. Metal-Free Click Chemistry Reactions on Surfaces. *Advanced Materials Interfaces* **2,** 1–42. ISSN: 21967350 (2015).

40. Tosatti, S., De Paul, S. M., Askendal, A., VandeVondele, S., Hubbell, J. A., Tengvall, P. & Textor, M. Peptide functionalized poly(L-lysine)-g-poly(ethylene glycol) on titanium: Resistance to protein adsorption in full heparinized human blood plasma. *Biomaterials* **24,** 4949–4958. ISSN: 01429612 (2003).

41. Eeftens, J. M., Torre, J. V. D., Burnham, D. R. & Dekker, C. Copper-free click chemistry for attachment of biomolecules in magnetic tweezers. *BMC Biophysics*, 1–7. ISSN: 2046-1682. http://dx.doi.org/10.1186/s13628-015-0023-9 (2015).

42. Janissen, R., Berghuis, B. A., Dulin, D., Wink, M., Laar, T. V. & Dekker, H. Invincible DNA tethers : covalent DNA anchoring for enhanced temporal and force stability in magnetic tweezers experiments, 1–10 (2014).

43. Kotagiri, N., Li, Z., Xu, X., Mondal, S., Nehorai, A. & Achilefu, S. Antibody Quantum Dot Conjugates Developed via Copper-Free Click Chemistry for Rapid Analysis of Biological Samples Using a Micro fl uidic Microsphere Array System (2014).

44. Gunnarsson, A., Jo, P., Marie, R. & Tegenfeldt, J. O. Single-Molecule Detection and Mismatch Discrimination of Unlabeled DNA Targets (2008).

45. Jacob, A., van IJzendoorn, L. J., de Jong, A. M. & Prins, M. W. J. Quanti fi cation of Protein - Ligand Dissociation Kinetics in Heterogeneous A ffi nity Assays (2012).

46. Beyer, M. K. The mechanical strength of a covalent bond calculated by density functional theory. **112,** 3–8 (2000).

47. Michel, R., Lussi, J. W., Csucs, G., Reviakine, I., Danuser, G., Ketterer, B., Hubbell, J. A., Textor, M. & Spencer, N. D. Selective Molecular Assembly Patterning : A New Approach to Micro- and Nanochemical Patterning of Surfaces for Biological Applications, 3281–3287 (2002).

48. Wattendorf, U., Kreft, O., Textor, M., Sukhorukov, G. B. & Merkle, H. P. Stable Stealth Function for Hollow Polyelectrolyte Microcapsules through a Poly (ethylene glycol) Grafted Polyelectrolyte Adlayer, 100–108 (2008).

49. Kenausis, G. L., Vo, J., Elbert, D. L., Huang, N., Hofer, R., Ruiz-taylor, L., Textor, M., Hubbell, J. A. & Spencer, N. D. Poly (L -lysine) - g -Poly (ethylene glycol) Layers on Metal Oxide Surfaces : Attachment Mechanism and Effects of Polymer Architecture on Resistance to Protein Adsorption †, 3298–3309 (2000).

50. Huang, N., Michel, R., Voros, J., Textor, M., Hofer, R., Rossi, A., Elbert, D. L., Hubbell, J. A. & Spencer, N. D. Poly (L -lysine) - g -poly (ethylene glycol) Layers on Metal Oxide Surfaces : Surface-Analytical Characterization and Resistance to Serum and Fibrinogen Adsorption, 489–498 (2001).

51. Weissgerber, T. L., Milic, N. M., Winham, S. J. & Garovic, V. D. Beyond Bar and Line Graphs: Time for a New Data Presentation Paradigm. *PLoS Biology* **13,** 1–10. ISSN: 15457885 (2015).

52. Waikar, S. S. & Bonventre, J. V. Creatinine Kinetics and the Definition of Acute Kidney Injury, 672–679 (2009).

53. Schlapak, R., Armitage, D., Saucedo-Zeni, N., Chrzanowski, W., Hohage, M., Caruana, D. & Howorka, S. Selective protein and DNA adsorption on PLL-PEG films modulated by ionic strength. *Soft Matter* **5,** 613–621. ISSN: 1744683X (2009).

54. Martens, K. J., Bader, A. N., Baas, S., Rieger, B. & Hohlbein, J. Phasor based single-molecule localization microscopy in 3D (pSMLM-3D): An algorithm for MHz localization rates using standard CPUs. *Journal of Chemical Physics* **148.** ISSN: 00219606. http://dx.doi.org/10.1063/1.5005899 (2018).

55. Hagedoorn, L. C. Comparison of grafting behavior of commercially available PLL- g -PEG and a tailor-made anti-fouling polymer (2018).

56. Steinmetz, L. M. & Jones, A. Sensing a revolution. *Molecular Systems Biology* **12,** 867. ISSN: 1744-4292 (2016).

57. Justino, C. I., Duarte, A. C. & Rocha-Santos, T. A. Recent progress in biosensors for environmental monitoring: A review. *Sensors (Switzerland)* **17.** ISSN: 14248220 (2017).

58. Qu, J. H., Dillen, A., Saeys, W., Lammertyn, J. & Spasic, D. Advancements in SPR biosensing technology: An overview of recent trends in smart layers design, multiplexing concepts, continuous monitoring and in vivo sensing. *Analytica Chimica Acta* **1104,** 10–27. ISSN: 18734324. https://doi.org/10.1016/j.aca.2019.12.067 (2020).

59. Kurnik, M., Pang, E. Z. & Plaxco, K. W. An Electrochemical Biosensor Architecture Based on Protein Folding Supports Direct Real-Time Measurements in Whole Blood. *Angewandte Chemie* **132,** 18600–18603. ISSN: 0044-8249 (2020).

60. Lubken, R. M., de Jong, A. M. & Prins, M. W. J. How Reactivity Variability of Biofunctionalized Particles Is Determined by Superpositional Heterogeneities. *ACS Nano* **15,** 1331–1341. ISSN: 1936086X (2021).

61. Bult, P. Design and Feasibility of Deep Learning Algorithms for Biosensing by Particle Mobility (2021).

62. Van Haaften, R. Brownian motion analysis on tethered particles to probe particle states Brownian motion analysis of tethered particles to probe particle states Bachelor End Project (2019).

63. Bjerketorp, J., Håkansson, S., Belkin, S. & Jansson, J. K. Advances in preservation methods: Keeping biosensor microorganisms alive and active. *Current Opinion in Biotechnology* **17,** 43–49. ISSN: 09581669 (2006).

64. Terpou, A., Papadaki, A., Lappa, I. K., Kachrimanidou, V., Bosnea, L. A. & Kopsahelis, N. Nutrients-11-01591 (1).Pdf. *Nutrients* **11,** 32. https://www.mdpi.com/2072-6643/11/7/1591 (2019).

65. Redway, K. F. & Lapage, S. P. Effect of carbohydrates and related compounds on the long-term preservation of freeze-dried bacteria. *Cryobiology* **11,** 73–79. ISSN: 10902392 (1974).

66. Crowe, J. H. & Hoekstra, F. A. John H. Crowe, Folkert (1992).

67. Wolkers, W. F., Walker, N. J., Tablin, F. & Crowe, J. H. Human platelets loaded with trehalose survive freeze-drying. *Cryobiology* **42,** 79–87. ISSN: 00112240 (2001).

68. Patist, C. M., Mulder, M. B., Gautier, S. E., Maquet, V., Jérôme, R. & Oudega, M. Freeze-dried poly(D,L-lactic acid) macroporous guidance scaffolds impregnated with brain-derived neurotrophic factor in the transected adult rat thoracic spinal cord. *Biomaterials* **25,** 1569–1582. ISSN: 01429612 (2004).

69. Kumar, S., Gallagher, R., Bishop, J., Kline, E., Buser, J., Lafleur, L., Shah, K., Lutz, B. & Yager, P. Long-term dry storage of enzyme-based reagents for isothermal nucleic acid amplification in a porous matrix for use in point-of-care diagnostic devices. *Analyst* **145,** 6875–6886. ISSN: 13645528 (2020).

70. Higashiyama, T. Novel functions and applications of trehalose: *Pure and Applied Chemistry* **74,** 1263–1269. https://doi.org/10.1351/pac200274071263 (2002).

71. Jovanović, N., Bouchard, A., Hofland, G. W., Witkamp, G. J., Crommelin, D. J. & Jiskoot, W. Distinct effects of sucrose and trehalose on protein stability during supercritical fluid drying and freeze-drying. *European Journal of Pharmaceutical Sciences* **27,** 336–345. ISSN: 09280987 (2006).

72. Leslie, S. B., Israeli, E., Lighthart, B., Crowe, J. H. & Crowe, L. M. Trehalose and sucrose protect both membranes and proteins in intact bacteria during drying. *Applied and Environmental Microbiology* **61,** 3592–3597. ISSN: 00992240 (1995).

73. Leathers, T. D. Biotechnological production and applications of pullulan. *Applied Microbiology and Biotechnology* **62,** 468–473. ISSN: 01757598 (2003).

74. Singh, R. S., Kaur, N., Rana, V. & Kennedy, J. F. Pullulan: A novel molecule for biomedical applications. *Carbohydrate Polymers* **171,** 102–121. ISSN: 01448617. http://dx.doi.org/10.1016/j.carbpol.2017.04.089 (2017).

75. Tabasum, S., Noreen, A., Maqsood, M. F., Umar, H., Akram, N., Nazli, Z. i., Chatha, S. A. S. & Zia, K. M. A review on versatile applications of blends and composites of pullulan with natural and synthetic polymers. *International Journal of Biological*

Macromolecules **120,** 603–632. ISSN: 18790003. https://doi.org/10.1016/j.ijbiomac.2018.07.154 (2018).

76. Bruls, D. M. *et al.* Rapid integrated biosensor for multiplexed immunoassays based on actuated magnetic nanoparticles. *Lab on a Chip* **9,** 3504–3510. ISSN: 14730189 (2009).

77. Ali, M. M., Brown, C. L., Jahanshahi-Anbuhi, S., Kannan, B., Li, Y., Filipe, C. D. & Brennan, J. D. A Printed Multicomponent Paper Sensor for Bacterial Detection. *Scientific Reports* **7,** 1–10. ISSN: 20452322. http://dx.doi.org/10.1038/s41598-017-12549-3 (2017).

78. Stevens, D. Y., Petri, C. R. & Yager, P. On-card dry reagent storage for disposable microfluidic immunoassays. *12th International Conference on Miniaturized Systems for Chemistry and Life Sciences - The Proceedings of MicroTAS 2008 Conference,* 188–190 (2008).

79. Spaanderman, D. Development of a ready-to-use BPM sensor (2021).

80. Lin, Y., Vermaas, R., Yan, J., de Jong, A. M. & Prins, M. W. J. Click-Coupling to Electrostatically Grafted Polymers Greatly Improves the Stability of a Continuous Monitoring Sensor with Single-Molecule Resolution. *ACS Sensors* **6,** 1980–1986. ISSN: 2379-3694 (2021).

81. Chiang, C. Y. *et al.* Fiber optic nanogold-linked immunosorbent assay for rapid detection of procalcitonin at femtomolar concentration level. *Biosensors and Bioelectronics* **151,** 111871. ISSN: 18734235. https://doi.org/10.1016/j.bios.2019.111871 (2020).

82. Gao, L. *et al.* DcR3, a new biomarker for sepsis, correlates with infection severity and procalcitonin. *Oncotarget* **9,** 10934–10944. ISSN: 19492553 (2018).

83. Schneider, H. G. & Lam, Q. T. Procalcitonin for the clinical laboratory: A review. *Pathology* **39,** 383–390. ISSN: 14653931 (2007).

84. Kocabaş, E., Sarikçioğlu, A., Aksaray, N., Seydaoğlu, G., Seyhun, Y. & Yaman, A. Role of procalcitonin, C-reactive protein, interleukin-6, interleukin-8 and tumor necrosis factor-α in the diagnosis of neonatal sepsis. *Turkish Journal of Pediatrics* **49,** 7–20. ISSN: 00414301 (2007).

85. Ruokonen, E., Nousiainen, T., Pulkki, K. & Takala, J. Procalcitonin concentrations in patients with neutropenic fever. *European Journal of Clinical Microbiology and Infectious Diseases* **18,** 283–285. ISSN: 09349723 (1999).

86. Herrmann, J. L., Blanchard, H., Lagrange, P. H. & Brunengo, P. TNFα, IL-1β and IL-6 plasma levels in neutropenic patients after onset of fever and correlation with the C-reactive protein (CRP) kinetic values. *Infection* **22,** 309–315. ISSN: 03008126 (1994).

87. Abdollahi, A., Shoar, S., Nayyeri, F. & Shariat, M. Diagnostic value of simultaneous measurement of procalcitonin, interleukin-6 and hs-CRP in prediction of early-onset neonatal sepsis. *Mediterranean Journal of Hematology and Infectious Diseases* **4.** ISSN: 20353006 (2012).

88. Iglesias, J., Marik, P. E. & Levine, J. S. Elevated serum levels of the type I and type II receptors for tumor necrosis factor-α as predictive factors for ARF in patients with septic shock. *American Journal of Kidney Diseases* **41,** 62–75. ISSN: 02726386. http://dx.doi.org/10.1053/ajkd.2003.50024 (2003).

89. Vigushin, D. M., Pepys, M. B. & Hawkins, P. N. Metabolic and scintigraphic studies of radioiodinated human C-reactive protein in health and disease. *Journal of Clinical Investigation* **91,** 1351–1357. ISSN: 00219738 (1993).

90. Lee, J. E., Seo, J. H., Kim, C. S., Kwon, Y., Ha, J. H., Choi, S. S. & Cha, H. J. A comparative study on antibody immobilization strategies onto solid surface. *Korean Journal of Chemical Engineering* **30,** 1934–1938. ISSN: 02561115 (2013).

91. Nellaiappan, S., Mandali, P. K., Prabakaran, A. & Krishnan, U. M. Electrochemical immunosensors for quantification of procalcitonin: Progress and prospects. *Chemosensors* **9,** 1–16. ISSN: 22279040 (2021).

92. Lim, J. M., Ryu, M. Y., Kim, J. H., Cho, C. H., Park, T. J. & Park, J. P. An electrochemical biosensor for detection of the sepsis-related biomarker procalcitonin. *RSC Advances* **7,** 36562–36565. ISSN: 20462069 (2017).

93. Molter, G. P., Soltész, S., Kottke, R., Wilhelm, W., Biedler, A. & Silomon, M. Procalcitoninplasmakonzentration und systemische inflammatorische antwort nach verschiedenen operativen eingriffen. *Anaesthesist* **52,** 210–217. ISSN: 00032417 (2003).

94. Leclerc, F., Cremer, R. & Noizet, O. Procalcitonin as a diagnostic and prognostic biomarker of sepsis in critically ill children. *Pediatric Critical Care Medicine* **4,** 264–266. ISSN: 15297535 (2003).

95. Jing, W., Wang, Y., Yang, Y., Wang, Y., Ma, G., Wang, S. & Tao, N. Time-Resolved Digital Immunoassay for Rapid and Sensitive Quantitation of Procalcitonin with Plasmonic Imaging. *ACS Nano* **13,** 8609–8617. ISSN: 1936086X (2019).

96. Carvalho, A. M., Manicardi, A., Montes, C. V., Gunnoo, S. B., Schneider, R. J. & Madder, A. Decoration of trastuzumab with short oligonucleotides: Synthesis and detailed characterization. *Organic and Biomolecular Chemistry* **15,** 8923–8928. ISSN: 14770520 (2017).

97. Van Geel, R., Wijdeven, M. A., Heesbeen, R., Verkade, J. M., Wasiel, A. A., Van Berkel, S. S. & Van Delft, F. L. Chemoenzymatic Conjugation of Toxic Payloads to the Globally Conserved N-Glycan of Native mAbs Provides Homogeneous and Highly Efficacious Antibody-Drug Conjugates. *Bioconjugate Chemistry* **26,** 2233–2242. ISSN: 15204812 (2015).

98. Linssen, M. & Lin, Y. Orientated antibody coupling for PCT-assay in BPM (2021).

99. Gajos, K., Szafraniec, K., Petrou, P. & Budkowski, A. Surface density dependent orientation and immunological recognition of antibody on silicon: TOF-SIMS and surface analysis of two covalent immobilization methods. *Applied Surface Science* **518,** 146269. ISSN: 01694332. https://doi.org/10.1016/j.apsusc.2020.146269 (2020).

100. Strunz, T., Oroszlan, K., Schäfer, R. & Güntherodt, H. J. Dynamic force spectroscopy of single DNA molecules. *Proceedings of the National Academy of Sciences of the United States of America* **96,** 11277–11282. ISSN: 00278424 (1999).

PUBLICATIONS

ARTICLES

1. **Lin, Y.**, Vermaas, R., Yan, J., de Jong, A. M., & Prins, M. W. J. "Click-Coupling to Electrostatically Grafted Polymers Greatly Improves the Stability of a Continuous Monitoring Sensor with Single-Molecule Resolution." *ACS Sensors* (2021).

2. Alvisi, N., Gutiérrez-Mejía, F. A., Lokker, M., **Lin, Y.**, de Jong, A. M., van Delft, F., & de Vries, R. "Self-Assembly of Elastin-like Polypeptide Brushes on Silica Surfaces and Nanoparticles." *Biomacromolecules* (2021).

3. Buskermolen, A., **Lin, Y.**, van Smeden, L., et al; (A.B., Y.L. and L.S. are equally contributing first authors.) "Continuous biomarker monitoring with single molecule resolution by measuring free particle motion" to be submitted.

ORAL PRESENTATIONS

1. **Lin, Y.**, Prins, M. W. J., de Jong, A. M., *Surface functionalization for biosensing with single-molecule resolution*, International MicroNano Conference, 12 December 2018, Amsterdam, the Netherlands.

2. **Lin, Y.**, Prins, M. W. J., de Jong, A. M., *Surface functionalization for continuous biosensing with single-molecule resolution*, CHAINS, 8 December 2020, Eindhoven, the Netherlands.

CURRICULUM VITÆ

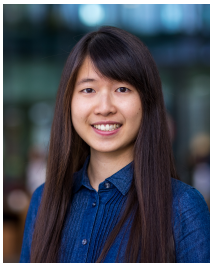

Yu-Ting Lin was born on the 3rd of May 1993 in Kaohsiung, Taiwan. She completed her primary and secondary education in Kaohsiung. After finishing her senior high school education at Kaohsiung Girls' Senior High School in 2011, she started her study of Chemical Engineering at National Taiwan University in Taipei.

In 2013, she started academic research in Professor Ling Chao's laboratory of Biomimetic Membrane Interfacial Phenomena and Engineering. In her senior year, she interned at Polysciences Asia Pacific, Inc., for one semester. She re-joined Professor Ling Chao's laboratory as a master student in 2015 and received her master degree in 2017. During her master project, she focused on developing a novel label-free method to directly measure the transport kinetics of membrane proteins embedded on cell membrane mimic bio-chips. She was trained for operating clean room equipment at the Institute of Physics, Academia Sinica.

In November 2017, she moved to Eindhoven and started working as a PhD student in the group of Molecular Biosensing for Medical Diagnostics (MBx) led by prof.dr.ir. Menno Prins at the Applied Physics department of Eindhoven University of Technology. Under the supervision of prof.dr.ir. Menno Prins and dr.ir. Arthur de Jong, she developed a robust molecular architecture and coupling process to immobilize biomolecules on anti-fouling surfaces for continuous monitoring biosensors, and furthermore explored analytical performances of particle-based biosensors. The main results and most relevant data of her PhD work are summarized in this thesis.

ACKNOWLEDGMENTS

Four years ago, I started searching for PhD positions in the Netherlands. I was lucky enough to be invited for an on-site interview at Eindhoven University of Technology. That was the first time I traveled to the Netherlands and I had a very nice experience back then. Fortunately, I got the opportunity to start my PhD journey at the MBx group. Doing a PhD is a big commitment, especially doing it aboard. I had to leave my family and leave the environment I grew up with. It all made me very nervous in the beginning. Plus the impression that only in rare cases can a PhD student finish within four years did not make my life easier. I had a hard time getting along with these ideas. Fortunately enough, with the help of my supervisors, friends, group members, and my supportive family, it all came to the end of a memorable adventure.

First of all, I would like to express my sincere gratitude to my two supervisors, Menno and Arthur, for their professional and personal support throughout the years. Without the two of you, I cannot imagine myself growing into an independent researcher. Menno has been giving me insightful guidance whenever I was stuck in my research as well as helping me a lot with my writing. I have had so much fun and really enjoyed doing experiments and executing our ideas during the past four years. Arthur, as my daily supervisor, has always helped me with all sorts of things and at the same time with such patience. From giving me suggestions on my experimental plans, to manuscript writing and all the way to my career development. It is a great pleasure and honor to have Menno and Arthur as my supervisors.

I deeply appreciate all members of the MBx group for all of the open-minded discussions, friendliness, and fun group activities that have made my PhD life memorable and enjoyable. Special thanks to Junhong, Yuyang, Laura and Rafiq. Junhong gave me a lot of critical suggestions and feedback on my experiments. Whenever I encounter problems, I always first reach out to you. I would like to thank you for sharing your expertise with me

and inspiring me with your enlightening ideas. Yuyang is the first person I contacted when I started applying for this PhD position. I bothered you a lot throughout the past four years. I really appreciate that you are always willing to devote your time and effort to help me solve my problems. Laura has always been very spontaneous in helping me, not only with my research but also when I was learning Dutch. You help me get through the challenges as an international student. So I would like to thank you for being so considerate and for all our fun moments in the office. I would also want to thank Rafiq for all the support. We started our PhD journey together, but since I was new to the group by that time, you kindly gave me all the instructions I needed. Your attitude towards perfection is everlasting and encouraged me to never give up on improving myself.

Thank you to Renko, Nicolo, and all members of the Gecko project for the invaluable collaboration. Last but not least, I want to express my thankfulness to my defense committee members, prof.dr.ir. I.K. Voets, dr. dipl.-ing. A. Sobota, prof.dr.ir. J. Huskens, and dr. R.J. de Vries, for their critical reviews and advice on my research.

特別感謝我的爸媽還有我哥一直以來都支持我的決定，雖然因爲疫情的關係暫時無法見面，但遠在荷蘭的我都還是有感受到你們的關心。最後，我還要感謝始終陪伴在我身邊的致嘉，感謝你好脾氣的包容我的一切。

Yu-Ting Lin